THESIS

IN-SITU ^{13}C CP-MAS NMR STUDY OF DILUTE ACID BIOMASS PRETREATMENT ON ^{13}C ENRICHED POPLAR WOOD

Submitted by

Benjamin D. Kohn

Department of Chemistry

In partial fulfillment of the requirements

For the Degree of Master of Science

Colorado State University

Fort Collins, Colorado

Fall 2011

Master's Committee:

Advisor: Gary Maciel

Elliot Bernstein
A. Ted Watson

ABSTRACT

IN-SITU ^{13}C CP-MAS NMR STUDY OF DILUTE ACID BIOMASS PRETREATMENT ON ^{13}C ENRICHED POPLAR WOOD

In situ ^{13}C NMR measurements are reported on ^{13}C-enriched powdered poplar wood that is subjected to pretreatment with water and 0.5 M sulfuric acid as a function of time at 150 ^{o}C. ^{13}C MAS (magic-angle spinning) spectra were obtained in both the CP (cross polarization) and DP (direct polarization) modes, the contrasts in this combination yielding valuable qualitative information on the effect of pretreatment on local molecular mobilities. In addition, spin-lattice relaxation values for ^{13}C and for ^{1}H, as well as cross polarization time constants T_{CH}^{-1} and $T_{1\rho H}^{-1}$, were measured on dry wood, and on wood 10 % in 0.5 M H_2SO_4 before, during and after treatment for lignin peaks and for holocellulose peaks in the ^{13}C NMR spectra, as indicators of the degree of molecular motion for those two structural entities. The results show that a substantial fraction of the solid/semi-solid biomass in 0.5 M H_2SO_4 is converted at elevated temperatures to a) chemically different and more mobile structures and/or b) locally similar structures with enhanced atomic-level mobilities, and that some fraction of this 'mobilized' biomass does not return to the original level of immobility upon cooling the acid-treated biomass back to room temperature.

TABLE OF CONTENTS

LIST OF FIGURES

LIST OF TABLES

LIST OF APPENDICES

CHAPTER 1 — INTRODUCTION

The past thirty years have seen a rise in awareness of the importance in finding a replacement for fossil fuels. There are many possible methods of energy generation that will be necessary in order to replace fossil fuels. One such method is the generation of ethanol from lignocellulosic biomass, which represents a renewable and carbon neutral supplement for fossil fuel use. The lignocellulose-to-fuel conversion scheme is currently understood in terms of empirical observation before and after each processing step. The logical optimization of any chemical process is facilitated via molecular level knowledge of the chemistry that occurs in situ. This study lays the framework for using solid state nuclear magnetic resonance to elucidate molecular level detail during chemically interesting steps of the lignocellulose-to-fuel conversion scheme.

Lignocellulose is a general chemical descriptor for the energy storage material produced by all species that use photosynthesis as their primary means of energy generation, and is the most abundant source of renewable carbon in our biosphere. The genesis of renewable and sustainable biofuels usually begins with the loosening of the components of lignocellulose; cellulose, hemicellulose and lignin. In the chemical literature, this process is referred to as *biomass pretreatment* and has been the subject of vigorous scientific inquiry. All studies to date have involved measurements of the system *before* and *after* the attempted separation. Using solid state ^{13}C nuclear magnetic resonance spectroscopy, this thesis outlines the first *in situ* measurements performed on a lignocellulosic substrate undergoing a pretreatment process, in an effort to evaluate the

molecular level consequences that occur *during* biomass pretreatment. Such knowledge may have broad impact on the processing of biofuels.

The specific lignocellulose used in this study comes from debarked stem wood of a narrowleaf cottonwood tree (*populus angustifolia*) that has been enriched with ^{13}C. The introduction will begin with a brief review of the relevant biological processes for the genesis of lignocellulose, followed with the chemistry of biomass pretreatment. Finally, the theory relevant to ^{13}C NMR spectroscopy used in analysis of lignocellulose in this study will be presented.

1.1 Wood Chemistry

Trees have been and continue to be of great importance to human society. They have been used to build, furnish and heat our homes for centuries. Initially, studies of trees were limited to gross anatomical features.[1] The study of the microscopic structures of trees began with the advent of the light microscope.[1] American research into the physical and chemical properties of trees began in earnest with the establishment of the US Forest Service Products Laboratory in 1910.[1] To date, properties such as mass-volume relationships, solid structure, capillary structure, adsorption, diffusion, thermal, mechanical, electrical and surface have been studied and many of these properties have been quantified.[1]

Trees are perennial seed bearing plants (spermatophytae), which are classified into two broad categories known as 'softwoods' (gymnosperms) and 'hardwoods' (angiosperms).[2-3] The main morphological components of a tree include the roots, stem, bark and leaves. In general, wood is an anisotropic material, with respect to its

anatomical, physical and chemical properties.[2,3] Wood is made up of different cell types, performing the necessary functions of mechanical support, water transport and metabolism. Wood cells are chemically heterogeneous, built from a complex polymeric matrix of structural components including carbohydrates, e.g., cellulose and hemicellulose, and phenolic moieties, e.g., lignin. These macromolecular substances are not uniformly distributed within the wood cell, and their relative concentrations vary depending on the structural component under interrogation.

Tree nutrients are manufactured through photosynthesis, primarily in the leaves, to provide the tree with energy and the propensity for growth.[2-4] Photosynthesis involves a number of reaction sequences producing primarily D-glucose, from carbon dioxide and water in the presence of chlorophyll and light.[2-4] Wood is the result of cell division utilizing the products of photosynthesis. After cell division, each cell undergoes successive development phases including enlargement, wall thickening, lignification and death. Most wood cells complete all development phases over the course of a few weeks.[2-4]

Carbohydrates, such as cellulose and hemicellulose, together known as holocellulose, constitute 70-80 wt % of woody biomass.[2-6] Phenolic moieties, of which lignin is the major component, account for 18 – 25 wt % of woody biomass.[2-6] The remaining biomass is classified as extraneous material consisting of terpenes, aliphatic acids, proteins and inorganic material, all of which constitute < 5% of the woody biomass.[2-6]

Cellulose is the main structural component found in the cell walls of all plants and is the world's most abundant and important biopolymer.[2-6] The molecular structure of cellulose is shown in Figure 1. Cellulose is a polydispersed homopolysaccharide consisting of β-D-glucopyranose (β-D-Glcp) residues, polymerized via 1→4 glycosidic bonds, with all substituents of the β-D-Glcp residues equatorially oriented.

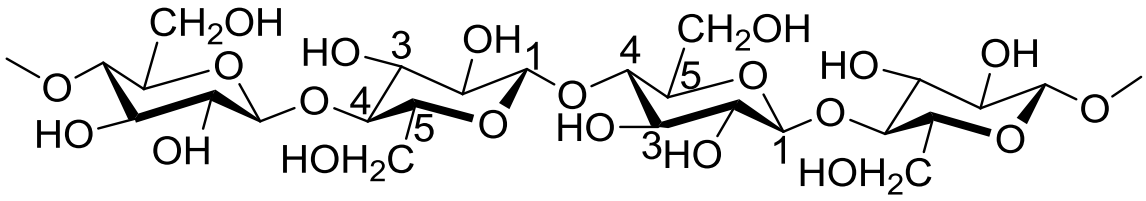

Figure 1. Molecular structure of cellulose (β-D-glucopyranose.)

The equatorial orientation of the C_1-O-C_4 glycosidic linkage minimizes the interactions between pyranose ring substituents and stabilizes the chain units.[2-3] The smallest cellulosic strand is termed an 'elementary fibril', due to the the strong tendancy for intra- and intermolecular hydrogen bonding, elementary fibrils aggregate to form fibrils. The fibrils pass through several regions of monoclinic and triclinic unit cells, depending on the specific arrangement of hydrogen bonds and as a result the fibrils aggregate into strands that are known as 'microfibrils'. Resulting in a long, linear macromolecule that has a degree of polymerization on the order of 10^4 residues, and corresponds roughly to a molecular mass of 1.6 million daltons.[2-5] The overall structure is relatively inert during most chemical treatments and soluble in very few solvents.[2-5]

The other naturally occuring carbohydrate-based polymer in wood, hemicellulose, is a heteropolysaccharide, and is less well defined than cellulose. The most common hemicellulose in hard wood is 4-O-methylglucuronoxylan,[2-3] shown in Figure 2. There

are many different types of hemicellulose. The most common saccharides typically found in hemicellulose are the pentose residues, D-xylose, L-arabinose, and D- arabinose. The hexose residues in hemicellulose are less abundant and vary among D-glucose, D-mannose and D-galactose. Also present in hemicellulose are uronic acids (carboxylic acid derivatives of hexose moeities). The chemical and thermal stability of hemicellulose is generally lower than that of cellulose, presumably due to a lack of crystallinity and a lower degree of polymerization, roughly 10^2 residues.[3]

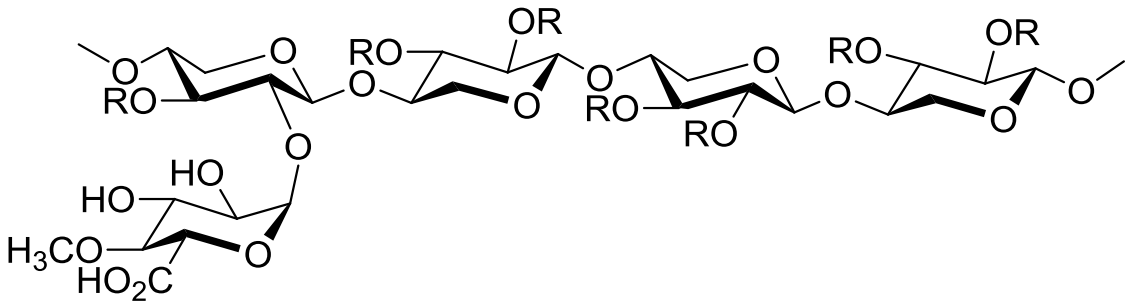

Figure 2. Molecular structure of glucoronoxylan. R can be H or acetyl group

Lignin is the second most abundant biopolymer after cellulose.[2-6] In a typical hardwood, the biosynthesis of lignin arises from a radical initiated polymerization with sinapyl alcohol (syringyl unit) and coniferyl alcohol (guayacil unit) as starting materials; these monomers are shown in Figures 3a and b, respectively. Figures 3c and d show two

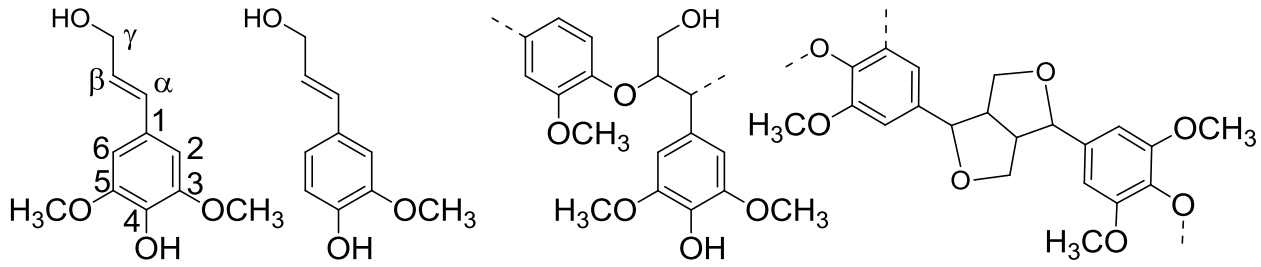

Figure 3. Building blocks of hardwood lignin. a: Sinapyl alcohol, b: Coniferyl alcohol. Hardwood lignin sub-unit structures. c: β-4’ ether linkage, d: β-β syringiresinol.

of the most common dimer moeities found in lignin. Lignin commonly polymerizes via β–O–4' ether linkages, and {α,β,γ}-{α,β,γ} alkyl or ether linkages.[2-7] Although these are the most common moeities,[2-7] in general lignin can polymerize from the 3, 4, 5, α, β and/or γ carbon atoms of either syringyl or guaiacyl moeities. The lignin polymer forms a random, three-dimensional network that acts as the 'glue' that holds cellulose and hemicellulose together, imparting strength to the middle lamella and secondary cell wall of the plant cells. In the lignocellulose complex, lignin and holocellulose participate in a combination of covalent and hydrogen bonding,[7] resulting in the structural stability and chemical recalcitrance of wood.

1.2 Biomass Pretreatment

Due to the non-renewable nature of fossil fuel, there has been vigorous research activity in converting wood into a liquid fuel, such as ethanol.[8-15] The conversion of wood to liquid fuel represents a clean, renewable and sustainable fuel source. The process of converting wood into a liquid fuel is known as *lignocellulosic biomass conversion*.[16-23] Typically, the lignocellulose-to-fuel conversion scheme takes place via a four step process: harvesting, pretreatment, fermentation, and purification. The first step involves the removal of the tree from the ground, transportation to a processing facility and subsequent pulverization of the tree to a suitably small particle size. In the second step, pretreatment, the now particulate wood is chemically treated to loosen the lignocellulose complex, thereby increasing the pore size distribution and facilitating enzymatic access to the remaining cellulose. The pretreated product is then typically treated by suitable enzymes to facilitate the depolymerization of cellulose and to ferment the resulting sugar monomers to yield ethanol and/or other chemically useful products.

It is the second step of the biomass conversion process that is of primary interest to our laboratory and is the focus of this study. This project focuses on providing molecular level information about the mobility of the lignocellulose complex *during* the pretreatment step. The changes of particular interest are those that 'disentangle' the components of lignocellulose in such a way as to facilitate conversion of woody biomass into chemically useful products, e.g., ethanol. The elucidation of molecular mobility may provide a fundamental basis for judging the mechanism for the pretreatment step, making major improvements in biomass conversion more likely.

Biomass pretreatments (BP) reported for lignocellulosic materials include acid hydrolysis, alkali swelling, solvent explosion, and exposure to supercritical fluids.[7] The acid hydrolysis pretreatment process uses either high concentration (40 - 80%) mineral acid under ambient temperature or dilute (0.5 - 2%) mineral acid under elevated temperature (120-200 ^{o}C).[2-7] This study is focused on BP via acid hydrolysis, using dilute (0.5 M) sulfuric acid as the pretreatment acid at 150 ^{o}C. BP by this approach is typically thought to be complete in 20 – 30 minutes.[24-39]

There is an abundance of work on the separation of lignocellulose into its constituents, cellulose, hemicellulose and lignin.[2-39] These works involve study of the system *before* and *after* the pretreatment process, but not *during* pretreatment. This thesis project will begin to fill this knowledge gap, using solid state ^{13}C nuclear magnetic resonance (NMR) to elucidate the structural alterations and dynamics of lignocellulose in situ, *during* BP. The acquisition of in situ measurements, using ^{13}C NMR spectroscopy is not possible using biomass containing the natural abundance of ^{13}C, 1.1 %, due to the several hours necessary to complete signal averaging for the natural-abundance ^{13}C NMR

experiment. It was decided early in the project planning that ^{13}C enriched wood would be a necessary starting material. To this end, a quantity of *populus angustifolia* was grown in an environment containing $^{13}CO_2$ as the primary source of carbon for photosynthesis.

1.3 Line Narrowing and Signal Enhancement Techniques of NMR Spectroscopy

Nuclear Magnetic Resonance (NMR) is a popular and versatile technique that is used to characterize molecular structure and dynamics.[41] Over the past 40 years, nuclear magnetic resonance spectroscopy has been successfully employed in the characterization of semi-solid samples of biological origin.[41-54] The acquisition of 'high-resolution' spectra from solid and semi-solid samples, such as lignocellulose, benefit from the use of signal enhancement via cross polarization (CP) and line narrowing techniques such as magic-angle spinning (MAS), and high power proton decoupling.[55-62] The physical sources of line broadening in NMR and line narrowing techniques necessary to gain useful chemical insight will be reviewed in this section.

1.3.1 The Dipolar Interaction

Nuclei with spin $\geq$ ½ produce local magnetic fields that slightly alter the magnetic fields experienced by other, nearby, nuclei. This effect is the *dipole-dipole interaction* and can result in line broadening of the magnetic resonance spectrum. The fast tumbling motion of molecules in the liquid phase averages the dipolar interaction to zero, which is at least partly responsible for the much narrower lines for liquid samples than those typically observed in solid samples.

The ^{1}H–^{13}C heteronuclear dipolar interaction, being common due to the abundance and proximity of ^{1}H in organic solids, adds a source of line broadening in the

^{13}C NMR spectra of organic solids that is not normally observed in solution state ^{13}C NMR spectra (because of rapid molecular tumbling). Often one makes use of high power proton decoupling during the data acquisition phase of the experiment to suppress heteronuclear $^{1}H - ^{13}C$ dipolar interactions during signal acquisition. This is achieved by irradiating the sample at the proton Larmor frequency, ν_H, and thus causing rapid transitions between ^{1}H spin states. The effect of such rapid transitions between ^{1}H spin states is that the ^{13}C nuclei experience an average of zero for the dipolar fields produced by the two ^{1}H spin states and a narrowing of the peaks in the ^{13}C NMR spectra is observed. The heteronuclear dipolar interaction that exists between ^{1}H and ^{13}C nuclei in most organic compounds that make possible certain useful techniques, including *cross polarization* (*vida infra*).

1.3.2 Cross Polarization

A substantial hurdle in the solid state ^{13}C NMR experiment is the low sensitivity of the ^{13}C nuclide, due to both a low natural abundance (1.1 %) and a low gyromagnetic ratio (γ). The low sensitivity can be overcome to some degree by signal averaging. By repeating the experiment and adding the results together, the signal-to-noise ratio is increased by $N^{1/2}$, where N is the number of signal acquisitions to be averaged. Another hurdle in ^{13}C NMR is the, typically, long times one must wait for magnetization recovery between signal acquisitions, due to long spin lattice relaxation times for ^{13}C as compared to ^{1}H spin lattice relaxation times.

In order to circumvent the long times necessary for ^{13}C T_1 recovery and increase the available signal, a now common method employed to analyze solid or semi-solid

samples is the cross-polarization (CP) technique.[55-60] In this technique, nuclear spin polarization is transferred from a more abundant, higher-γ nucleus, such as ^{1}H, to a lesser abundant, lower-γ nucleus, such as ^{13}C. Since the spins experience the ^{1}H-^{13}C dipolar interaction, spin polarization can be transferred from the ^{1}H spin system to the ^{13}C spin system if the two spin systems can be brought into thermal contact. Thermal contact is made between the ^{1}H and ^{13}C spin systems when one uses long radio frequency (RF) pulses at both the ^{1}H and ^{13}C Larmor frequencies (ν_H and ν_C) with amplitudes (B_{1H} and B_{1C}) set to satisfy the Hartmann-Hahn match[63] condition:

$$\gamma_H B_{1\,H} = \gamma_C B_{1\,C} \qquad (1.8)$$

When the above relationship is satisfied, the Zeeman energies of both ^{1}H and ^{13}C spin systems have been shown to be equal in a doubly rotating frame; and mutual ^{1}H–^{13}C spin 'flip-flops' become a very efficient method for spin polarization transfer[63]. During cross polarization, the ^{13}C nuclei experience a change in polarization that may increase by a factor determined by the ratio of the γ values, γ_H/γ_C, which, in this case, is nearly a factor of four. The polarization enhancement experienced by the ^{13}C nuclei depends on the duration of the match condition and details of the kinetics of the relevant spin states.

In addition to the signal enhancement brought by CP, the CP technique benefits from the fact that the generation of ^{13}C magnetization is dependent upon the state of the ^{1}H spins before Hartmann-Hahn contact is established. A consequence of this is that one need wait only for ^{1}H spin lattice relaxation before one repeats data acquisition, which tends to be much faster than ^{13}C spin-lattice relaxation. Hence, the CP technique avoids

the ^{13}C T_1 'bottleneck' by generating the ^{13}C magnetization from the ^{1}H magnetization present in the wood sample.

1.3.3 Chemical Shift Anisotropy

In addition to the dipolar interaction, a second contribution to line broadening in solid state NMR spectra is the chemical shift anisotropy. The chemical shift arises from the circulation of electrons, induced by the strong, static magnetic field, $\mathbf{B_o}$, around nuclei. This circulation in turn creates magnetic fields, opposing $\mathbf{B_o}$, that ultimately act to alter the local magnetic field, $\mathbf{B_{loc}}$, at the nucleus. Nuclei in different chemical and electronic environments will experience different $\mathbf{B_{loc}}$ fields, and will therefore resonate at slightly differing frequencies. Information about the chemical structure of a molecule can be obtained in the NMR experiment because nuclei in different chemical and electronic environments have different resonance frequencies or *chemical shifts*. This forms a major basis by which chemical structures can be identified using NMR spectroscopy.

In general, chemical shielding is sensitive to both the local chemical environment and the orientation of the molecule with respect to $\mathbf{B_o}$. For most solid samples, where relatively little molecular motion exists, the orientation of the molecule must be considered. For a powder of randomly oriented crystallites or a corresponding amorphous material, a distribution of chemical shift values is expected for each functional group, reflecting both the chemical shift tensor and the statistical probability of each orientation of the molecule.[55-60] It is expected that for sp or sp^2 carbon atoms the CSA is typically spread over 100 – 200 ppm, while for sp^3 carbon atoms the CSA typically spreads over only 50 ppm. The resulting 'powder pattern' would be spread over

a wide frequency range and is a manifestation of the geometrical dependence of the shielding parameter; this is referred to as the chemical shift anisotropy, CSA.

1.3.4 Magic Angle Spinning

It would be very difficult to relate chemical structure to individual peaks or peak areas in the ^{13}C NMR spectra of complex organic solids without a method to reduce the CSA powder pattern to a sharp peak that corresponds to its isotropic average. If a solid sample is rotated about an axis that forms an angle, β, with respect to $\mathbf{B_o}$, one finds an average of the energy of interaction.[60] It has been shown[60] that if β is set to β_m 54.74°, the 'magic angle', then $(3\cos^2\beta - 1 = 0)$ and one acquires the time averaged, isotropic value of the chemical shift. This procedure is called magic angle spinning (MAS).

MAS is used extensively in solid state NMR to improve spectral resolution by collapsing the CSA powder pattern to the average, isotropic, value of the chemical shift[60]. In order to achieve the greatest benefit from MAS, the sample spinning speed needs to be on the same order of magnitude or greater than the interaction energy one wishes to collapse. Using spinning speeds smaller than the CSA, results in the observation of spinning side bands (SSB), due to an additional modulation of the local magnetic fields, observable at interval values of the spinning speed. A MAS speed of 6 kHz is required to reduce the SSB to very small amplitudes at the field strength employed in this work.

The ^{13}C–^{13}C scalar interaction is of little concern for naturally occurring wood samples, as the natural abundance of ^{13}C nuclei is small enough, 1.1 %, to make the occurrence of adjacent ^{13}C–^{13}C spin pairs rare. The ^{13}C enriched wood studied in this thesis project is different, because of the occurrence of numerous ^{13}C-^{13}C pairs in the

sample. Thus, one could have additional line broadening due to ^{13}C–^{13}C scalar interactions, which are not averaged at all by MAS.[60]

1.4 Spin Dynamics

Spin lattice relaxation characterizes the interaction between the nuclear spin states and all possible mechanisms by which energy dissipation may occur in order achieve the return of the perturbed nuclear spin system to thermal equilibrium.[55-60] The modulation of magnetic dipole-dipole interactions from the rotational, translational or vibrational degrees of freedom can provide efficient mechanisms for spin lattice relaxation.[55-60] In a solid or semi-solid sample, where motional degrees of freedom of are severely restricted, spin lattice relaxation occurs via rotational and vibrational oscillations of the local magnetic fields that surround the nucleus of interest. The oscillations that have the greatest effect on ^{1}H spin lattice relaxation, T_{1H}, occur at ν_H and at twice ν_H, while those with the greatest effect on ^{13}C spin lattice relaxation, T_{1C}, occur at ν_C and at the ^{1}H-^{13}C flip-flop frequency, $\nu_C \pm \nu_L$.

There are several possible interactions responsible for causing magnetic field fluctuations by which spin lattice relaxation may occur in a solid or semi-solid sample. Modulation of the dipolar interaction, arising from the random thermal motions of adjacent nuclei, is considered to be the dominant interaction in diamagnetic solid or semi-solid samples. Measurement of spin lattice relaxation can be made by monitoring the return of the z-component of the magnetization of the sample back to thermal equilibrium after a perturbation.

The relevant CP kinetics involve two parameters, T_{CH} and $T_{1\rho H}$. The time constant T_{CH}^{-1} determines the time it takes for the generation of magnetization during cross polarization and is dependent upon the static contribution of the heteronuclear ^{1}H-^{13}C dipolar interaction to provide an efficient mechanism for polarization transfer.[59] Hence T_{CH}^{-1} is expected to be shorter for rigid structural components and will increase as the mobility of a structural component increases.

$T_{1\rho H}$ is the time constant for the decay of ^{1}H magnetization that is spin-locked in the frame of reference rotating about the $\mathbf{B_{1H}}$ field that is used to satisfy the Hartmann-Hahn match condition (eq. 1.8), and is therefore sensitive to oscillations that occur at or near the $\mathbf{B_{1H}}$ field strength, B_{1H}. In addition, $T_{1\rho H}$ is effected by magnetic field oscillations occurring at ν_H and at $2\ \nu_H$.[59] The measurement of T_{CH} and $T_{1\rho H}$ is performed by systematically varying the amount of time during which the ^{1}H and ^{13}C spins satisfy the Hartmann-Hahn match condition.[48-50]

The interpretation of $T_{1\rho H}$ values is made difficult by the existence of several potentially important mechanisms, even for much simpler chemical systems than wood.[64-65] However, one can often usefully make relatively straightforward qualitative interpretations of T_{CH} data in terms of atomic-level mobilities. As the temperature of a system increases, the thermal energy and therefore the motion of the system will increase; this should manifest itself as an increased value for T_{CH}.

By performing a systematic study of the above mentioned relaxation time constants, one should be able to estimate the extent that the components of lignocellulose have been mobilized by the 0.5 M H_2SO_4 pretreatment.

CHAPTER 2 — EXPERIMENTAL

Several technical challenges were overcome in order to carry out the work outlined in this thesis. First is the ^{13}C enrichment of *populus angustifolia*, necessary to conclude signal averaging over time periods prior to completion of pretreatment. Second is the design of a sample cell. Third is the modification and calibration of a variable temperature MAS apparatus capable of reaching 150 ^{o}C. The remainder of this section is devoted to the experimental NMR procedures.

2.1 Photosynthetic ^{13}C Enrichment of *Populus Angustifolia*

Since wood is the result of cell division that uses the products of photosynthesis, sufficient ^{13}C enrichment of wood has been obtained by growing trees in a $^{13}CO_2$ atmosphere.[66] To this end, a glove box was outfitted to be a growth chamber for poplar trees, specifically narrowleaf cottonwood (*populus angustifolia).* Three clippings were 'rooted' and provided by S. Skogerboe of the Fort Collins Nursery. The clippings were removed of natural abundance growth prior to placement in the enrichment chamber. The light cycle was set to be 18:6 hour light:dark cycle for the 6 month growth period. After a total of 50 liters of $^{13}CO_2$ was consumed (99 atom % ^{13}C: 10 liters Icon lot#CM326-09-10544; 10 liters Icon, lot#CM326-09-10699; 10 liters Isotec, lot#TP1846; 20 liters Cambridge Isotopes Laboratory, lot#91A0219/|1-11490). Only one of the three original clippings survived the enrichment process. This remaining tree was removed from the growth chamber and separated according to morphology into fractions of old stem, new stem, debarked stem, bark, leaf and root. The biomass fractions were then

dried at 105 ^{o}C for 24 hours, then stored in 2 dram vials in a descicator. A portion of the debarked stem was ground to pass through 40 mesh for the NMR analysis.

2.2 Ampoule Design

There are three considerations that must be met in the design of a suitable sample cell. The cell must be i) chemically inert, ii) NMR inactive under the relevant conditions, and iii) able to withstand an internal pressure of up to 20 atm. Boro-silicate glass meets all these criteria and an ampoule fashioned from this material is the sample cell used in the work described in this thesis. Sealing glass ampoules is, in general, a simple task, but sealing ampoules with the symmetry necessary to be used under MAS conditions is difficult. In order to achieve a 3.5 kHz spinning speed, the sample and rotor demand a tolerance of ±0.0002 inches about the center of symmetry. It was therefore necessary to design and build a mechanical system for performing this task with better reliability than one could achieve by hand. The design details are located in Appendix A.

2.3 Chemical Treatments

A solution of 0.5 M H_2SO_4 (98 % EMD lot# 48109) was prepared. Then a 10 % slurry of wood in water or sulfuric acid was prepared with 20 mg of ^{13}C-enriched biomass in a 7 mm (O.D.) glass ampoule. The sample was immediately frozen in liquid nitrogen to prevent chemical reaction, and the ampoule flame sealed. The ampoule was inserted into a 9.5 mm zirconia rotor sleeve and loaded into the corresponding 9.5 mm CP-MAS NMR probe. After acquisition of room temperature spectra, the variable temperature stack was then set to 150 ^{o}C sample temperature and the reaction monitored by ^{13}C CP-MAS and DP-MAS NMR, in situ.

2.4 The NMR experiments

A Chemagnetics CMX II type spectrometer with a 4.7 T magnetic field was used to perform the NMR experiments described in this thesis. All NMR experiments were carried out at 50.2 MHz for ^{13}C and 199.7 MHz for ^{1}H. The probe used in these experiments was a modified 9.5 mm Chemagnetics CP-MAS probe, tuned to ^{13}C and ^{1}H. The B_1 field strengths employed were each about 50 kHz. The sealed ampoule was loaded into a 9.5 mm zirconia sleeve, braced by a thin kel-F sleeve and enclosed with a triple o-ring drive tip and cap. One-minute CP acquisitions were acquired using 60 acquisitions and 1 s pulse delay. Nine-minute DP acquisitions were acquired using 120 acquisitions and a 4.5 s pulse delay. Spectral data sets for relaxation measurements were acquired using 300 acquisitions and a 1 s delay between reinitiation of the timing diagram. Relaxation measurements carried out at 150 ^{o}C were performed after the sample had been through one heating and cooling cycle.

2.4.1 DP-MAS

The simplest ^{13}C NMR technique performed in this project was the direct polarization (DP) or Bloch decay technique. In this mode, the net magnetization of the sample is tilted from the z-axis into the transverse plane by a strong, short $\pi/2$ radio frequency (RF) pulse. After the $\pi/2$ pulse, the macroscopic magnetization is digitally sampled and stored as a free induction decay (FID). The FID signal then undergoes Fourier transformation to reveal the frequency components present in the signal, resulting in the NMR spectrum. The timing diagram is shown in Figure 5. For ^{13}C detection, high power ^{1}H decoupling is used during the sampling of the ^{13}C magnetization.

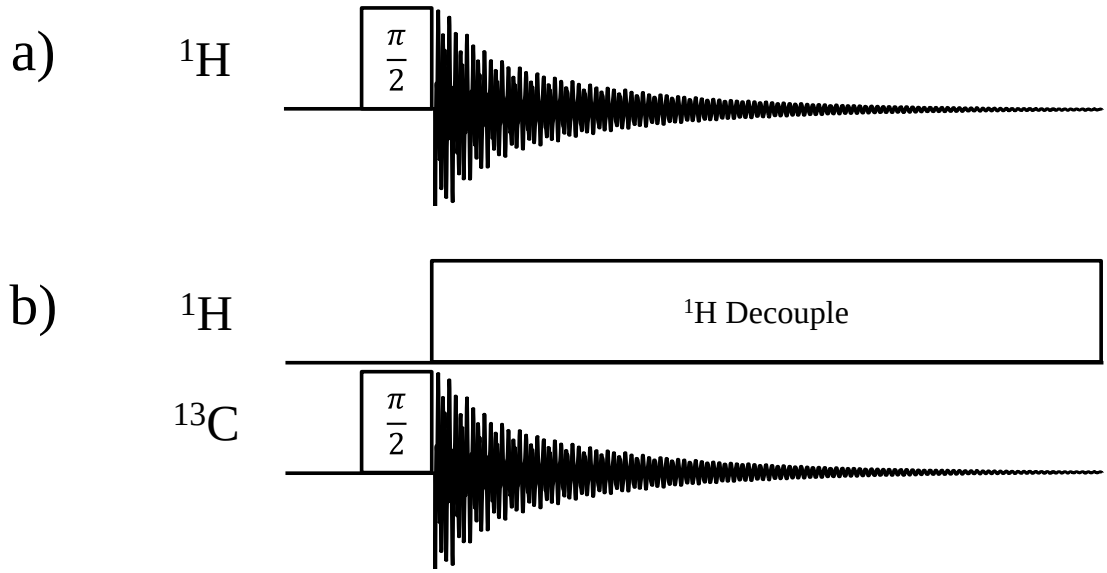

Figure 5. a) direct polarization for acquisition of ^{1}H NMR signal. b) direct polarization for acquisition of ^{13}C NMR signal.

2.4.2 CP-MAS

The timing diagram for the CP pulse sequence is shown in Figure 6. The initial $\pi/2$ ^{1}H RF pulse (a-b) brings the ^{1}H magnetization into the transverse plane. The following, long, RF pulse (mix) is phase shifted by 90^o with respect to the initial $\pi/2$ RF pulse, resulting in spin locking of the ^{1}H magnetization during simultaneous

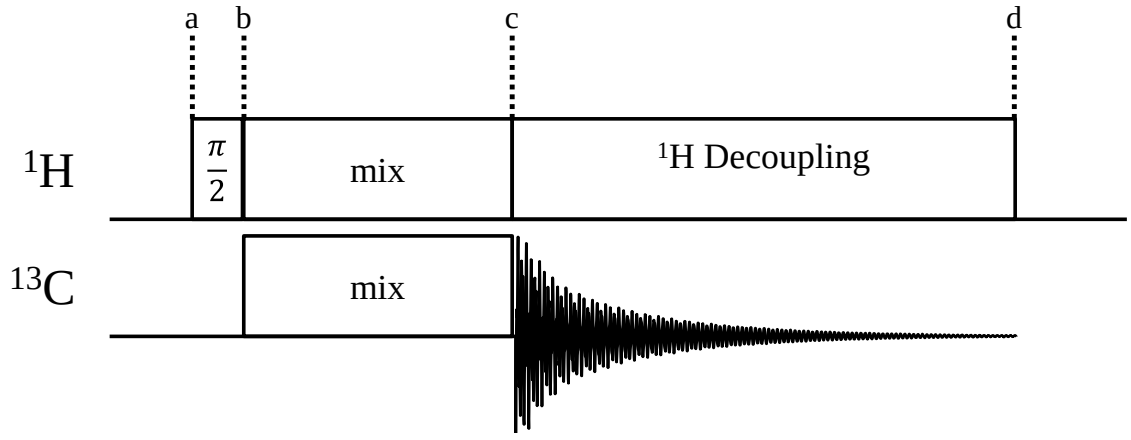

Figure 6. Timing Diagram for acquisition of ^{13}C signal via ^{1}H-^{13}C cross polarization.

application of ^{13}C radiation to satisfy the Hartmann-Hahn match condition (b-c). During the mix period (b-c) the ^{13}C magnetization grows via the CP process at a rate determined by the constant, T_{CH}^{-1}, and the ^{13}C magnetization decays according to $T_{1\rho H}$ processes. High power ^{1}H decoupling (c-d) is necessary to eliminate the effects of the heteronuclear dipolar interaction during detection.

There are several useful variants of this basic CP pulse sequence used in the project described in this thesis. One useful variant of this technique is to insert a delay, typically 40 μs, between the end of mixing and the beginning of detection, point (c) in Figure 6. The delay allows for dephasing of ^{13}C magnetization via the ^{1}H-^{13}C dipole-dipole interaction, resulting in attenuation of the signals from ^{13}C nuclei with directly bound ^{1}H nuclei. The resulting spectrum contains signals mainly from carbon atoms with no directly attached hydrogen atoms, substituted aromatic carbon atoms of lignin, and moieties with a very high degree of mobility, i.e., methyl groups, and liquid like components. This technique is commonly refered to as the *interrupted decoupling* or *dipolar dephasing* technique[48-52].

A second variant of the CP technique used in this thesis project is the measurement of cross polarization kinetics by variable contact time measurements. In this technique, the mix time (b-c) is varied and, following digital storage and Fourier transformation, the resulting peak areas were integrated and then were then fit according to the bi-exponential expression

$$M(\tau) = M_{\infty}\left(\frac{T_{1\rho H}}{T_{1\rho H} - T_{CH}}\right)\left(e^{-\tau/T_{1\rho H}} - e^{-\tau/T_{CH}}\right) \qquad (2.1)$$

where M_∞ is the magnetization acquired in the limit of infinitely fast cross polarization ($T_{CH} \rightarrow 0$) and infinitely slow rotating frame relaxation ($T_{1\rho H} \rightarrow \infty$). The variable contact-time spectral data sets acquired, as well as the mathematical fitting that generated T_{CH} and $T_{1\rho H}$ values are shown in Appendix C.

A third variant of the CP technique used in this thesis project is the measurement of T_{1H} by saturation recovery of ^1H, as detected (via CP) by ^{13}C, the timing diagram for this technique is shown in Figure 7. In this technique, there is a 'saturation comb' of $\pi/2$ degree pulses emitted on the ^1H channel. The effect of the saturation comb is to equalize the ^1H spin state populations, producing zero net proton magnetization.

The saturation comb is followed by a recovery period (t) during which the ^1H magnetization recovers according to ^1H spin lattice relaxation. The recovered magnetization is then cross polarized to ^{13}C for detection. Following digital storage and Fourier transformation, the resulting peak areas were integrated and then were then fit according to the expression

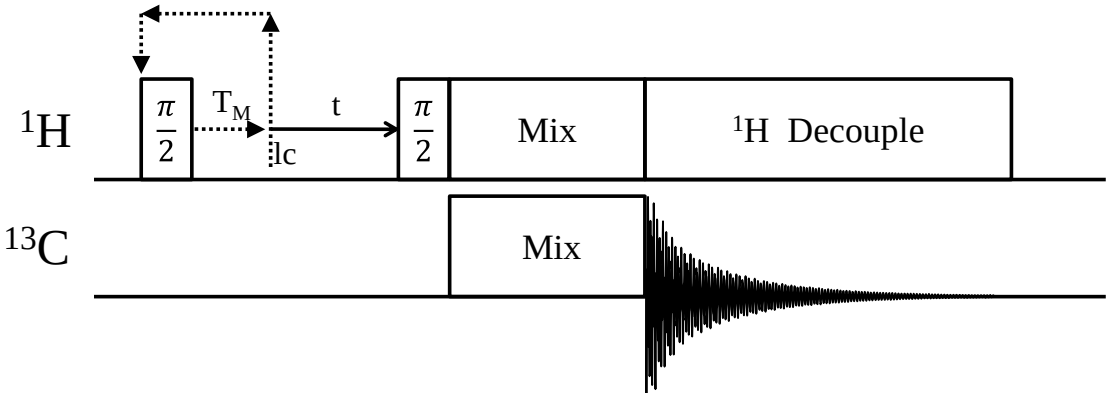

Figure 7. Timing diagram for saturation recovery pulse sequence. lc defines number of saturation pulses [100]. T_M defines delay between saturation pulses. t defines the saturation recovery time and is a varied parameter in this experiment.

$$M(t) = M\left(1 - e^{-t/T_{1H}}\right) \qquad (2.2)$$

where M is the thermal equilibrium value of the ^{1}H magnetization. The spectra acquired as well as the mathematical fitting that generated values of T_{1H} are shown in Appendix D.

The final CP-based technique performed in this thesis project is the measurement of T_{1C} by the method outlined by Torchia.[67] This is performed by inserting store and read pulses, separated by a recovery period (t) after the CP mix period. The store pulse brings the ^{13}C magnetization, generated from CP, back to the z-axis, where the ^{13}C magnetization will decay in the period t back toward its thermal equilibrium state via ^{13}C spin lattice relaxation.

After the recovery period, t, the resulting magnetization is detected after the read pulse. Figure 8 shows the timing diagram for the Torchia technique. Following digital storage and Fourier transformation, the resulting peak areas were integrated and then were then fit according to the expression

$$M(t) = M\left(e^{-t/T_{1C}}\right) \qquad (2.3)$$

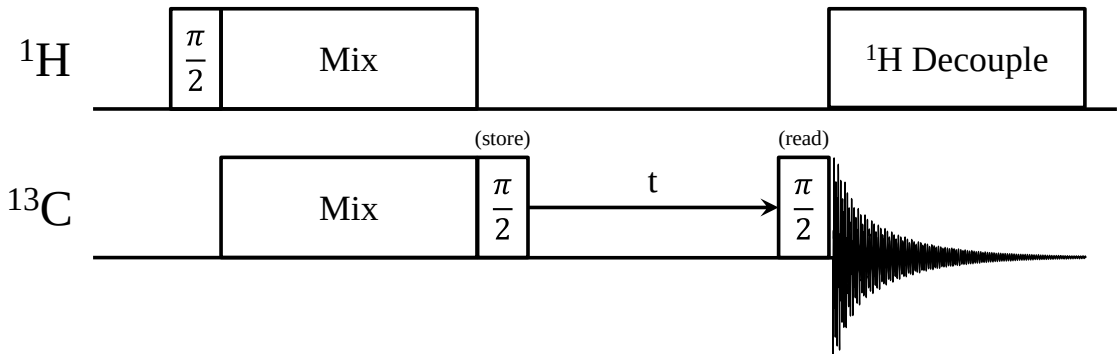

Figure 8. Timing diagram for measurement of T_{1C} by the method outlined by Torchia.[67]

where M is the value of the ^{13}C magnetization generated from CP. The spectra acquired and the mathematical fitting that generated the T_{1C} values are shown in Appendix E.

2.5 Variable Temperature NMR

A Chemagnetics variable-temperature stack (VTS) was modified and used for the NMR experiments that were not carried out at ambient temperature, 30 ^{o}C. The Chemagnetics VTS is designed to mate with the modified Chemagnetics NMR probe, deliver hot air to the spinning module, and serve as a vent for the hot air to leave the spinning module. The temperature controller used was a REX-F900 (RKC Instrument INC.), which was connected to a platinum resistance thermometer, located 10 cm above the sample. The REX-F900 read-out display was calibrated to the sample temperature using ^{1}H DP NMR to measure i) the frequency difference between the ^{1}H signals of ethylene glycol, a well-known NMR thermometer, and ii) the sharpening of spectral features due to the s $\rightarrow$ l phase transition of pure organic compounds.[68-71]

2.5.1 Calibration of Variable Temperature Stack via NMR Thermometry.

Ethylene glycol has seen much use as a standard for calibrating the sample temperature of an NMR probe.[68-71] The ^{1}H NMR spectrum of ethylene glycol shows two signals, one from ^{1}H on aliphatic carbon atoms and the other from the hydroxyl ^{1}H. As the temperature of the system is increased, the frequency difference between these two peaks decreases. Furthermore, the decrease is cited as being linear up to 400 K.[68] In this work, the linearity of the frequency difference as a function of applied temperature is shown to be valid up to 430 K. There is, however, caution placed on using ethylene glycol at such high temperatures, due to an increase of the ^{1}H T_1 (from 700 ms at 30 ^{o}C to

3s at 150 ^{o}C). ^{1}H T_1 effects were overcome by using a 10 s pulse delay at elevated temperatures.

The sample temperature was calculated measuring the proton chemical shift difference and comparing it to a calibration curve generated from previously published calibration curves. The standard deviation about the mean temperature calculated in this fashion was 2 ^{o}C. Correlating the sample temperature, as measured by ^{1}H frequency difference, to the setting temperature of the REX-F900 allows one to predict the REX-F900 setting that one needs to achieve a specific sample temperature.

2.5.2 Calibration of Variable Temperature Stack via Melting Point.

The ^{1}H NMR spectrum of an organic solid is typically very broad, without some type of line-narrowing technique applied. As the temperature is increased and the sample begins to undergo the melting phase transition, the atomic level mobility of the sample increases. When the melting point is reached, the NMR signal due to the molecules now in the liquid phase begins to grow, and levels off to a constant intensity when the entire sample has melted. The melting point of an organic compound provides an alternative method for temperature calibration.

To calibrate the VTS via melting points, tetramethylbenzene (mp = 79 – 80 ^{o}C) and trans-cinnamic acid (mp = 132 - 133 ^{o}C) were chosen as melting point standards, based on having sharp melting points that would confirm or refute the validity of the ethylene glycol temperature calibration. After measuring the selected compound's melting point in a Thomas Hoover Capillary Melting Point Apparatus, the sample was loaded into an ampoule, sealed, and inserted into a 9.5 mm zirconia MAS rotor and spun

at 3.5 kHz MAS. The spinning is necessary to simulate air flow conditions that are similar to what is present during the *in-situ* ^{13}C MAS experiments, not for the reduction of line width necessary in a typical ^{1}H MAS experiment (typically requiring a much higher MAS speed). At each temperature, the system was given ten minutes to reach a thermal steady state, at which point a ^{1}H DP spectrum was acquired. This process was performed first in ten degree steps, to qualitate the melting point, and again in one degree steps to quantitate the melting point. The spectra used for temperature calibration, and resultant calibration plots are found in Appendix B.

CHAPTER 3 — RESULTS.

3.1 Deconvolution

The combination of cross polarization, magic angle spinning and high power proton decoupling yields the narrowest possible peaks in the ^{13}C CP-MAS NMR analysis of solid and semi-solid samples.[58] However, the linewidths observed in a CP-MAS spectrum are typically greater than those observed in a liquids NMR spectrum and complex materials, such as wood, have many overlapping peaks. In order to gain chemically useful information, it is often necessary to deconvolve the NMR spectrum into a series of curves with Lorentzian distributions. Figure 9a shows the CP-MAS spectrum of 50 mg ^{13}C enriched wood acquired with high-powered ^{1}H decoupling at a MAS rate of 7kHz, sufficiently fast to complete averaging of line broadening effects at this field, 4.7 T. Figure 9b shows the deconvolved spectrum determined by fitting figure 9a to a series of twelve lorentzian distributions, shown in Figure 9c. It has been shown that there are more than twelve contributions to the chemical shift spectrum of wood.[48-50] The signal-to-noise ratio in these experiments does not allow for fitting of small contributions (i.e., side chain groups of lignin) in the baseline.

The deconvolution procedure allows one to determine the center frequency, maximum intensity, and width of each deconvolved chemical shift signal in a highly over-lapped spectrum. The center frequency and peak widths from the deconvolution are shown in Table 1 with the chemical shift assignments for each peak.

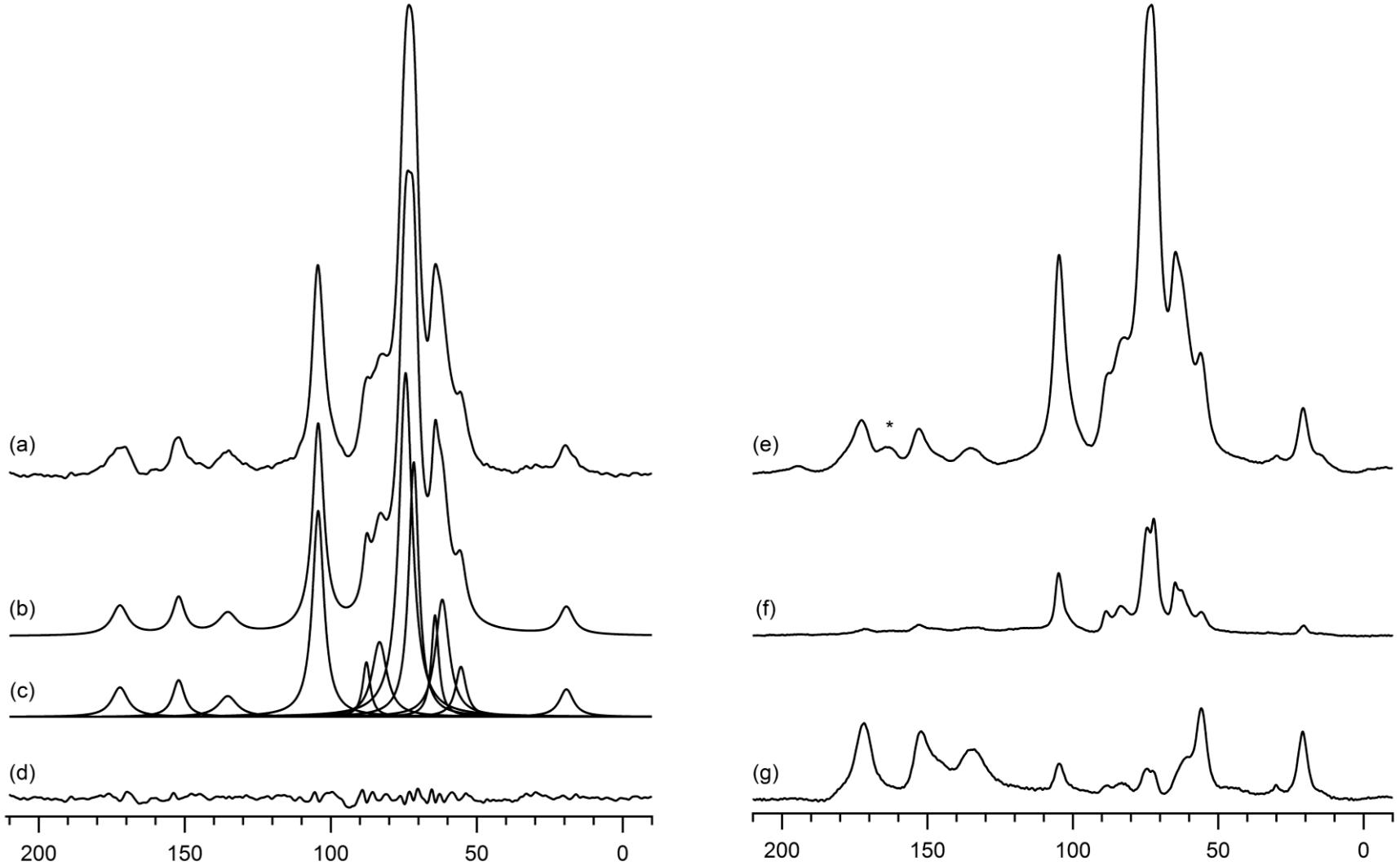

Figure 9. ^{13}C CP-MAS spectra of (a) 20 mg ^{13}C enriched wood, 7 kHz MAS, (b) Deconvolution of (a). (c) individual peaks whose sum is (b). (d) residual found from subtraction of (b) from (a). (e) 50 mg ^{13}C enriched wood, 3.5 kHz MAS. (f) 500 mg natural-abundance wood, 3.5 kHz MAS. (g) 40 μs dipolar dephasing result on ^{13}C enriched wood from (e). Number of acquisitions = 1800, Contact time = 1 ms, pulse delay = 1 s. * denotes spinning side band

The center frequency and peak widths found in this manner were used as initial criteria in measuring integrated areas for the relaxation measurements.

3.2 Determination of ^{13}C enrichment via ^{13}C NMR.

A total of ten ^{13}C CP-MAS spectra were acquired for ^{13}C enriched poplar with an amount of 50 mg and ten ^{13}C CP-MAS spectra were acquired for natural abundance poplar with a 500 mg amount. Figure 9e shows the average of ten ^{13}C CP-MAS NMR spectra of 50 mg of ^{13}C enriched poplar wood and Figure 9f shows the average of ten ^{13}C CP-MAS NMR spectra of 500 mg of natural-abundance poplar wood. Since the intensity of the NMR signal is proportional to the number of ^{13}C spins in the sample, the following relation was used to determine the level of ^{13}C enrichment:

$$x\,\%\,{}^{13}C = \frac{I_E m_N (1.1\,\%{}^{13}C)}{I_N m_E} \qquad (3.1)$$

where I_E is the total integrated intensity of a ^{13}C enriched lignocellulose sample, m_N is the mass of natural abundance lignocellulose, I_N is the total integrated intensity from integration of a natural abundance lignocellulose, and m_E is the mass of ^{13}C enriched material. Using (eq. 3.1), one obtains 70 ± 6 % ^{13}C for the sample studied.

3.3 Peak Assignments.

Table 1 summarizes the ^{13}C chemical shift assignments that are most relevant to this study. These assignments were taken as 'rough consensus' values from the rather extensive literature on ^{13}C NMR of wood or wood-related samples.[41-54] The numbers given in the table should be considered to have uncertainties of roughly ±2 ppm, because of a number of factors, including i) variations in non-nearest-neighbor structures (e.g.,

Table 1. Selected[a] ^{13}C Chemical Shift Assignments[b].

Peak[a] (ppm)	Width (Hz)	Assignment
22	292	acetate methyls in hemicellulose
56	219	methoxyl groups of lignin
62	283	C6 of amorphous cellulose and hemicellulose
66	153	C6 of crystalline cellulose and hemicellulose
73	206	C2, C3 and C5 of crystalline cellulose and hemicellulose
75	271	C2, C3 and C5 of amorphous cellulose and hemicellulose
84	309	C4 of amorphous cellulose and hemicellulose
89	157	C4 of crystalline cellulose and hemicellulose
105	237	C1 of cellulose and hemicellulose
135	390	C1 of lignin
153	245	C3 and C5 of lignin
173	334	Carbonyl of lignin, carboxyl group of hemicelluloses

[a] The most relevant and reliable assignments relevant, especially for intense peaks, for the issues addressed in this particular study.
[b] Numbers taken as a 'consensus' from references 41 - 54. Values relative to TMS.

alkyl substitution on aromatic rings of lignin), ii) bulk magnetic susceptibility effects and iii) varying chemical shift referencing methods among different laboratories.

One can see that the natural-abundance spectrum is slightly sharper than that based on the ^{13}C-enriched sample; this difference is presumably the manifestation of unresolved J_{CC} couplings in the enriched sample, which are not averaged by MAS, and ^{13}C-^{13}C dipolar couplings that are not completely averaged by 3.5 kHz MAS.

The weak peak at about 174 ppm represents carbonyls of lignin and of the acetate and other carboxyl groups of hemicellulose. The broad peaks at 153 and 135 ppm are due to the aromatic signals of lignin. The peak at 105 ppm corresponds to C1 of cellulose, with superimposed signal from C1 of hemicellulose. The peaks at 89 and 84 ppm are C4 signals from polysaccharides. The peak at about 89 ppm comes from highly ordered polysaccharides, e.g., cellulose, and the 84 ppm peak from polysaccharides that are

amorphous, e.g., hemicellulose and cellulose surface fibers; the same type of crystalline-vs-amorphous interpretation holds for the polysaccharide C6 peaks at 66 and 63 ppm as well as the C2, C3, and C5 peaks at about 73 and 75 ppm. The sharp peak at 56 ppm arises from methoxyl groups of lignin and possibly of hemicellulose. The weak peak at 22 ppm corresponds to acetate methyl groups in hemicellulose.

Figure 9g shows the dipolar-dephasing ^{13}C CP-MAS spectrum of the ^{13}C enriched sample of Figure 9e. In comparing Figures 9e and 9g, one sees that the intensities of the carbohydrate C-H peaks in Figure 9g have been reduced by 90 % relative to those in 9e. The lignin, carbonyl and methyl peaks show a 10 - 20 % loss of intensity due at least in part to the disappearance of i) spinning side bands resultant from the carbohydrate chemical shift anisotropy or ii) reduced overlap with carbohydrate peaks. The spectra in both Figure 9e and Figure 9g show a small peak at 30 ppm, presumably due to aliphatic methylene side chain carbons of lignin; this peak is not seen in Figure 9f due to the low signal-to-noise in the spectra of natural-abundance wood samples.

3.4 Effects of Pretreatment Treatment on ^{13}C NMR Spectrum.

Since cross polarization relies upon the static component of ^{1}H-^{13}C dipolar interaction, the 'mobilization' of any portion or segment of biomass due to a treatment will reduce the observed ^{13}C CP-MAS intensity of that portion of the biomass. Hence, an observed reduction of ^{13}C CP-MAS intensity resulting from a treatment can be due to some combination of i) conversion of the observed structure into other structure(s) and ii) the mobilization of certain structural component(s).

3.4.1 Pretreatment Transformations.

^{13}C MAS spectra were obtained in both the CP (cross polarization) and DP (direct polarization) modes as a function of heating time on samples of ^{13}C-enriched poplar wood that were in a 10 % slurry with i) pure water and heated at 150 ^{o}C (Figure 10), and ii) 0.5 M H_2SO_4 at 150 ^{o}C (Figure 11). Both CP and DP modes were employed because these two modes respond very differently to atomic-level mobility. The CP mode depends upon a static component of ^{1}H-^{13}C dipolar interactions, while the DP mode relies entirely on ^{13}C spin-lattice relaxation, hence ^{13}C-spin interactions that have time-dependences with components in the Larmor ($10^7 – 10^8$ Hz) frequency range. Therefore, highly rigid wood components will yield intensities preferentially in the CP mode, while highly mobile (liquid-like) components yield intensities only in the DP mode. Components in the intermediate mobility range may generate ^{13}C intensity to some degree in both modes.

The experiments leading to Figures 10 and 11 were carried out by using CP-MAS and DP-MAS techniques applied in alternating measurements of 1 min CP, 9 min DP, 1 min CP, 9 min DP, etc. Each of the two series of experiments employed one sample over a total of 500 min (including 10 min at 30 ^{o}C for each sample before and after heating and 10 min of cool-down at the end of heating) and generated 51 separate spectra in each mode. When each sample had reached the elevated temperature (typically after about 3 minutes), the spectrometer probe was electronically retuned, so that any observed reduction in ^{13}C NMR intensity is not largely due to probe tuning.

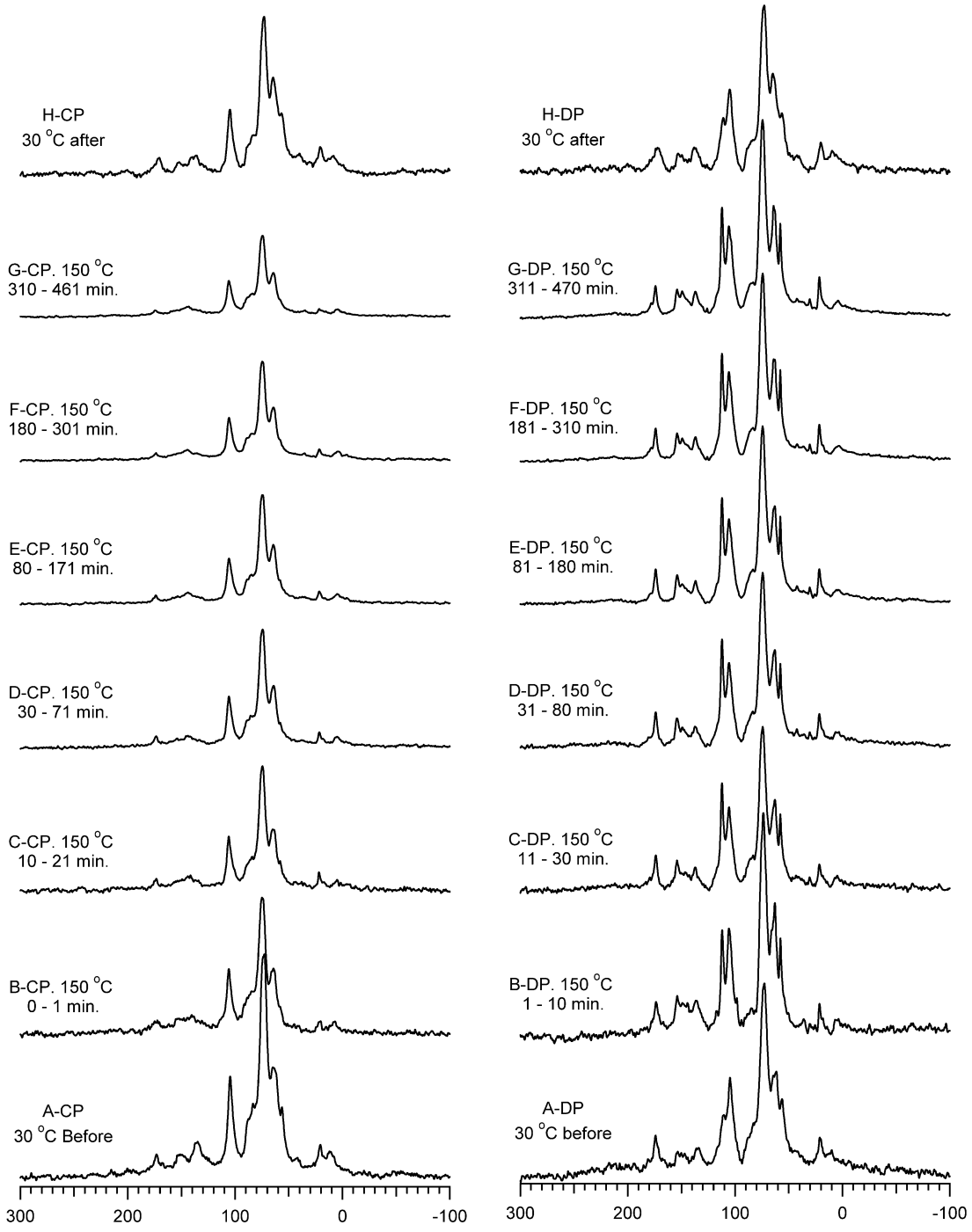

Figure 10. Left: ^{13}C CP-MAS results on 20 mg wood, 10 % in H_2O, time span of one min., separated by nine min. DP segments. Right: ^{13}C DP-MAS results on 20 mg wood, 10 % in H_2O, time span of nine min., separated by one min. CP segments.

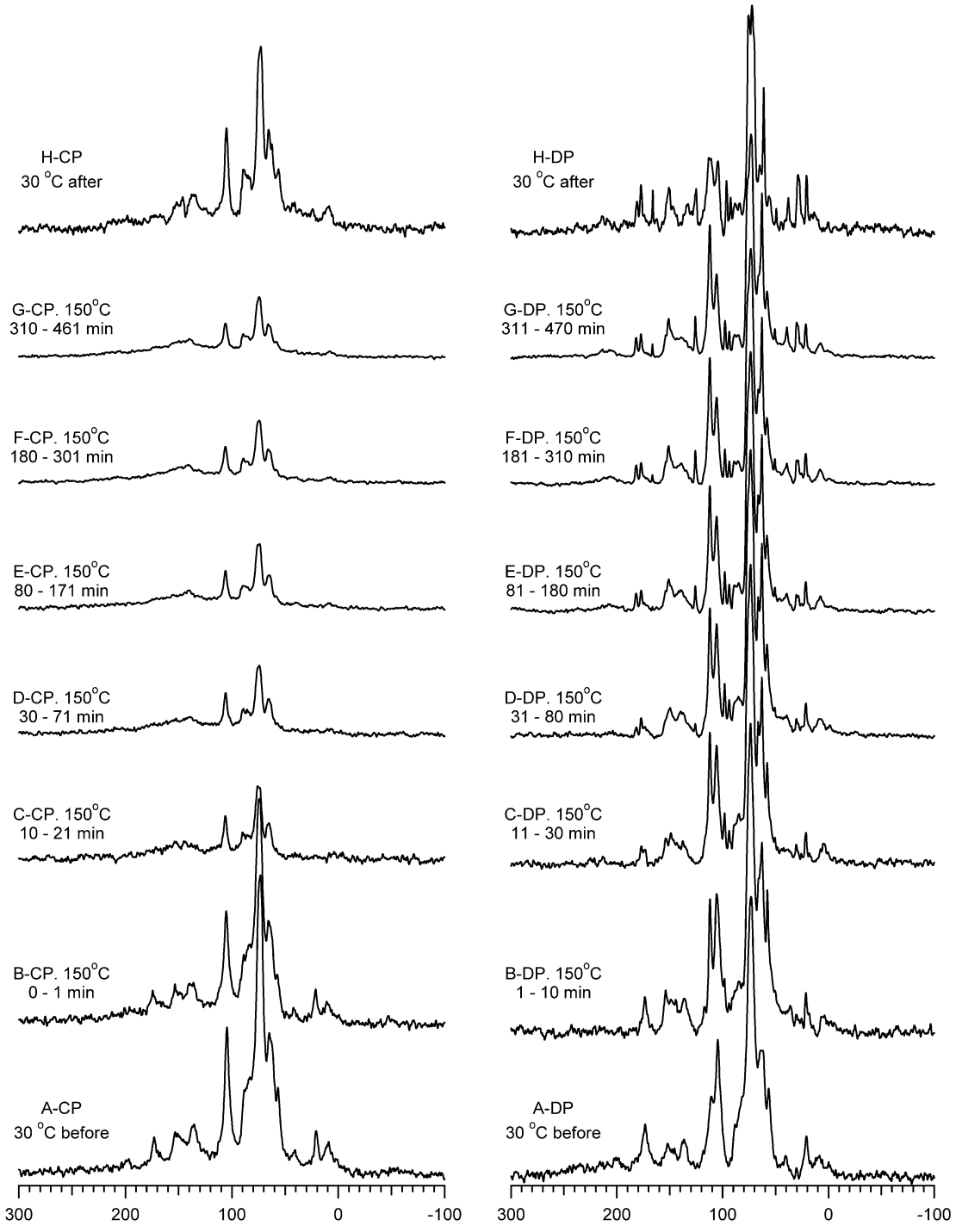

Figure 11. Left: ^{13}C CP-MAS results on 20 mg enriched wood, 10 % in 0.5 M H_2SO_4, time span of one min., separated by nine min. DP segments. Right: ^{13}C DP-MAS results on 20 mg wood, 10 % in 0.5 M H_2SO_4, time span of nine min., separated by one min. CP segments.

Not all the spectra are shown in Figures 10 and 11; instead several instances of signal-averaging of the stored data were employed over time spans during which substantial variations are not seen among the several individual spectra. Appendices F and G contain all spectra that went into the signal averaging of Figures 10 and 11, respectively.

The series of measurements made on a water-saturated poplar sample at 150 ^{o}C (Fig. 10) were carried out as a type of 'control' experiment, to examine what, if any changes in the sample/spectra occur in the absence of added acid. The spectra of Figure 10 show some interesting features. First, while the main features of the CP-MAS and DP-MAS spectra of the initial, unheated sample (Fig. 10A) are very similar, there are some substantial differences, as one might expect from the reasons stated above regarding the relationships between intensity and mobility. As the heating begins, these CP-vs-DP differences increase; most notably the intensities in the CP-MAS spectra decrease with time and new, more highly resolved DP-MAS peaks appear and increase in intensity with time. These changes are apparent even in the spectra obtained after one minute at elevated temperature. Changes in the CP-MAS spectra over the period from 10 min to 301 min are gradual; most of the overall changes in CP-MAS spectra have occurred within ten minutes. By the time 5.0 – 5.5 hours of heating at 150 ^{o}C has occurred, more than 60 % of the CP-MAS intensity has been lost (Fig. 10G-CP) and only about half of the 'lost' intensity returns when the sample is returned to 30 ^{o}C (Fig. 10H–CP). In the corresponding DP-MAS spectra, there is no substantial loss of overall spectral intensity with time; in fact there is an apparent increase in the intensity of the 5.0 – 5.5 hr spectrum (Fig. 10G-DP), some of which is lost, along with intensity of the sharpest peaks, when

the sample is cooled back down to 30 ^{o}C (Fig. 10H–DP). The overall sharpness of the DP-MAS spectrum at 150 ^{o}C is decreased when the sample is cooled back to 30 ^{o}C, reflecting an overall loss of liquid-like character in the sample at the lower temperature. There is no large overall loss in DP-MAS intensity from the pre-heating 30 ^{o}C spectrum (Fig. 10A–DP) to the post-heating 30 ^{o}C spectrum (Fig. 10H–DP).

Only about 30 % of NMR intensity would be lost in the 30 ^{o}C to 150 ^{o}C change because of the Boltzmann factor and all of that loss should be recovered in the return to 30 ^{o}C. Thus, the loss of CP-MAS intensity during heating is due to a combination of the conversion of immobile structural components into a) more mobile forms of the same components and/or b) other, more mobile structural components. Some of that enhanced mobility (resulting reduced CP-MAS intensity) is reversed when the sample is cooled back to room temperature.

Detailed examination of Figure 10 (and its 102–spectra version, Appendix F) reveals that, in the CP spectra, there is an intensity decrease to about 36 % of the initial CP intensity with heating and a return to about 60 % of the initial CP signal intensity when the sample is returned to 30 ^{o}C. The lignin-aromatic-carbon intensity between about 110 and 150 ppm is only marginally detected in the CP spectra of samples heated at 150 ^{o}C, but at least partially recovers when the sample is cooled back to 30 ^{o}C (Fig. 10H–CP). Essentially the same kind of behavior is seen for the carbonyl/carboxyl peak at about 173 ppm and for the aliphatic carbon peaks in the 10 – 20 ppm range. In the DP spectra, there is an additional peak at about 111 ppm that becomes very intense at 150 ^{o}C and returns to its initial intensity upon return to 30 ^{o}C.

As expected, 150 ^{o}C heating of the 0.5 M H_2SO_4-treated sample yields much more dramatic changes in the ^{13}C MAS spectra (Fig. 11). The most drastic changes in both the CP-MAS and the DP-MAS spectra occur within about 10 minutes after the sample reaches 150 ^{o}C (Fig. 11C). The loss of CP-MAS intensity is much more dramatic, about 75 % of the initial CP intensity, after about 10 minutes and remains essentially constant throughout roughly 8 hours of heating (Fig. 11C–CP to Fig. 11G–CP). Again, some of the lost CP-MAS intensity (about half of the initial value) is restored upon cooling to 30 ^{o}C (Fig. 11H-CP). As the 150 ^{o}C/0.5 M H_2SO_4 pretreatment progresses, the DP-MAS spectra display even more sharp peaks throughout the spectrum, indicating liquid-like behavior, than in the corresponding 150 ^{o}C treatment with pure water. And, unlike the 150 ^{o}C/water case, with 0.5 M H_2SO_4 treatment at 150 ^{o}C, the sharp features of the DP-MAS spectra obtained at 150 ^{o}C between about 10 and 470 min (Fig. 11C–DP to Fig. 11G–DP) are retained, even enhanced, when the sample is cooled back to 30 ^{o}C (Fig. 11H–DP).

In the CP spectra, the peaks at 22 and 173 ppm (due to acetoxy groups of hemicellulose) disappear after 20 minutes, and do not reappear when the sample is returned to 30 ^{o}C; this indicates that the acetate moieties in hemicellulose have been hydrolyzed irreversibly. However, the same spectral regions in the DP spectra do not disappear, but show a decrease in line width, and the carbonyl/carboxyl peak at 173 ppm seems to split into two peaks at 178 and 181 ppm. In addition, several sharp peaks are formed at 167, 125, 97, 93, 50, and 29 ppm.

3.4.2 Interpretation of Alternating CP-MAS and DP-MAS Spectra.

In the 150 ^{o}C H_2O treatment (Fig. 10), all the peaks in the CP spectra decrease in intensity, but roughly half of this intensity returns when the sample is cooled back to 30 ^{o}C after heating. This intensity decrease is due to a combination of a general loosening of the wood structure (yielding a smaller fraction of the wood structure that is sufficiently immobile to support $^{1}H \rightarrow {}^{13}C$ cross polarization) without major changes in *local* 'monomer-level' (molecular building block) structure of the wood. In the DP spectra, the peaks at 22 ppm (acetate methyls), 56 ppm (methoxy groups), 112 ppm (uncertain assignment, *vide infra*) and 173 ppm (acetate carbonyl carbons) become narrow at 150 ^{o}C and broaden upon return to 30 ^{o}C; these results suggest that there is no hydrolysis of wood components due to H_2O treatment to an extent that is detected by ^{13}C MAS NMR.

The above-mentioned narrowing effects are probably also due to the general loosening of the wood structure invoked above for rationalizing the CP-MAS results; this loosening provides some averaging (line-narrowing of broadening due to chemical shift dispersion). The broad lines seen in Figure 10-H-DP probably indicate that the level of mobility retained when the sample is brought back to 30 ^{o}C is sufficient to partially interfere with the CP process, but not sufficient to retain the averaging/narrowing effect seen in DP-MAS spectra at 150 ^{o}C.

In the 150 ^{o}C H_2SO_4 treatment (Fig. 11), the CP-MAS peaks at 22 and 173 ppm (due to acetate esters) are not present after 20 minutes of treatment and are not present in the CP-MAS spectra after cooling back to 30 ^{o}C. All other peaks decrease in intensity, about half of which returns after cooling to 30 ^{o}C. This intensity decrease is in part due to the general 'loosening' effect invoked above for the 150 ^{o}C H_2O treatment, but can

also be identified with a heating-produced decrease in the amount of carbon that has sufficiently low atomic-level mobility to support $^{1}H \rightarrow ^{13}C$ CP; this can be seen by comparing the M^*_{∞} values listed for the carbohydrate region in Tables 2 and 4 (*vide infra*) for the 30 ^{o}C samples before and after the 150 ^{o}C treatment, respectively.

In the DP spectra of Figure 10, the peak at 22 ppm (methyl of acetate) becomes narrow at 150 ^{o}C and remains narrow on return to 30 ^{o}C, suggesting hydrolysis of hemicellulose acetate groups to acetic acid. The peak at 30 ppm is due to aliphatic carbons of lignin. After 10 minutes of heating this peak begins to increase in intensity, all of which is retained after treatment. Since the side-chain content of lignin is very unlikely to be increased by the 150 ^{o}C/H_2SO_4 treatment, this increased intensity is most likely due to some other kind of chemical transformation, e.g., the formation of levulinic acid (a well-known degradation/dehydration product of simple sugars;[2] ***(4)*** of Figure 12), whose sp^3 carbons may also contribute to the intensity of this peak. Figure 12 shows the structure and chemical shift assignments of the degradation products resultant from the 0.5 M H_2SO_4/150 ^{o}C treatment.

The sharp DP peak in Figure 11 at 39 ppm appears after 60 min of heating and also increases in intensity during heating, most of this intensity increase remaining after treatment. This peak is most likely due to the aliphatic carbon atoms in levulinic acid (***4***) [3]. The DP peak at 50 ppm in Figure 11 appears after 60 minutes and is most likely methanol, a result of methoxy ether hydrolysis. The methoxy (ether) peak at 56 ppm becomes very narrow at the beginning of heating and gradually decreases in intensity as treatment progresses, supporting the idea of hydrolysis of methoxy carbons from hemicellulose and lignin. The peak at 62 ppm (C6 of hexose and C5 of pentose units) in

Figure 11 becomes narrow and increases in intensity at 150 ^{o}C and remains narrow after cooling back to 30 ^{o}C. This sharp peak is most likely the C5 carbon of hydrolyzed pentose units and C6 carbon of hydrolyzed hexose units from hemicellulose.

The DP peak at 66 ppm (C6 of cellulose) in Figure 11 appears to decrease as heating progresses and does not recover intensity upon the return to 30 ^{o}C, suggesting a possible decrease in the crystalinity of cellulose. The DP peaks at 73 and 75 in Figure 11 do not show major changes, but these peaks are difficult to interpret in detail because they are most likely the result of overlapping peaks from the C2, C3 and C5 carbons of

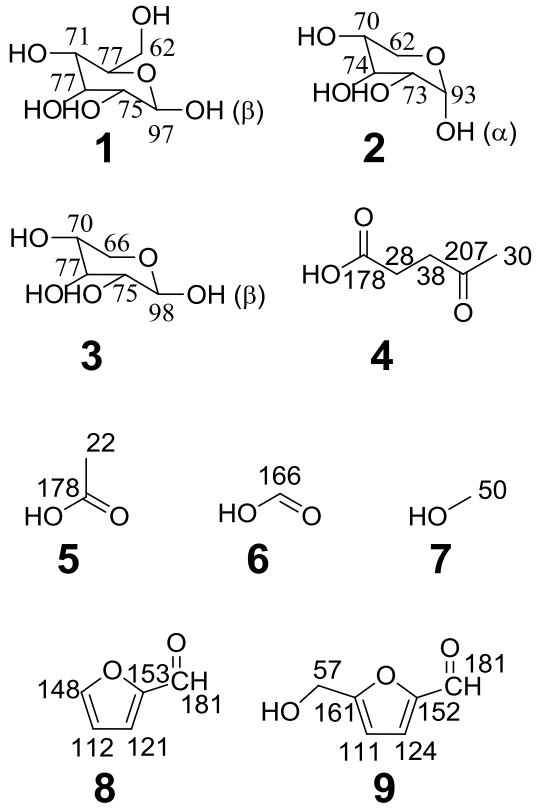

Figure 12. Structures of presumed products of hemicellulose hydrolysis during dilute sulfuric acid pretreatment. **1**. β-D-Glucopyranose. **2**. α-D-Xylopyranose. **3**. β-D-Xylopyranose. **4**. Levulinic acid. **5**. Acetic acid. **6**. Formic acid. **7**. Methanol. **8**. Furfural. **9**. Hydroxymethyl-furfural.

cellulose, hemicellulose, and from the C2, C3 and C4 carbons of monosaccharides in the hydrolyzate. The DP peaks at 84 and 89 ppm (due to C4 carbons of cellulose and hemicellulose) in Figure 11 decrease in intensity as treatment progresses, also indicating transformations within the holocellulose fraction.

There are two new DP peaks formed at 93 and 97 ppm (Figure 11), most likely due to C1 in the α and β orientations, respectively, of hydrolyzed sugars. The DP peak at 97 ppm in Figure 10 has greater intensity than the peak at 93 ppm, consistent with the expectation that the β orientation will be more prevalent than the α orientation in a saccharidic solution.[3] The DP-MAS peak at 105 ppm (C1 of cellulose and hemicellulose) in Figure 11 decreases in the H_2SO_4/150 ^oC treatment due to hydrolysis of polysaccharide linkages; this 'lost' intensity may be at least partially responsible for increased intensities in the peaks at 93 and 97 ppm.

The DP-MAS peak at 112 ppm in Figure 11 becomes very narrow in the H_2SO_4/150 ^oC treatment and broadens on return to 30 ^oC; this peak is likely due to sp^2 carbons of furfural (***8***), an intermediate in the formation of levulinic acid (***4***).[2] The DP-MAS peak at 125 ppm appears after 60 minutes of heating and increases in intensity during treatment; all of the intensity is recovered on return to 30 ^oC. This 125 ppm peak is most likely due to sp^2 carbons of furfural (***8***). The DP-MAS intensity of the peaks at 135 ppm (aromatic C1 carbon of some lignin structures) and 153 ppm (aromatic C3 and C5 of lignin) appear to show slight intensity changes, but mainly linewidth changes in the H_2SO_4/150 ^oC treatment. The DP-MAS peak at 167 ppm appears after 200 minutes of H_2SO_4/150 ^oC treatment and is most likely a result of the formation of formic acid, a

degradation product formed in the transformation of 5-hydroxymethyl furfural (***9***) to levulinic acid (***4***).[2]

The DP-MAS peak at 173 ppm (carboxyl carbon region), which is rather broad before heating, is apparently transformed into one or more sharp peaks in the 150 ^{o}C heated and post-heating 30 ^{o}C samples. This implies a substantial mobilization and chemical transformation, e.g., hydrolysis, of all detectable carboxy moieties. The DP-MAS peak at 178 ppm begins to form after 20 minutes of treatment and remains after treatment. This peak is due to carbonyl groups, including those of carboxylic acid moieties, e.g., levulinic acid (***4***), acetic acid (***5***) and possibly of hydrolyzed uronic acids of hemicellulose. The DP-MAS peak at 181 ppm appears after 60 minutes of heating and remains upon return to 30 ^{o}C; this is suggestive of carbonyl carbons (*vide supra*), possibly the aldehyde carbon of furfural (***8***).[3]

3.5 Variable Contact Time Studies

Variable-contact-time (VCT) experiments were carried out on four samples: a sample of dry poplar wood at 30 ^{o}C (Table 2), a sample of poplar in 0.5 M H_2SO_4 at 30 ^{o}C *before* treatment at 150 ^{o}C (Table 3), a sample of poplar in 0.5 M H_2SO_4 *during* treatment at *150 ^{o}C* (Table 4) and a sample of poplar in 0.5 M H_2SO_4 at 30 ^{o}C *after* treatment at 150 ^{o}C (Table 5). Analysis of the VCT results by fitting the data to the accepted equation[36,41] yields values of the parameters, T_{CH}, $T_{1\rho H}$ and M_{∞} , which are summarized in Tables 2-5. See Appendix E for spectra and mathematical fitting procedures.

In Tables 2-5 M_∞ is the value that the CP-generated magnetization would have if the polarization-transfer process were infinitely fast and if rotating-frame proton spin-lattice relaxation were infinitely slow. This number, when corrected by a well-established factor due to incomplete ^1H spin-lattice relaxation, $\{1 - \exp(-t/T_{1H})\}^{-1}$, yields a number M^*_∞ that should faithfully represent the population of ^{13}C sites that were available for cross polarization; these parameters are collected in Tables 2 – 5.

In comparing the T_{CH} results reported in Tables 2 and 3 for dry wood and wood treated with 0.5 M H_2SO_4, both at 30 ^oC, one sees that the addition of 0.5 M H_2SO_4 to poplar wood at 30 ^oC causes almost no changes that are detectable via T_{CH} values, with the exception of the low-shielding peaks at 153 ppm and 173 ppm. These same peaks are dramatically reduced in intensity in the CP-MAS spectrum in the early stages of heating and are only marginally recovered when the sample is cooled back down to 30 ^oC. This behavior probably reflects hydrolysis of acetate esters and phenolic ethers or esters of lignin, so that the final sample contains a much smaller quantity of unhydrolysed entities as part of the solid-like (CP-detectable) material. And, the unhydrolyzed acetate and phenoxy moieties that remain after 0.5 M H_2SO_4 addition at 30 ^oC are apparently more rigid (smaller T_{CH} values) than their pre-hydrolysis ancestors.

Table 2. Variable contact time results on dry poplar at 30 °C.

Peak[a]		M_∞[b]	M^*_∞[c]	$T_{1\rho H}$ (ms)	T_{CH} (μs)
	22	2.1 ± 0.1	2.4 ± 0.1	10 ± 1	66 ± 5
L	56	5.0 ± 0.1	5.8 ± 0.1	11 ± 1	52 ± 5
	62	8.2 ± 0.2	9.7 ± 0.2	10 ± 1	32 ± 3
C	66	8.1 ± 0.2	9.7 ± 0.2	11 ± 2	31 ± 3
C	73	17.8 ± 0.6	21.3 ± 0.6	10 ± 1	36 ± 5
	75	17.5 ± 0.6	20.9 ± 0.6	10 ± 1	36 ± 5
	84	10.6 ± 0.4	12.6 ± 0.4	10 ± 1	36 ± 5
C	89	2.5 ± 0.6	3.0 ± 0.6	11 ± 1	36 ± 4
C	105	7.5 ± 0.2	9.0 ± 0.2	11 ± 1	41 ± 5
L	135	4.5 ± 0.2	5.2 ± 0.2	13 ± 2	80 ± 10
L	153	2.7 ± 0.1	3.2 ± 0.1	14 ± 2	150 ± 20
	173	2.6 ± 0.1	3.0 ± 0.1	12 ± 1	200 ± 30

[a] Peak positions in ppm. L signifies a lignin peak, C signifies a cellulose peak and others are from hemicellulose and minor contributions from amorphous cellulose.

[b] M_∞ represents the transverse ^{13}C magnetization that would have been generated if the CP transfer had been infinitely fast and if rotating-frame ^1H spin-lattice relaxation had been infinitely slow.

[c] M^*_∞ is the corresponding M_∞ value that has been corrected by the factor, $\{1 - \exp(-t/T_{1H})\}^{-1}$, for incomplete ^1H spin-lattice relaxation between CP scans.

Table 3. Variable contact time results on 10 % poplar in 0.5 M H_2SO_4 at 30 ^oC *before* pretreatment at 150 ^oC.

Peak[a]		M_∞[b]	M^*_∞[c]	$T_{1\rho H}$ (ms)	T_{CH} (μs)
	22	0.8 ± 0.1	0.9 ± 0.1	10 ± 1	66 ± 9
L	56	2.2 ± 0.1	2.5 ± 0.1	7 ± 1	53 ± 6
	62	4.2 ± 0.2	5.2 ± 0.2	6 ± 1	33 ± 5
C	66	3.9 ± 0.2	4.8 ± 0.2	8 ± 1	30 ± 5
C	73	8.5 ± 0.5	10.7 ± 0.5	7 ± 1	34 ± 7
	75	7.7 ± 0.5	9.6 ± 0.5	7 ± 1	33 ± 8
	84	4.5 ± 0.3	5.5 ± 0.3	9 ± 1	32 ± 8
C	89	1.2 ± 0.1	1.5 ± 0.1	10 ± 2	34 ± 8
C	105	3.7 ± 0.3	4.7 ± 0.3	8 ± 1	36 ± 9
L	135	1.6 ± 0.1	1.9 ± 0.1	18 ± 1	93 ± 6
L	153	0.8 ± 0.1	0.9 ± 0.1	24 ± 4	90 ± 10
	173	0.6 ± 0.1	0.7 ± 0.1	27 ± 4	110 ± 10

[a] Peak positions in ppm. L signifies a lignin peak, C signifies a cellulose peak and others are from hemicellulose and minor contributions from amorphous cellulose.

[b] M_∞ represents the transverse ^{13}C magnetization that would have been generated if the CP transfer had been infinitely fast and if rotating-frame ^1H spin-lattice relaxation had been infinitely slow.

[c] M^*_∞ is the corresponding M_∞ value that has been corrected by the factor, $\{1 - \exp(-t/T_{1H})\}^{-1}$, for incomplete ^1H spin-lattice relaxation between CP scans.

Table 4. Variable contact time results on 10 % poplar in 0.5 M H_2SO_4 *during* pretreatment at 150 ^{o}C.

Peak[a]		M_∞[b]	M^*_∞[c]	$T_{1\rho H}$ (ms)	T_{CH} (μs)
	22				
L	56	1.0 ± 0.1	1.5 ± 0.1	24 ± 1	36 ± 5
	62	1.8 ± 0.1	2.7 ± 0.1	24 ± 2	37 ± 4
C	66	1.9 ± 0.1	2.8 ± 0.1	24 ± 2	34 ± 3
C	73	3.9 ± 0.1	5.8 ± 0.1	26 ± 3	39 ± 4
	75	3.6 ± 0.1	5.3 ± 0.1	25 ± 3	38 ± 4
	84	2.4 ± 0.1	3.5 ± 0.1	22 ± 3	44 ± 5
C	89	0.6 ± 0.1	0.9 ± 0.1	21 ± 3	46 ± 6
C	105	1.7 ± 0.1	2.5 ± 0.1	24 ± 2	46 ± 4
L	135	1.3 ± 0.1	1.8 ± 0.1	24 ± 5	130 ± 30
L	153	0.6 ± 0.1	0.8 ± 0.1	20 ± 3	160 ± 30
	173				

[a] Peak positions in ppm. L signifies a lignin peak, C signifies a cellulose peak and others are from hemicellulose and minor contributions from amorphous cellulose.

[b] M_∞ represents the transverse ^{13}C magnetization that would have been generated if the CP transfer had been infinitely fast and if rotating-frame ^{1}H spin-lattice relaxation had been infinitely slow.

[c] M^*_∞ is the corresponding M_∞ value that has been corrected by the factor, $\{1 - \exp(-t/T_{1H})\}^{-1}$, for incomplete ^{1}H spin-lattice relaxation between CP scans.

No signal is observed at 22 or 173 ppm due to hydrolysis of acetate ester moeities

Table 5. Variable contact time results on 10 % poplar in 0.5 M H_2SO_4 at 30 ^oC *after* pretreatment at 150 ^oC.

Peak[a]		M_∞[b]	M^*_∞[c]	$T_{1\rho H}$ (ms)	T_{CH} (μs)
	22				
L	56	1.4 ± 0.1	1.7 ± 0.1	24 ± 3	53 ± 3
	62	2.2 ± 0.1	2.8 ± 0.1	21 ± 2	33 ± 3
C	66	2.5 ± 0.1	3.2 ± 0.1	23 ± 2	30 ± 3
C	73	5.2 ± 0.2	6.7 ± 0.2	23 ± 3	36 ± 5
	75	4.6 ± 0.1	5.9 ± 0.1	22 ± 3	35 ± 4
	84	3.3 ± 0.1	4.1 ± 0.1	21 ± 3	37 ± 5
C	89	1.0 ± 0.1	1.3 ± 0.1	21 ± 3	39 ± 5
C	105	2.3 ± 0.1	3.0 ± 0.1	23 ± 3	40 ± 5
L	135	2.2 ± 0.1	2.6 ± 0.1	30 ± 6	120 ± 20
L	153	1.0 ± 0.1	1.2 ± 0.1	28 ± 8	150 ± 40
	173				

[a] Peak positions in ppm. L signifies a lignin peak, C signifies a cellulose peak and others are from hemicellulose and minor contributions from amorphous cellulose.

[b] M_∞ represents the transverse ^{13}C magnetization that would have been generated if the CP transfer had been infinitely fast and if rotating-frame ^1H spin-lattice relaxation had been infinitely slow.

[c] M^*_∞ is the corresponding M_∞ value that has been corrected by the factor, $\{1 - \exp(-t/T_{1H})\}^{-1}$, for incomplete ^1H spin-lattice relaxation between CP scans.

No signal is observed at 22 or 173 ppm due to hydrolysis of acetate ester moeities

Comparison of the T_{CH} values for the poplar/0.5 M H_2SO_4 samples, summarized in Tables 2 – 5, reveal that the addition of sulfuric acid to the sample at 30 ^oC does not have a substantial effect on the mobility of carbon atoms with directly attached hydrogen atoms. However, the addition of sulfuric acid results in an apparent decrease of T_{CH} for oxygen bound sp^2 carbon atoms.

The T_{CH} values for corresponding chemical shifts appear to be larger (implying greater atomic-level mobility) when the sample is at 150 ^oC (Table 3), although the differences are at the edge of experimental uncertainties – with an exception for the methoxy peak (56 ppm), for which T_{CH} is clearly smaller at 150 ^oC than at 30 ^oC. This exception may reflect a decrease in methyl group mobility due to some unknown steric constraint during hydrolysis of methyl ethers. Upon return of the sample temperature back to 30 ^oC, the T_{CH} values show a return to a similar level of mobility present before pretreatment.

3.6 Spin Lattice Relaxation Results

Measurements of ^1H T_1 values were made, by a well-established ^{13}C-detection method,[72] on the same four systems represented in Tables 2 – 5. One sees from the results collected in Table 6 that, for any *one* of these four systems, the ^1H T_1 values are almost the same, within experimental error, for the entire ^{13}C chemical shift range sampled. This behavior is typical of solids, as efficient ^1H spin diffusion during a recovery period tends to yield an average ^1H T_1 value for all sites in a sample. Inspection of Table 5 also reveals that the 'spin-diffusion-averaged' ^1H T_1 values of this table differ *between* samples. Most noteworthy are the facts that a) the 'spin-diffusion-averaged' ^1H T_1 values of the two 30 ^oC samples in 0.5 M H_2SO_4, before and after heating at 150 ^oC, are nearly the same, and

Table 6. Summary of T_{1H} results on dry poplar at 30 ^{o}C, and on 10 % poplar in 0.5 M H_2SO_4 at 30 ^{o}C before and after treatment at 150 ^{o}C, and during treatment at 150 ^{o}C

Peak[a]	T_{1H}^{Dry} (s)	T_{1H}^{Before} (s)	T_{1H}^{During} (s)	T_{1H}^{After} (s)
22	1.0 ± 0.1	1.1 ± 0.1	[b]	[b]
56	1.0 ± 0.1	1.0 ± 0.1	1.8 ± 0.1	1.2 ± 0.1
62	1.1 ± 0.1	1.2 ± 0.1	1.8 ± 0.1	1.3 ± 0.1
66	1.1 ± 0.1	1.2 ± 0.1	1.8 ± 0.1	1.3 ± 0.1
73	1.1 ± 0.1	1.3 ± 0.1	1.8 ± 0.1	1.3 ± 0.1
75	1.1 ± 0.1	1.3 ± 0.1	1.7 ± 0.1	1.3 ± 0.1
84	1.1 ± 0.1	1.2 ± 0.1	1.7 ± 0.1	1.3 ± 0.1
89	1.1 ± 0.1	1.2 ± 0.1	1.7 ± 0.1	1.3 ± 0.1
105	1.1 ± 0.1	1.3 ± 0.1	1.8 ± 0.1	1.3 ± 0.1
135	1.0 ± 0.1	1.1 ± 0.1	1.5 ± 0.1	1.1 ± 0.1
153	1.1 ± 0.1	1.0 ± 0.1	1.6 ± 0.2	1.2 ± 0.1
173	1.0 ± 0.1	1.0 ± 0.1	[b]	[b]

[a] Peak positions in ppm.
[b] Not observed under these conditions.

b) the 'spin-diffusion-averaged' ^{1}H T_1 value(s) of the sample in 0.5 M H_2SO_4 measured *during* heating at 150 ^{o}C are roughly 50 % larger at 150 ^{o}C than those measured at 30 ^{o}C before and after heating.

^{13}C T_1 measurements were made by the Torchia method[67] on the same four systems represented in Tables 2 – 6. The results are summarized in Table 7. Unlike what is typically encountered with ^{13}C in natural abundance, where ^{13}C T_1 values can vary dramatically from one type of molecular site to another in a given sample, in this case of high ^{13}C enrichment, the variation among T_{1C} values for the various carbon sites are significant, but small, both within a sample and between samples. In addition, the values reported here for ^{13}C spin lattice relaxation are less than half those previously reported on wood samples[43]. These observations are likely the result of spin diffusion and spin lattice relaxation made efficient by the J_{CC} scalar interaction, hence ^{13}C-^{13}C spin flip-flops, as a result of ^{13}C enrichment.

Table 7. Summary of T_{1C} results on dry poplar at 30 ^{o}C, and on 10 % poplar in 0.5 M H_2SO_4 at 30 ^{o}C before and after treatment at 150 ^{o}C, and during treatment at 150 ^{o}C

Peak[a]	T_{1C}^{Dry} (s)	T_{1C}^{Before} (s)	T_{1C}^{During} (s)	T_{1C}^{After} (s)
22	3.9 ± 0.1	4.4 ± 0.3	[b]	[b]
56	3.8 ± 0.1	4.3 ± 0.2	5.9 ± 0.6	5.9 ± 0.4
62	3.9 ± 0.1	4.2 ± 0.1	3.9 ± 0.3	5.6 ± 0.3
66	4.2 ± 0.1	4.5 ± 0.1	3.7 ± 0.2	5.8 ± 0.2
73	4.3 ± 0.1	4.7 ± 0.1	4.1 ± 0.2	5.9 ± 0.1
75	4.2 ± 0.1	4.5 ± 0.1	4.1 ± 0.2	5.9 ± 0.2
84	4.1 ± 0.2	4.3 ± 0.2	4.3 ± 0.2	6.0 ± 0.4
89	4.4 ± 0.1	5.1 ± 0.3	4.4 ± 0.6	6.5 ± 0.5
105	4.4 ± 0.1	4.3 ± 0.2	4.1 ± 0.3	6.0 ± 0.3
135	4.2 ± 0.2	5.0 ± 0.4	4.7 ± 0.4	6.6 ± 0.5
153	4.6 ± 0.2	4.7 ± 0.4	4.1 ± 0.2	5.8 ± 0.4
173	4.5 ± 0.2	4.7 ± 0.6	[b]	[b]

[a] Peak positions in ppm.
[b] Not observed under these conditions.

SUMMARY AND CONCLUSIONS.

^{13}C NMR spectra, obtained by both DP-MAS and CP-MAS approaches, have allowed one to follow, via the populations of mobile and immobile structural segments, respectively, the progress of transformations that occur in ^{13}C-enriched poplar wood under 'pretreatment' with 0.5 M H_2SO_4 at 150 ^{o}C. While lignocellulose treated with just water does not undergo substantial changes, as would be represented by the presence of new, mobile species in the DP spectra, the sulfuric acid treatment shows the formation of both hydrolysis products, presumably from hemicellulose, and at longer times degradation products of the hydrolyzed sugars.

The time resolution available with the dramatically enhanced signal-to-noise characteristics that are achievable with ^{13}C-enriched samples demonstrates that the lignocellulose under pretreatment with 0.5 M H_2SO_4 at 150 ^{o}C reaches a maximum structural mobilization at about ten minutes pretreatment time. After this time, there is a substantial decrease in the rate of hemicellulose hydrolysis, suggesting that the major chemical changes to the structural mobility have already been completed. The relaxation results show that more information is desirable and necessary for a complete understanding of the dynamic processes that occur within lignocellulose during pretreatment. That there are relaxation results suggests that this frame work for studying in situ details of the BP chemistry has been successful and can allow for furthering scientific knowledge of the lignocellulose-to-fuel conversion scheme. Both in terms of

the changes in the chemical shift spectrum, acquired under CP and DP conditions, as well as in terms of molecular mobilities as measured by spin lattice relaxation and cross polarization dynamics.

There are a substantial number of experiments revealed to be possible (and necessary for a more complete understanding of the molecular mobility in this system) that one could perform on the ^{13}C enriched wood and similar, ^{13}C enriched lignocellulosic systems. Experiments necessary to obtain a more complete understanding of the in situ dynamics of the lignocellulose-to-fuel scheme include the execution of relaxation measurements at different field strengths, to elucidate the dependence of the correlation time on the Larmor frequency. Understanding of this correlation would allow one to quantitate the correlation time, hence molecular mobility of the ^{13}C enriched wood. Additionally, experiments performed at a variety of temperatures would be useful in determining the effect of temperature in the pretreatment process and in estimating activation parameters.

The time resolution available with the dramatically enhanced signal-to-noise characteristics that are achievable with ^{13}C-enriched samples should render detailed kinetic studies possible. The fundamental elucidation of the chemical kinetics of the pretreatment process would be very useful as empirical parameters for simulation studies and optimization of the industrial lignocellulose-to-fuel conversion scheme. The ^{13}C-enriched samples would also enable multi-dimensional NMR studies aimed at understanding the specific structural interactions that occur between lignin and holocellulose in whole wood.

In addition to the debarked stem wood examined in this study, several other morphological fractions of the poplar tree are available for study. Such studies would allow for a more complete understanding of the processing of whole trees to fuel. It is also possible to use the photosynthetic ^{13}C enrichment process used in the present study for analogous experiments of any plant species. Repeating these types of experiments on other biological substrates, e.g., algae, switch grass, sugar cane, etc… should provide the basis for an understanding of pretreatment as a general bioenergy processing technique.

REFERENCES

1) Cote, W. A.; Freudenberg, K.; Kisser, J.; Koch, P.; Kollmann, F. F. P.; Liese, W.; Marian, J. E.; Stamm, A. J.; Thunell, B.; Winkelmann, H. G.; Ylinen, A. *Wood Sci. Tech*, **1967**, *1*, 161-190

2) Sjöström, E., *Wood Chemistry Fundamentals and Applications*, 2nd Ed., Academic Press, New York, **1993**, Ch. 2.

3) Fengel, D., Wegener, G., *Wood Chemistry Ultrastructure Reactions*, Gruyter, New York, **1984**, Ch. 10

4) Cambel, N. A.; Reece, J.B. *Biology*, 7th ed.; Pearson: New York, **2004**

5) Browning, B. L. *The Chemistry of Wood*, Robert E. Krieger Publishing Company: New York, **1975**

6) Kintisch, E., *Science*, **2007**, *315*, 786.

7) McMillan, J. D. Pretreatment of Lignocellulosic Biomass in Enzymatic Conversion of Biomass for Fuels Production, American Chemical Society, Ch. 15 **1994**

8) McMillan, J. D. In *Biochemical Conversion of Cellulosic Feedstocks*, Conference on Biomass to Chemicals and Fuels: Science, Technology and Public Policy, Houston, TX, **2006**.

9) Sun, Y.; Cheng, J., *Biores. Technol*., **2002**, *83*, 1 – 11.

10) Sannigrahi, P.; Ragauskas, A. J., *Biofuels Bioprod. Bioref.*, **2010**, *4*, 209 – 226.

11) Kintisch, E., *Science*, **2007**, *315*, 786.

12) Tullo, A. H., *Chem. & Eng. News* **2007**, *85*, (48), 28-31.

13) Galbe, M.; Zacchi, G., *Appl. Microbiol. Biotechnol*., **2002**, *59*, 618-628.

14) Lynd, L. R.; Wyman, C. E.; Tillman, U. G., *Biotech. Prog*., **1999**, *15*, 777-793.

15) McMillan, J. D., in *Enzymatic Conversion of Biomass for Fuels Production*, Himmel, M. E.; Baker, J. O.; Overend, R. P., eds., *ACS Symp*. Ser., **1994**, *566*, 293 – 324.

16) McMillan, J. D., in *Enzymatic Conversion of Biomass for Fuels Production*, Himmel, M. E.; Baker, J. O.; Overend, R. P., eds., *ACS Symp*. Ser., **1994**, *566*, 293 – 324.

17) Taherzadeh, M. J.; Karimi, K., *Int. J. Mol. Sci*., **2008**, *9*, 1621 – 1651.

18) Mosier, N.; Wyman, C.; Dale, B.; Elander, R.; Lee, Y. Y.; Holtzapple, M.; Ladisch, M., *Bioresource Technol*., **2005**, *96*, 673 – 686.

19) Kumar, P.; Barrett, D. M.; Delwiche, M. J.; Stroeve, P., *Indust. Eng. Chem. Res*, **2009**, *48*, 3713-3729.

20) Taherzadeh, M. J.; Karimi, K., *Bioresources*, **2007**, *2*, 707 –738.

21) Taherzadeh, M. J.; Karimi, K., *Bioresources*, **2007**, *2*, 472 – 499.

22) Fan, L. T.; Lee, Y.-H.; Gharpuray, M. M., *Adv. Biochem. Eng*., **1982**, *23*, 157 – 187.

23) Millett, M. A.; Baker, A. J.; Satter, L. D., *Biotech. Bioeng. Symp*., **1976**, *6*, 125 – 153.

24) Cara, C.; Ruiz, E.; Oliva, J. M.; Saez, F.; Castro, E., *Bioresource Tech*., **2008**, *99*, 1869 – 1876.

25) Sun, Y.; Cheng, J. J., *Bioresource Tech*., **2005**, *96*, 1599 – 1606.

26) Yang, B.; Wyman, C. E., *Biotech. Bioeng*., **2004**, *86*, 88 – 95.

27) Schell, D. J.; Torget, R.; Power, A.; Walter, P. J.; Grohmann, K.; Hinman, N. D., *Appl. Biochem. Biotech.*, **1991**, *28/29*, 87 – 97.

28) Wyman, C. E., *Biomass Ann. Rev. Energy Envir*., **1999**, *24*, 189 – 226.

29) Torget, R.; Werdene, P.; Himmel, M.; Grohmann, K., *Appl. Biochem. Biotech*., **1990**, *24/25*, 115 – 126.

30) Allen, S. G.; Schulman, D.; Lichwa, J.; Antal, M. J., Jr.; Jennings, E.; Elander, R., *Ind. Eng. Chem. Res.*, **2001**, *40*, 2352 – 2361.

31) Nguyen, Q. A.; Tucker, M. P.; Keller, F. A.; Eddy, F. P., *Appl. Biochem. Biotech*., **2000**, 84-*86*, 561 – 576.

32) Lee, Y. Y.; Iyer, P.; Torget, R. W., *Adv. Biochem. Eng./Biotech*., **1999**, *65*, 93 – 115.

33) Saha, , B. C.; Bothast, R. J., *Appl. Biochem. Biotech*., **1999**, *76*, 65 – 77.

34) Nguyen, Q. A.; Tucker, M. P.; Boynton, B. L.; Keller, F. A.; Schell, D. J., *Appl. Biochem. Biotech.*, **1998**, *70-72*, 77 – 87.

35) Lee, K. C. P.; Bulls, M.; Holmes, J.; Barrier, J. W., *Appl. Bioch. Biotech*., **1997**, *66*, 1 – 23.

36) Torget, R.; Hsu, T., *Appl. Biochem. Biotech*., **1994**, *45/46*, 5 – 22.

37) Grethlein, H. E.; Allen, D. C.; Converse, A. O., *Biotech. Bioeng*., **1984**, *26*, 1498 – 1505.

38) Knappert, D.; Grethlein, H.; Converse, A., *Biotech. Bioeng*., **1980**, *22*, 1449 – 1463.

39) Knappert, D.; Grethlein, H.; Converse, A., *Biotech. Bioeng*., **1981**, *11*, 66 - 77.

40) Becker, E. D. *High Resolution NMR. Theory and Chemical Applications*, 3rd Ed., Academic Press, New York, 2000

41) Atalla, R. H.; Gast, J. C.; Sindorf, D. W.; Bartuska, V. J.; Maciel, G. E., *J. Am. Chem. Soc.*, **1980**, *102*, 3249 - 3251.

42) Pacchiano, R. A.; Sohn, W.; Chlanda, V. L.; Garbow, J. R.; Stark, R. E. *J. Agric. Food Chem*.,**1993**, *41*, 78 - 83.

43) Love, G. D.; Snape, C. E.; Jarvis, M. C., *Phytochem*., **1998**, *49*, 1191 - 1194.

44) Hatfield, G. R.; Maciel, G. E.; Erbatur, O.; Erbatur, G., *Anal. Chem*., **1987**, *59*, 172 - 179.

45) Earl, W. L.; VanderHart, D. H., *J. Am. Chem. Soc*., **1980**, *102*, 3251- 3152.

46) Earl, W. L.; VanderHart, D. H., *Macromol*., **1981**, *14*, 570 - 574.

47) Kolodziejski, W.; Frye, J. S.; Maciel, G. E., *Anal. Chem*., **1982**, *54*, 1419 –1424.

48) Davis, M. F.; Schroeder, H. R.; Maciel, G. E., *Holzforschung*, **1994**, *48*, 99 – 105.

49) Davis, M. F.; Schroeder, H. R.; Maciel, G. E., *Holzforschung*, **1994**, *48*, 186 – 192.

50) Davis, M. F.; Schroeder, H. R.; Maciel, G. E., *Holzforschung*, **1994**, *48*, 301 – 307.

51) Haw, J. F.: Maciel, G. E.; Schroeder, H. A., *Anal. Chem*., **1984**, *56*, 1323 – 1329.

52) Haw, J. F.; Maciel, G. E.; Biermann, C. J., *Holzforschung*, **1984**, *38*, 327 – 331.

53) Leary, G. J.; Morgan, K. R.; Newman, R. H.; Samuelsson, B.; Westermark, U., *Holzforschung*, **1986**, *40*, 221 – 224.

54) Freitas, J. C. C.; Bonagamba, T. J.; Emmerich, F. G., *Carbon* **2001**, *39*, 535-545.

55) Abraham, R. J.,: Fisher, J.; Loftus, P., *Introduction to NMR Spectroscopy*, John Wiley & Sons, New York, **1988**.

56) Fyfe, C. A., *Solid State NMR for Chemists*, C.F.C. Press, Guelph, Ontario, **1983**.

57) Duer, M. J., ed., *Solid-State NMR Spectroscopy – Principles and Applications*, Blackwell Science, Oxford, U.K., **2002**.

58) Maciel, G. E., Science,**1984**, *226*, 282-288.

59) Mehring, M., *Principles of High Resolution NMR in Solids*, 2nd ed., Springer-Verlag, New York, **1983**.

60) Stejskal, E. O.; Memory, J. D., *High Resolution NMR in the Solid State*, Oxford Univ. Press, Oxford, U.K., **1994**.

61) Farrar, T. C.; Becker, E. D., *Pulse and Fourier Transform NMR*, Academic Press, New York, **1971**, pp. 51 – 55.

62) Slichter, C. P., *Principles of Magnetic Resonance*, 2nd Ed., Springer-Verlag, pp. 164 – 167.

63) Hartmann, S.R.; Hahn, E.L., *Phys. Rev.* **1962**, *128*, 2042-2053

64) Garroway, A. N. *J. Magn. Reson.*, **1979**, *34*, 283- 293.

65) Schaefer, J.; Stejskal, E. O.; Buchdahl, R. *Macromol.*, **1975**, *8*, 291-296.

66) Lapierre, C.; Montis, B., Photosynthetically ^{13}C-Labelled Poplar Lignins: ^{13}C NMR Experiments. *Holzforschung* **1984**, *38*, 333-342

67) Torchia, D. A., *J. Magn. Reson.*, **1978**, *30*, 613-616.

68) Kaplan, M.L.; Bovey, F. A.; Cheng, H.N, *Anal. Chem* **1975**, 47, 1703-1705

69) Van Geet, A.L., *Anal Chem* **1968**, *40*, 2227

70) Varian Associates, Palo Alto, Calif. 94303, publication No. 87-202-006

71) Neuman, R.C.; Jonas, V., *J. Am. Chem. Soc.***1968**, *90*

72) Keeler, C.; Maciel, G. E., *Anal. Chem.*, **2003**, *75*, 2421-2432.

73) Kohn, B.; Maciel, G. E., *Energy Fuels*, **2011**, *25*, 2301-2313.

Appendix A

Ampoule Sealing

List of Figures

Making in situ measurements on a system under going biomass pretreatment via solid state NMR requires a non-standard sample container. Since the wood sample must be in H_2SO_4 or H_2O at 150 ^oC for times ranging from 30 minutes to 8 hours, the sample container must be resistant to corrosion, 15 atm pressure, and elevated temperatures up to 150 ^oC. Commercially available borosilicate glass tubing can satisfy these requirements. The glass tubing needs to be fashioned into a sample container, henceforth referred to as an ampoule, with dimensions similar to the solenoid coil of the NMR probe, and sealed. Figure A1 shows the unsealed empty ampoule and stem as received from the glass shop. The indentation near the bottom of the ampoule provides a target for the flame and reduces the time necessary to soften the glass for sealing.

Since the sealed ampoule will be spun at 3 kHz (180000 rpm), the symmetric

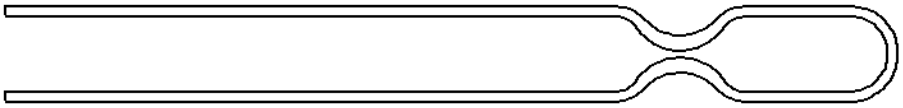

Figure A1. Unsealed empty glass ampoule.

uniformity and precision of the seal are demanding. Therefore an ampoule guide was designed to facilitate the symmetric uniformity of the seal. Figure A2 shows top and side views of the ampoule guide. The ampoule guide consists of a single piece of brass, center drilled to an inside diameter that is 100 μm larger than the O.D. of the desired ampoule; then the upper half of the guide's outside diameter is reduced from 1.5" to 0.75". The reduced side is then clamped in the mill and four 0.25" holes are drilled ninety degrees apart. The guide is then put back in the lathe, chucking the reduced side, and the bottom is parted in half, resulting in two 0.25" thick plates. The two plates are joined by 0.25"

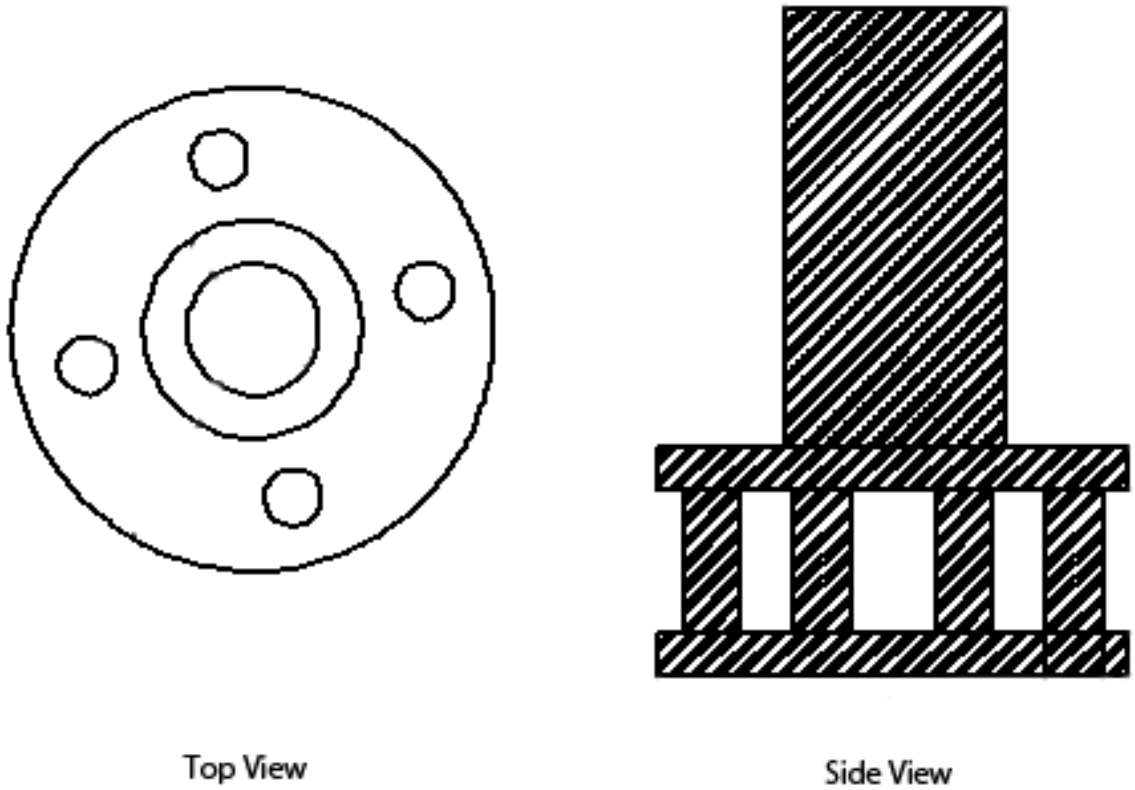

Figure A2. Top and side views of the ampoule guide.

dowel pins, each 1" in length, placed through the previously existing 0.25" holes. This process ensures the alignment of the center drilled hole of the ampoule guide.

The next challenge of the ampoule guide is holding the ampoule in place while performing the seal. The solution was to create ampoule clamps. The ampoule clamps are made from Teflon, cut to a length of one inch and turned to a diameter of one inch, then center drilled to the same I.D. as the ampoule's O.D. The clamp is then mounted on the mill and an axial channel is cut along the direction parallel to the center hole. The clamp is rotated 90^{o} and drilled through the center of the axial channel. This hole is tapped with 1/4-20 threads on one side of the axial channel and drilled to 11/16 " on the other side of the axial channel. Tightening of a bolt in this half-threaded channel will fix the ampoule in place during the sealing process. During ampoule sealing, the ampoule

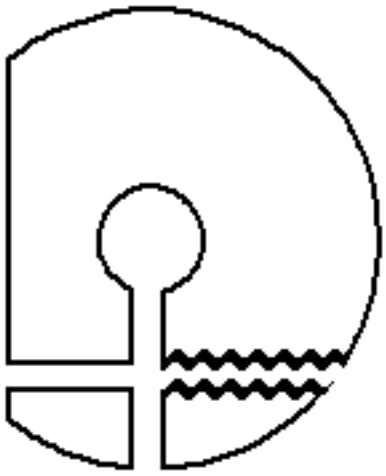

Figure A3. Top view of ampoule clamp

clamp is held in place with a three-fingered clamp. Figure A3 shows the top view of ampoule clamp.

Figure A4 shows the four-tipped torch designed and built for this project, for symmetric application of heat to the glass. Copper tubes, 0.25" O.D., connected with Swagelok® fittings, were used as plumbing for the torch fuel mixture. The four tips are slightly off center to maximize the effect of heating provided by the flame splash. It was decided early in this work that application of reduced pressure during the sealing process would facilitate an even seal and nearly eliminate the escape of solvent. To this end, the ampoule is connected to a vacuum manifold during the sealing process.

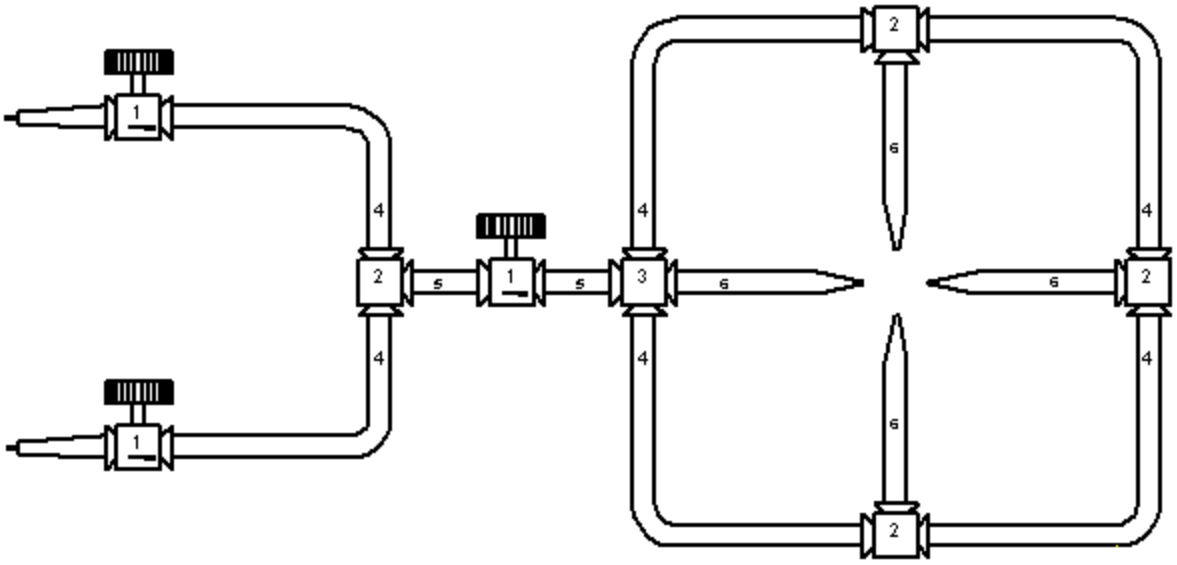

Figure A4. Four-tipped torch. 1. Needle Valve. 2. 3-way fitting. 3. 4-way-fitting. 4. 1/4" copper tube with 90^{o} bend. 5. Straight copper tube. 6. Torch tip.

To summarize the ampoule sealing process, the ampoule is loaded with 20 mg enriched biomass and 200 μl solvent (H_2O or H_2SO_4), to create a 10 % slurry. The ampoule is then frozen in liquid nitrogen. The freezing is necessary to prevent, as much as possible, the solvent from evaporating and degassing during the sealing process. The ampoule is then clamped and inserted into the ampoule guide. When the flame is applied to the ampoule, under reduced pressure, the area softened by the flame begins to collapse. When the walls of the ampoule coalesce in the center, the ampoule is pulled vertically for two inches and the flow of oxygen to the torch is stopped via a foot pedal. After the ampoule is pulled, the flow of methane to the torch is removed, the torch is vented and all needle valves are closed. The sample is then re-frozen in liquid nitrogen and the ampoule is cut from the stem by a diamond knife and polished, briefly, by flame.

Figures A5 and A6 show photographs of an ampoule clamped inside the ampoule guide and loaded into the four-tipped torch.

Figure A5. Photograph of an ampoule, inside the ampoule guide and held by the ampoule clamps.

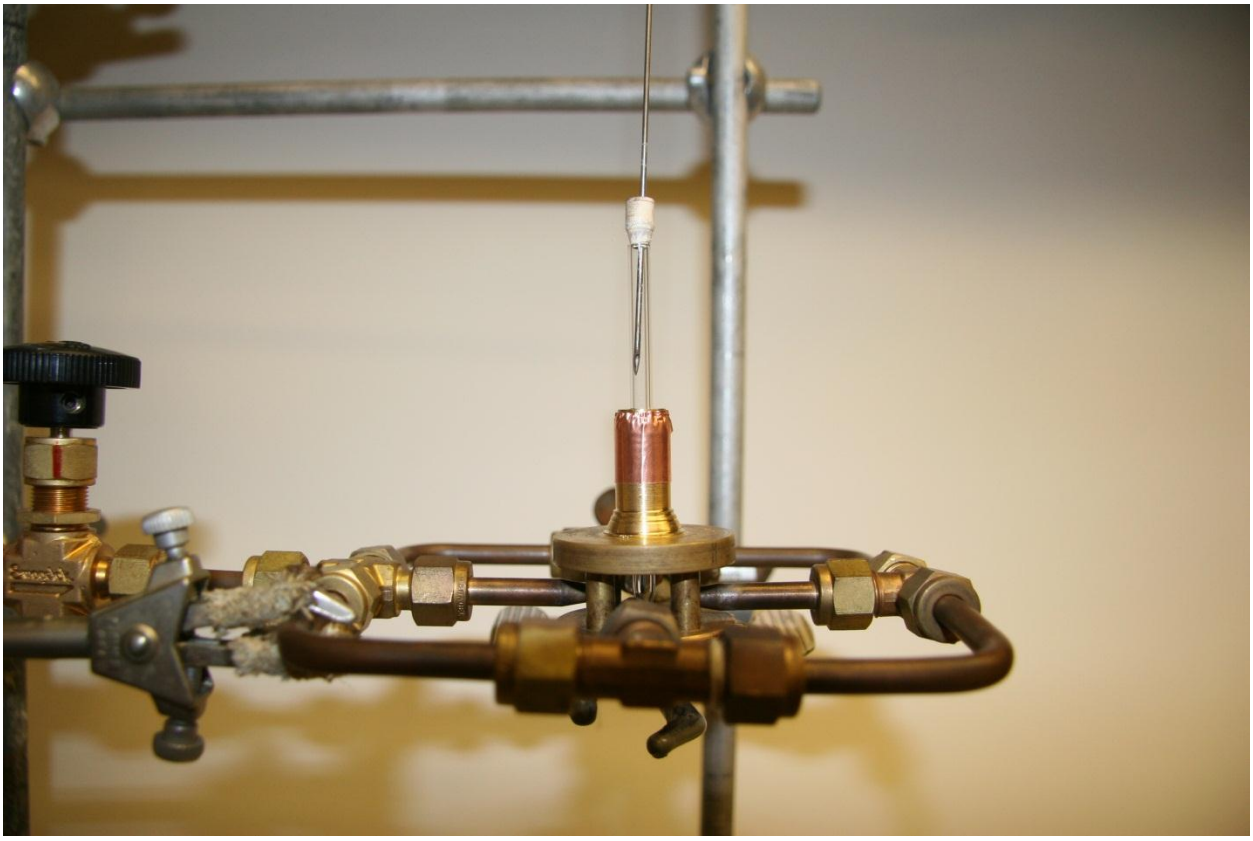

Figure A6. Photograph of ampoule in ampoule guide and connected to the four-tipped torch.

Appendix B

Variable Temperature Stack

List of Figures

In solid state nuclear magnetic resonance, the sample temperature can be changed and monitored by using an apparatus called a variable temperature stack (VTS). Figure B1 shows the VTS, mated to a solid state NMR probe.

It was decided that it would be better to rebuild the heater core of the VTA rather than to reuse the previous configuration (heavily modified based on commercially delivered product from Chemagnetics). In rebuilding the VTS, a piece of one half inch quartz tube is used to contain the heater coil and act as a mixing chamber for freshly heated air. The exhaust air from the NMR probe flows through the VTS around the outside of the quartz tube. The heater coil was wound by hand and the length of heater wire was set to provide a resistance of 50 Ω. A platinum resistance thermometer was mounted on a piece of Teflon and placed twelve inches downstream of the heater coil, at the point where the hot air exits and the exhaust air enters the VTS.

The VTS is controlled by a REX-F900 temperature control unit (RKC Instruments). The REX-F900 uses a proprietary PID (Proportional Integral Differential) algorithm to provide pulsed AC electricity to the heater coil. In brief, the PID algorithm measures the temperature with a platinum thermometer, compares the

Figure B1. Variable temperature stack mated to NMR probe

measurement to the setting temperature and adjusts the length of the AC pulse and separation between AC pulses to reach and maintain the target temperature. However, the REX-F900 can moniter the temperature only *within the VTS apparatus*. Knowledge of the temperature *within the ampoule* is critical to this study. Thus, two methods of temperature calibration were employed in this study: the ethylene glycol NMR thermometer and the method of melting points.

A previously reported ethylene glycol NMR thermometer[68-70] was employed. The ethylene glycol NMR thermometer works by measuring the frequency difference between the two ^{1}H signals of ethylene glycol. Previous works have yielded the following calibration equations for the calculation of the sample temperature in ^{o}C.

$$\text{Becker}^{68}: \; T_{sample}(^{o}C) = 466.5 - 0.461 * (\Delta\nu * 220) - 273.15 \qquad \text{(B.1)}$$

$$\text{Neuman}^{68}: \; T_{sample}(^{o}C) = 193.8 + -1.691 * (\Delta\nu * 60) \qquad \text{(B.2)}$$

$$\text{Van Geet}^{69}: \; T_{sample}(^{o}C) = 466 - 1.694 * (\Delta\nu * 60) - 273.15 \qquad \text{(B.3)}$$

$$\text{Van Geet}^{69}: \; T_{sample}(^{o}C) = 193.2 + -1.705 * (\Delta\nu * 60) \qquad \text{(B.4)}$$

$$\text{Van Geet}^{69}: \; T_{sample}(^{o}C) = 192.8 + -1.695 * (\Delta\nu * 60) \qquad \text{(B.5)}$$

$$\text{Varian}^{70}: \; T_{sample}(^{o}C) = 188 + -1.656 * (\Delta\nu * 60) \qquad \text{(B.6)}$$

where $\Delta\nu$ is the measured frequency difference between the two ^{1}H signals. Figure B2 shows the ^{1}H NMR spectra of ethylene glycol collected during temperature calibration. For temperature calibration, the REX-F900 was set to a target temperature, e.g. 100 ^{o}C, and allowed to equilibrate for 10 minutes. After 10 minutes had passed, the NMR

spectrum was acquired and the frequency difference, $\Delta\nu$, measured. This procedure was repeated in 10 ^{o}C increments on the REX-F900. The six expressions, Eq. B.1-B.6, were used to calculate the sample temperature for the observed frequency difference, $\Delta\nu$, at each setting temperature on the REX-F900. The average temperature calculated from B1-6 was used to determine the sample temperature for each REX-F900 setting temperature. The standard deviation about the mean value for each frequency difference was used as an estimate of the error.

The second method used for temperature calibration was the method of melting points. To confirm the ethylene glycol measurements, the melting points of two organic solids, tetramethyl benzene (79-80 ^{o}C) and trans-cinnamic acid (132-135 ^{o}C) were measured in a Thomas-Hoover melting point apparatus. 100 mg of each sample was then sealed in an ampoule. The setting temperature of the REX-F900 was then increased until the ^{1}H NMR spectrum showed a peak, signifying that the solid has been converted to the liquid phase and thus melted. The REX-F900 setting temperature was continually increased until the intensity of the ^{1}H had reached a maximum value (an arbitrary intensity that is unchanged as the sample temperature continues to be increased beyond the melting point of the target compound). Figures B3 and B4 show the ^{1}H NMR spectra of tetramethylbenzene and trans-cinnamic acid, respectively, acquired during the melting point calibration method.

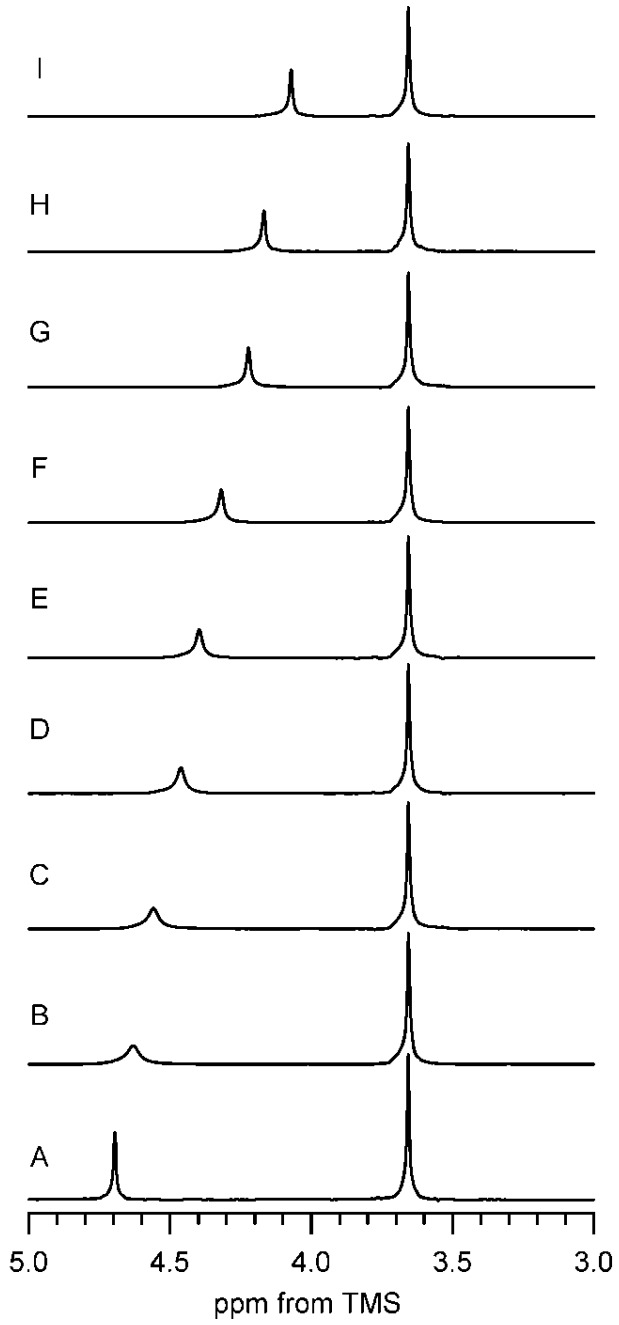

Figure B2. ^{1}H NMR spectra of ethylene glycol as a function of REX-F900 RTD temperature setting, ^{o}C: A; 80, B; 100, C; 110, D; 120, E; 130, F; 140, G; 150, H; 160, I; 170.

Melting point calibration points were estimated by taking the average temperature from which the peak had grown by 10 % and 90 % of the maximum value. The RTD error bars were determined by taking the difference between the 10 and 90 % temperatures and the determined average value. The sample temperature was estimated by calculating the average of the melting point range, as determined by the capillary melting point method and by the average of the 10 % and 90 % melted signal intensities. The standard deviation about the mean value was used to estimate the error bars in the sample temperature dimension.

Figure B5 shows the calibration plot generated from these two calibration methods, showing the sample temperature on the abscissa and the REX-F900 setting value on the ordinate. The regression equation was used to determine the REX-F900 setting value that would yield the desired sample temperature.

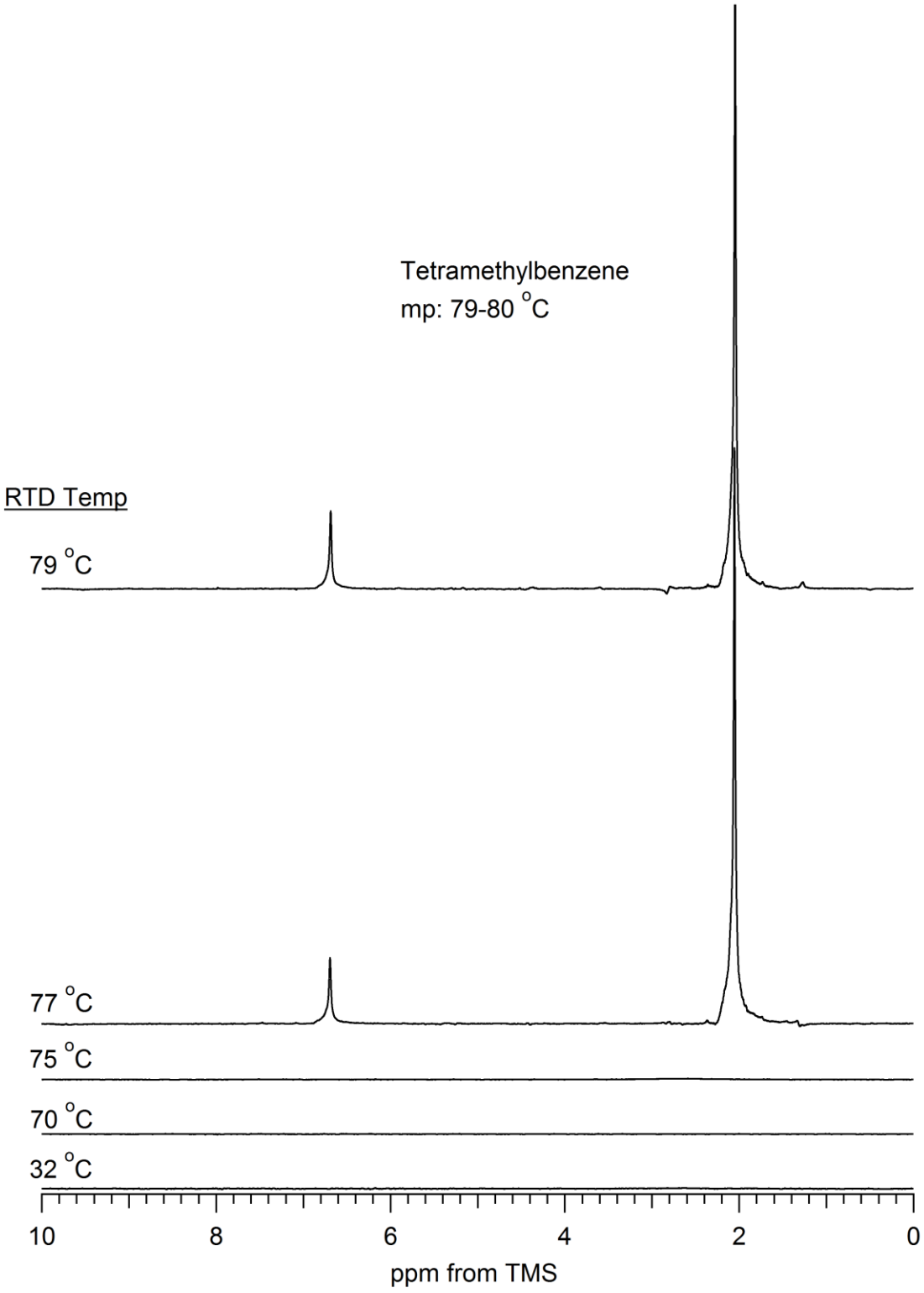

Figure B3. ^{1}H NMR spectra of tetramethylbenzene as a function of calibrated temperature.

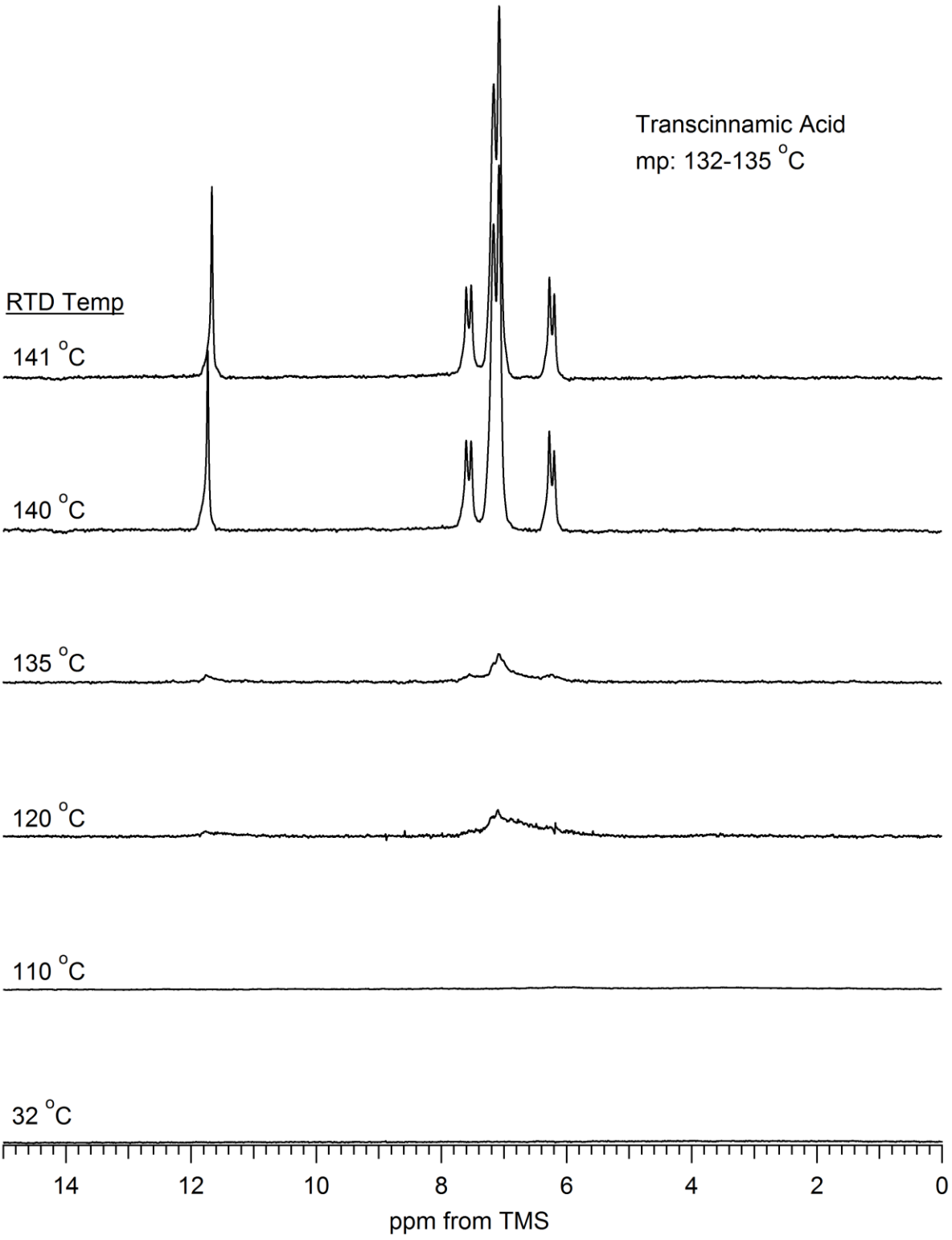

Figure B4. ^{1}H NMR spectra of trans-cinnamic acid as a function of calibrated temperature.

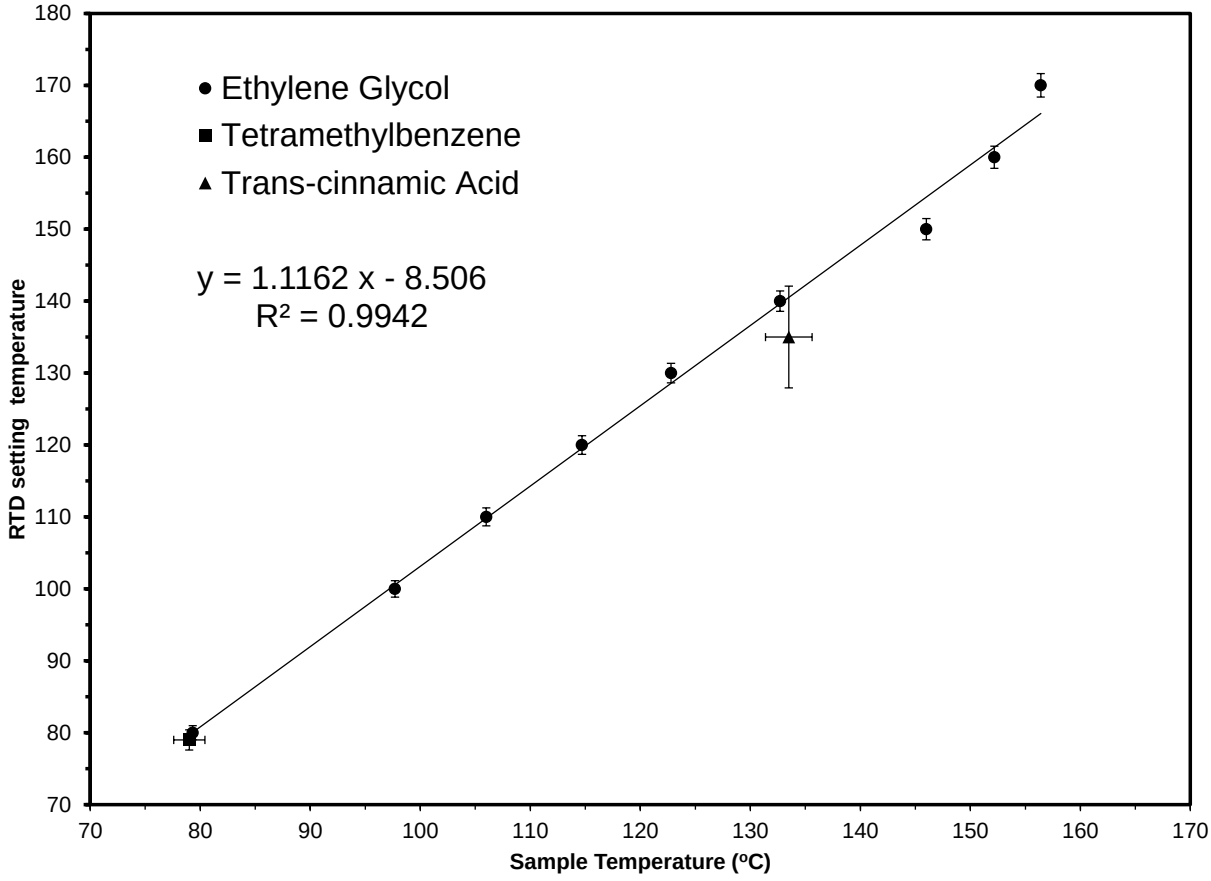

Figure B5. Calibration plot for variable temperature stack.

Appendix C

Variable-contact-time results

List of Figures

C4. Variable-contact-time experiment at 30 ^{o}C *after* pretreatment of 10 % poplar in 0.5 M H_2SO_4 at 150 ^{o}C.

C4a. Experimental ^{13}C CP-MAS NMR spectra.

C4b. Curve fitting of $T_{1\rho H}$, T_{CH}, M_{∞} to cellulose peaks in experimental ^{13}C CP-MAS NMR spectra.

C4c. Curve fitting of $T_{1\rho H}$, T_{CH}, M_{∞} to hemicellulose peaks in experimental ^{13}C CP-MAS NMR spectra.

C4d. Curve fitting of $T_{1\rho H}$, T_{CH}, M_{∞} to lignin peaks in experimental ^{13}C CP-MAS NMR spectra.

List of Tables

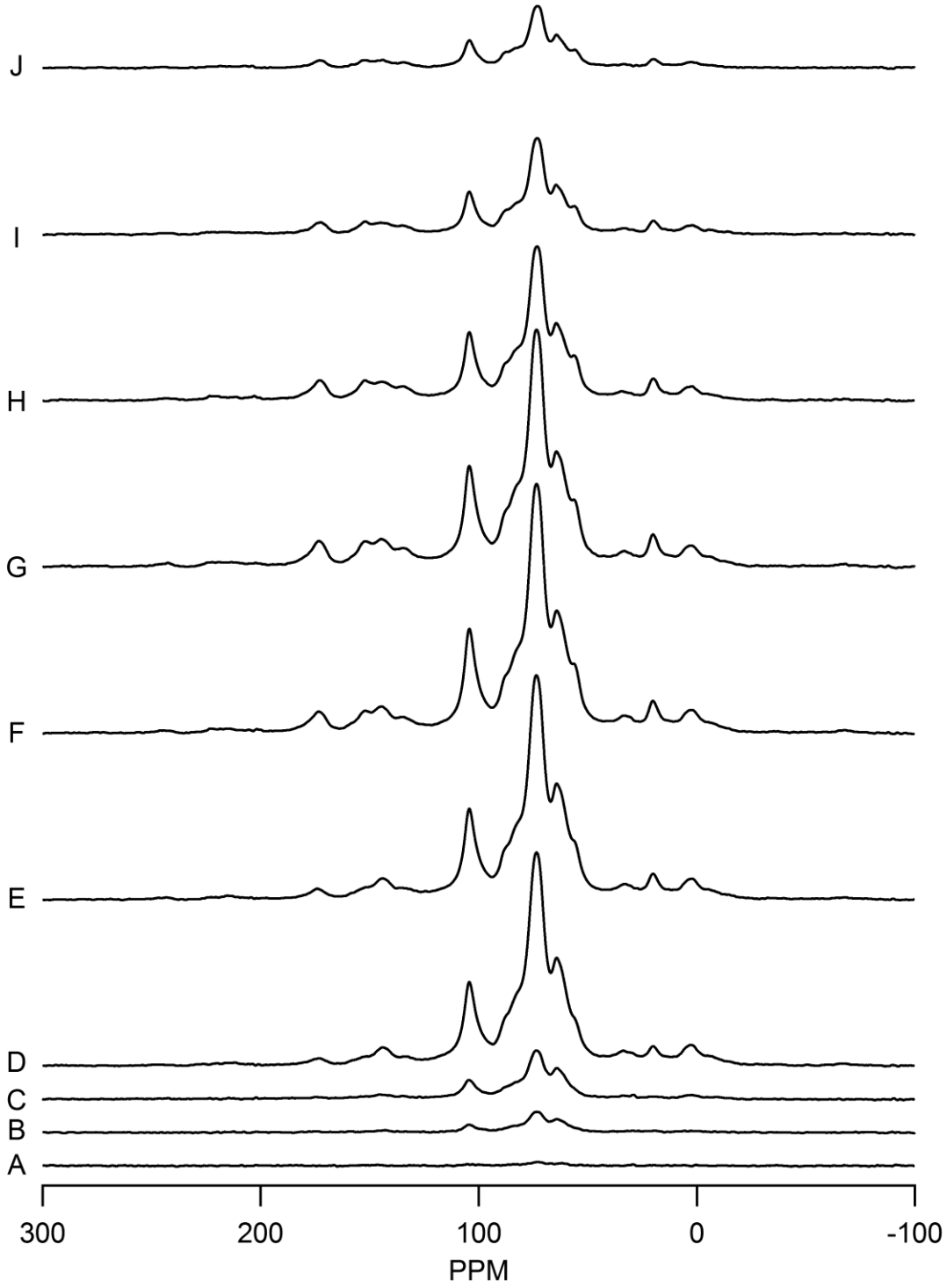

Figure C1a. CP-MAS spectra acquired from variable-contact-time experiment on 20 mg enriched dry wood at 30 ^{o}C. Contact times: A. 1 μs. B. 5 μs. C. 10 μs. D. 50 μs. E. 100 μs. F. 500 μs. G. 1 ms. H. 5 ms. I. 10 ms. J. 15 ms.

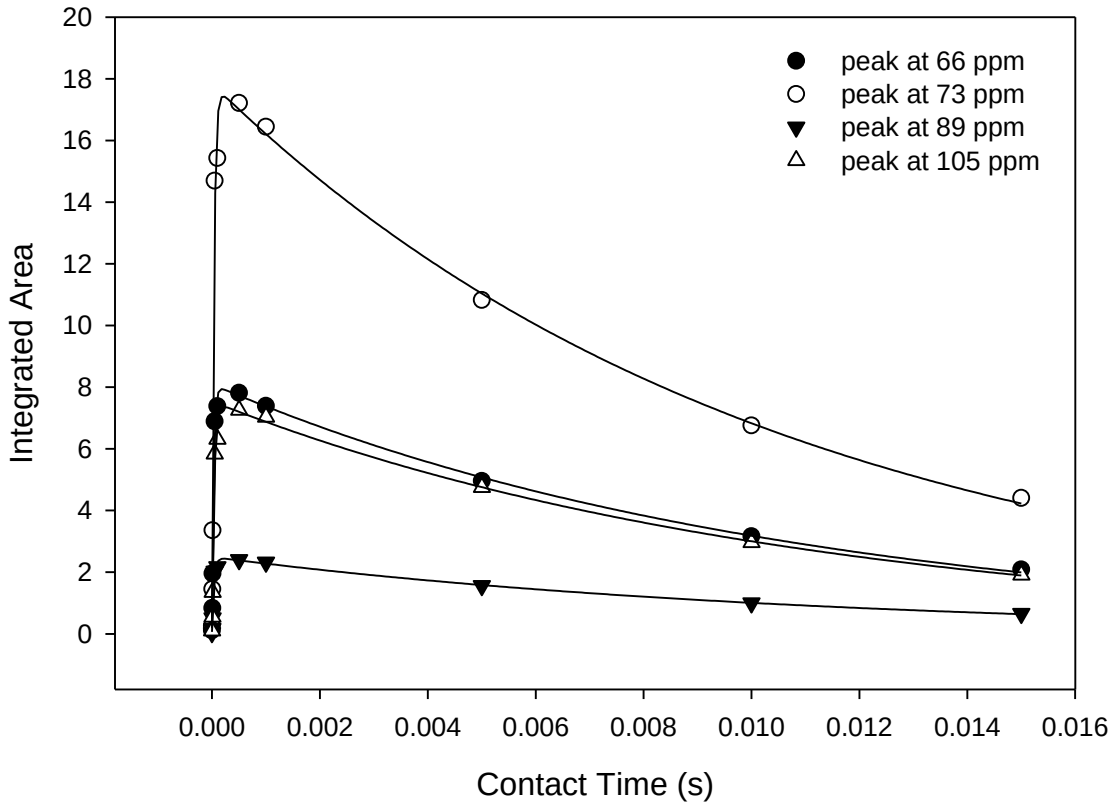

Figure C1b. Curve fitting of variable-contact-time results for integrated intensities of cellulose peaks in CP-MAS ^{13}C NMR spectra (Fig. C1a) of dry poplar at 30 ^{o}C to eq. 2.1.

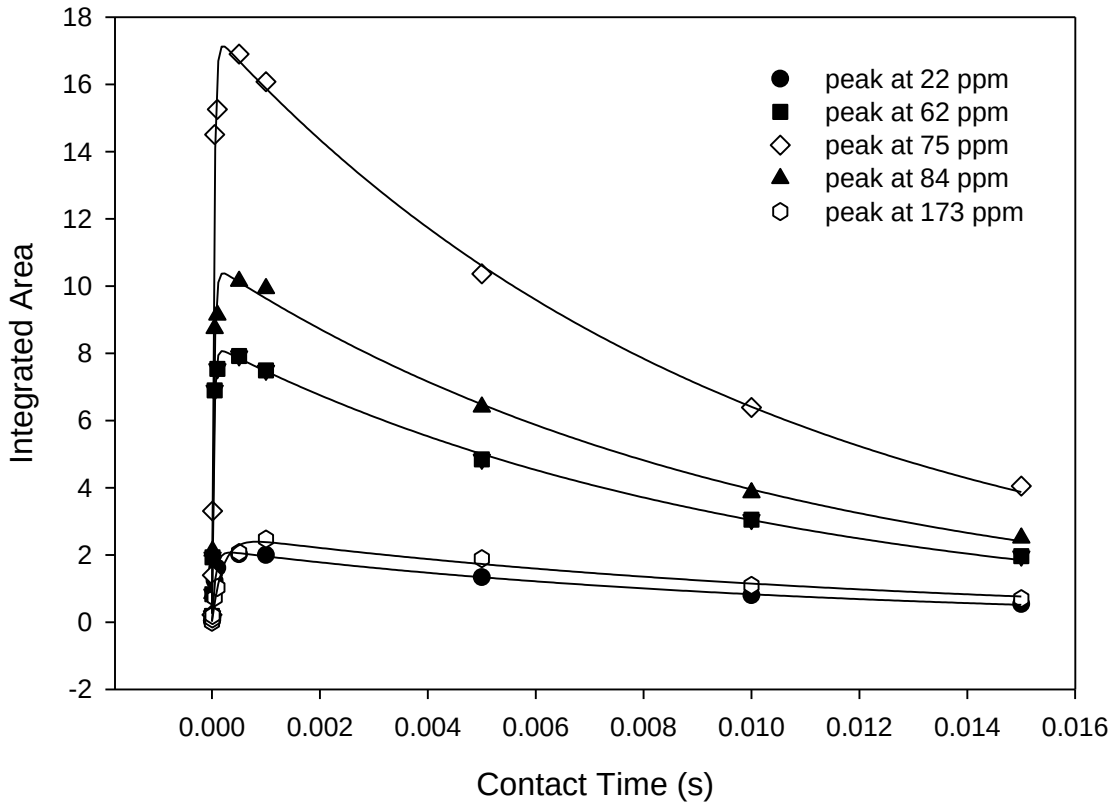

Figure C1c. Curve fitting of variable-contact-time results for integrated intensities of hemicellulose peaks in CP-MAS ^{13}C NMR spectra (Fig. C1a) of dry poplar at 30 ^{o}C to eq. 2.1.

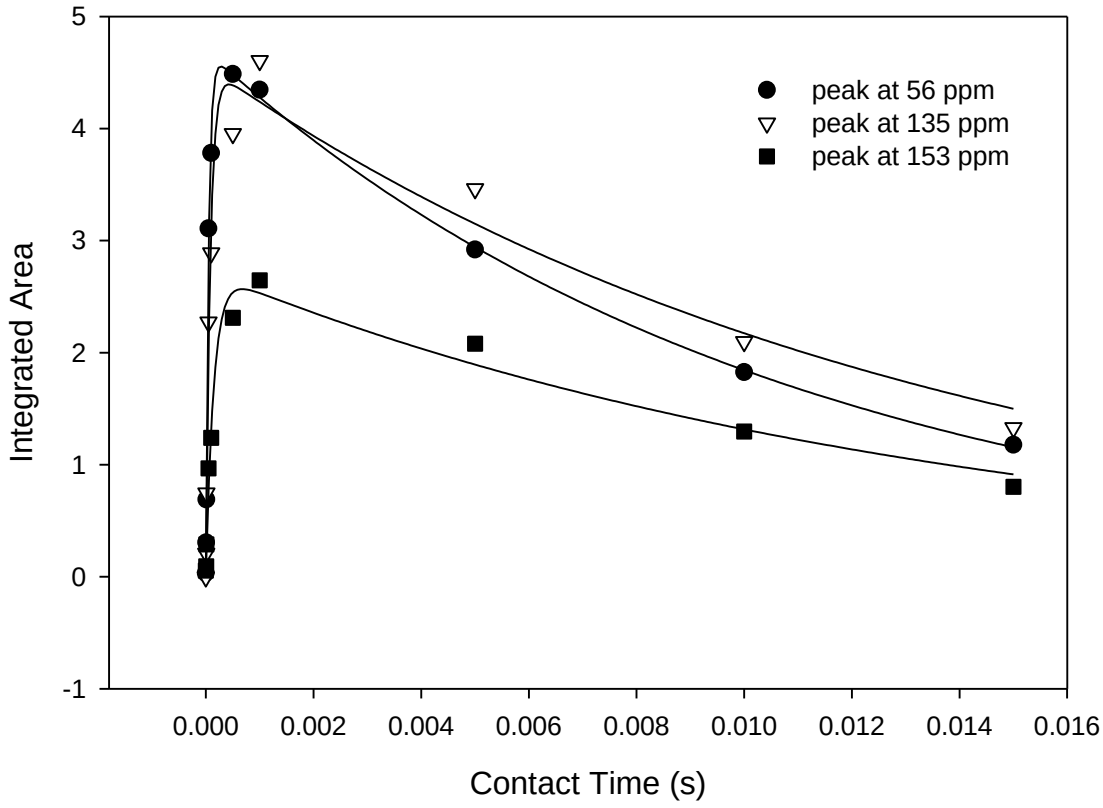

Figure C1d. Curve fitting of variable-contact-time results for integrated intensities of lignin peaks in CP-MAS ^{13}C NMR spectra (Fig. C1a) of dry poplar at 30 ^{o}C to eq. 2.1.

Table C1. Variable-contact-time curve fitting results on dry poplar at 30 ^{o}C

	Peak[a]	M_{∞}[b]	M^*_{∞}[c]	$T_{1\rho H}$ (ms)	T_{CH} (μs)
	22	2.1 ± 0.1	2.4 ± 0.1	10 ± 1	66 ± 5
L	56	5.0 ± 0.1	5.8 ± 0.1	11 ± 1	52 ± 5
	62	8.2 ± 0.2	9.7 ± 0.2	10 ± 1	32 ± 3
C	66	8.1 ± 0.2	9.7 ± 0.2	11 ± 2	31 ± 3
C	73	17.8 ± 0.6	21.3 ± 0.6	10 ± 1	36 ± 5
	75	17.5 ± 0.6	20.9 ± 0.6	10 ± 1	36 ± 5
	84	10.6 ± 0.4	12.6 ± 0.4	10 ± 1	36 ± 5
C	89	2.5 ± 0.6	3.0 ± 0.6	11 ± 1	36 ± 4
C	105	7.5 ± 0.2	9.0 ± 0.2	11 ± 1	41 ± 5
L	135	4.5 ± 0.2	5.2 ± 0.2	13 ± 2	80 ± 10
L	153	2.7 ± 0.1	3.2 ± 0.1	14 ± 2	150 ± 20
	173	2.6 ± 0.1	3.0 ± 0.1	12 ± 1	200 ± 30

[a] Peak positions in ppm. L signifies a lignin peak, C signifies a 'crystalline' cellulose peak and others are from hemicellulose and minor contributions from amorphous cellulose.

[b] M_{∞} represents the transverse ^{13}C magnetization that would have been generated if the CP transfer had been infinitely fast and if rotating-frame ^{1}H spin-lattice relaxation had been infinitely slow.

[c] M^*_{∞} is the corresponding M_{∞} value that has been corrected by the factor, $\{1 - \exp(-t/T_{1H})\}^{-1}$, for incomplete ^{1}H spin-lattice relaxation between CP scans.

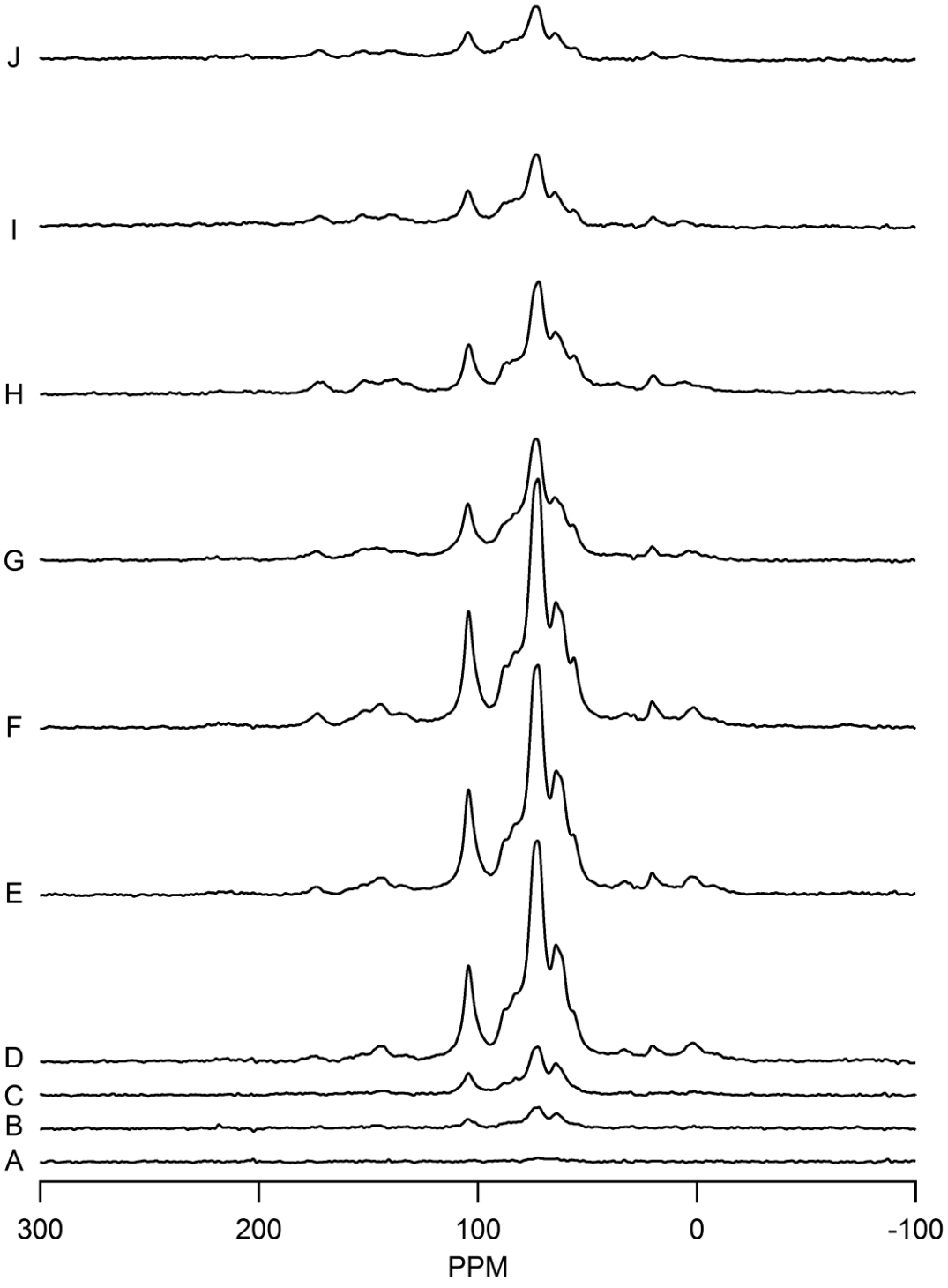

Figure C2a. CP-MAS spectra acquired from variable-contact-time experiment on 20 mg enriched wood 10 % in 0.5 M H_2SO_4 at 30 ^{o}C *before* pretreatment. Contact times: A. 1 μs. B. 5 μs. C. 10 μs. D. 50 μs. E. 100 μs. F. 500 μs. G. 1 ms. H. 5 ms. I. 10 ms. J. 15 ms.

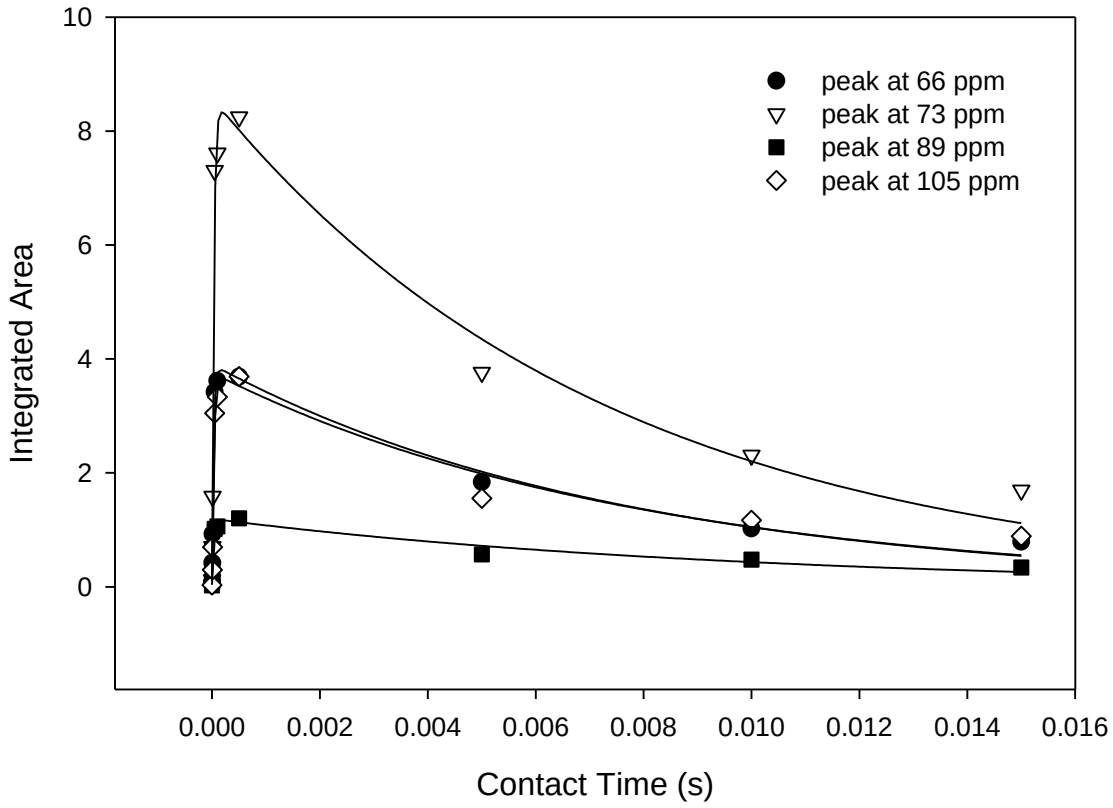

Figure C2b. Curve fitting of variable-contact-time results for integrated intensities of cellulose peaks in CP-MAS ^{13}C NMR spectra (Fig. C2a) on 20 mg enriched wood 10 % in 0.5 M H_2SO_4 at 30 ^{o}C *before* pretreatment to eq. 2.1.

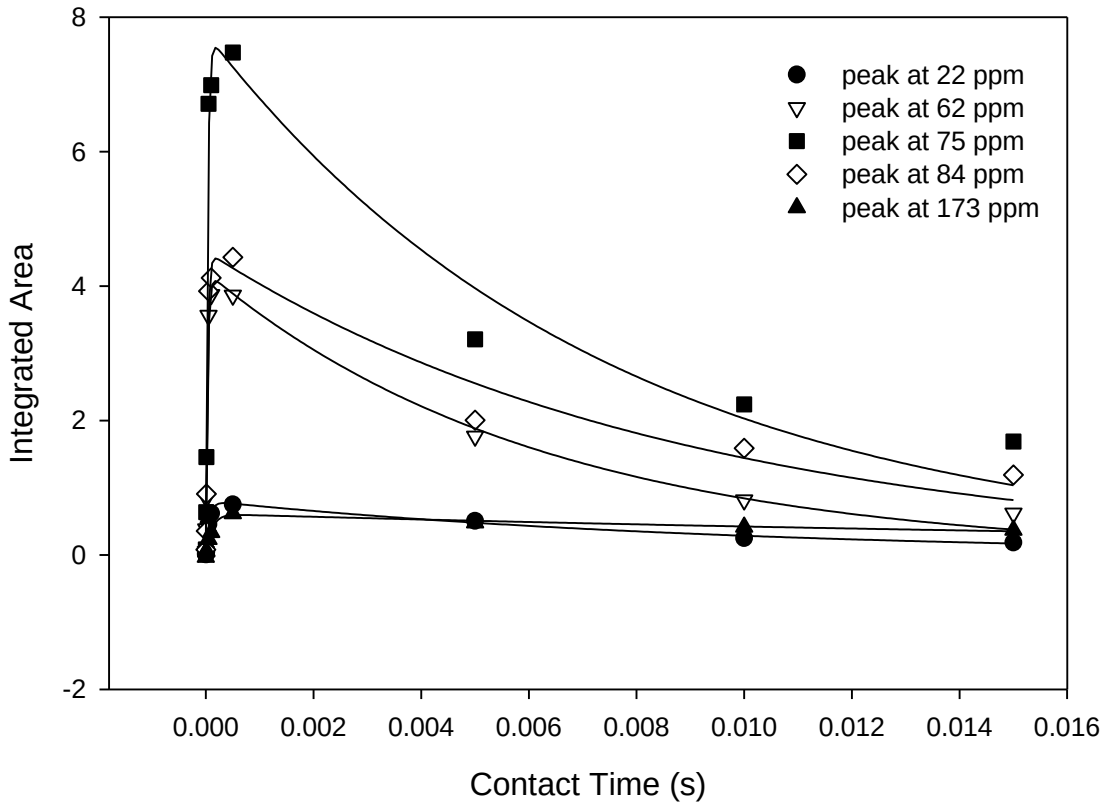

Figure C2c. Curve fitting of variable-contact-time results for integrated intensities of hemicellulose peaks in CP-MAS ^{13}C NMR spectra (Fig. C2a) on 20 mg enriched wood 10 % in 0.5 M H_2SO_4 at 30 ^{o}C *before* pretreatment to eq. 2.1.

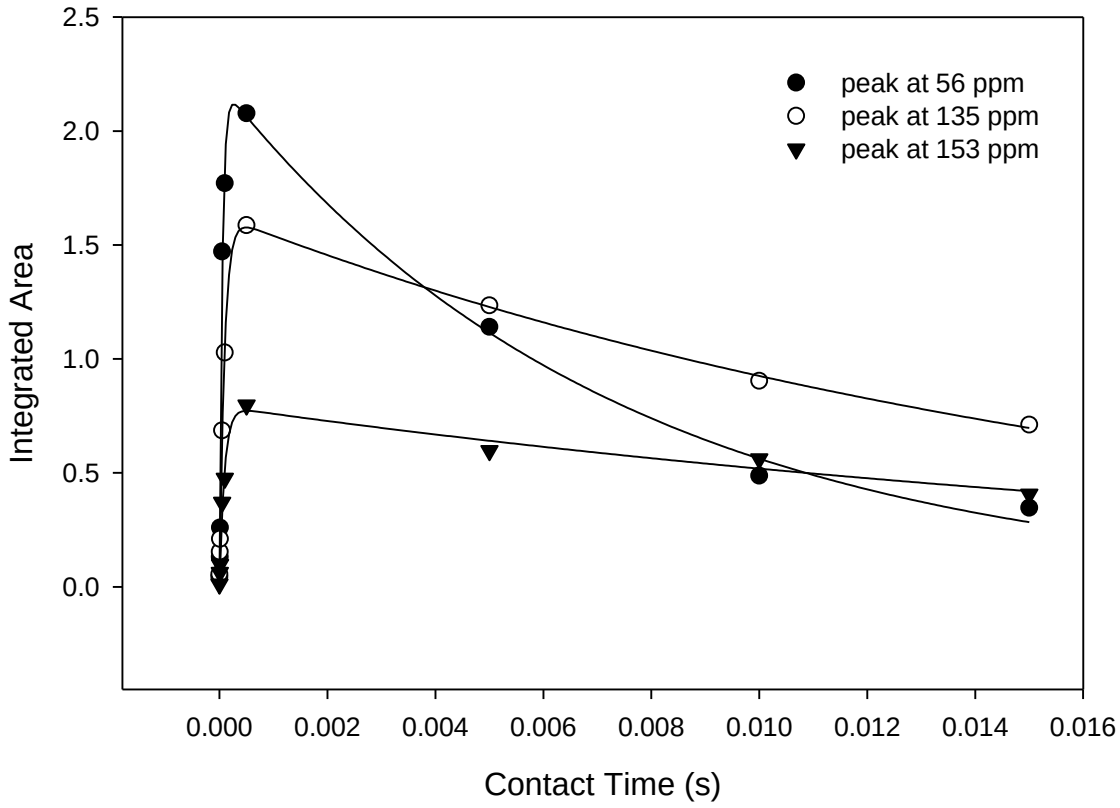

Figure C2d Curve fitting of variable-contact-time results for integrated intensities of lignin peaks in CP-MAS ^{13}C NMR spectra (Fig. C2a) on 20 mg enriched wood 10 % in 0.5 M H_2SO_4 at 30 ^{o}C *before* pretreatment to eq. 2.1.

Table C2. Variable-contact-time **c**urve fitting results on 10 % poplar in 0.5 M H_2SO_4 at 30 ^oC *before* pretreatment.

	Peak[a]	M_∞[b]	M^*_∞[c]	$T_{1\rho H}$ (ms)	T_{CH} (μs)
	22	0.8 ± 0.1	0.9 ± 0.1	10 ± 1	66 ± 9
L	56	2.2 ± 0.1	2.5 ± 0.1	7 ± 1	53 ± 6
	62	4.2 ± 0.2	5.2 ± 0.2	6 ± 1	33 ± 5
C	66	3.9 ± 0.2	4.8 ± 0.2	8 ± 1	30 ± 5
C	73	8.5 ± 0.5	10.7 ± 0.5	7 ± 1	34 ± 7
	75	7.7 ± 0.5	9.6 ± 0.5	7 ± 1	33 ± 8
	84	4.5 ± 0.3	5.5 ± 0.3	9 ± 1	32 ± 8
C	89	1.2 ± 0.1	1.5 ± 0.1	10 ± 2	34 ± 8
C	105	3.7 ± 0.3	4.7 ± 0.3	8 ± 1	36 ± 9
L	135	1.6 ± 0.1	1.9 ± 0.1	18 ± 1	93 ± 6
L	153	0.8 ± 0.1	0.9 ± 0.1	24 ± 4	90 ± 10
	173	0.6 ± 0.1	0.7 ± 0.1	27 ± 4	110 ± 10

[a] Peak positions in ppm. L signifies a lignin peak, C signifies a 'crystalline' cellulose peak and others are from hemicellulose and minor contributions from amorphous cellulose.

[b] M_∞ represents the transverse ^{13}C magnetization that would have been generated if the CP transfer had been infinitely fast and if rotating-frame ^1H spin-lattice relaxation had been infinitely slow.

[c] M^*_∞ is the corresponding M_∞ value that has been corrected by the factor, $\{1 - \exp(-t/T_{1H})\}^{-1}$, for incomplete ^1H spin-lattice relaxation between CP scans.

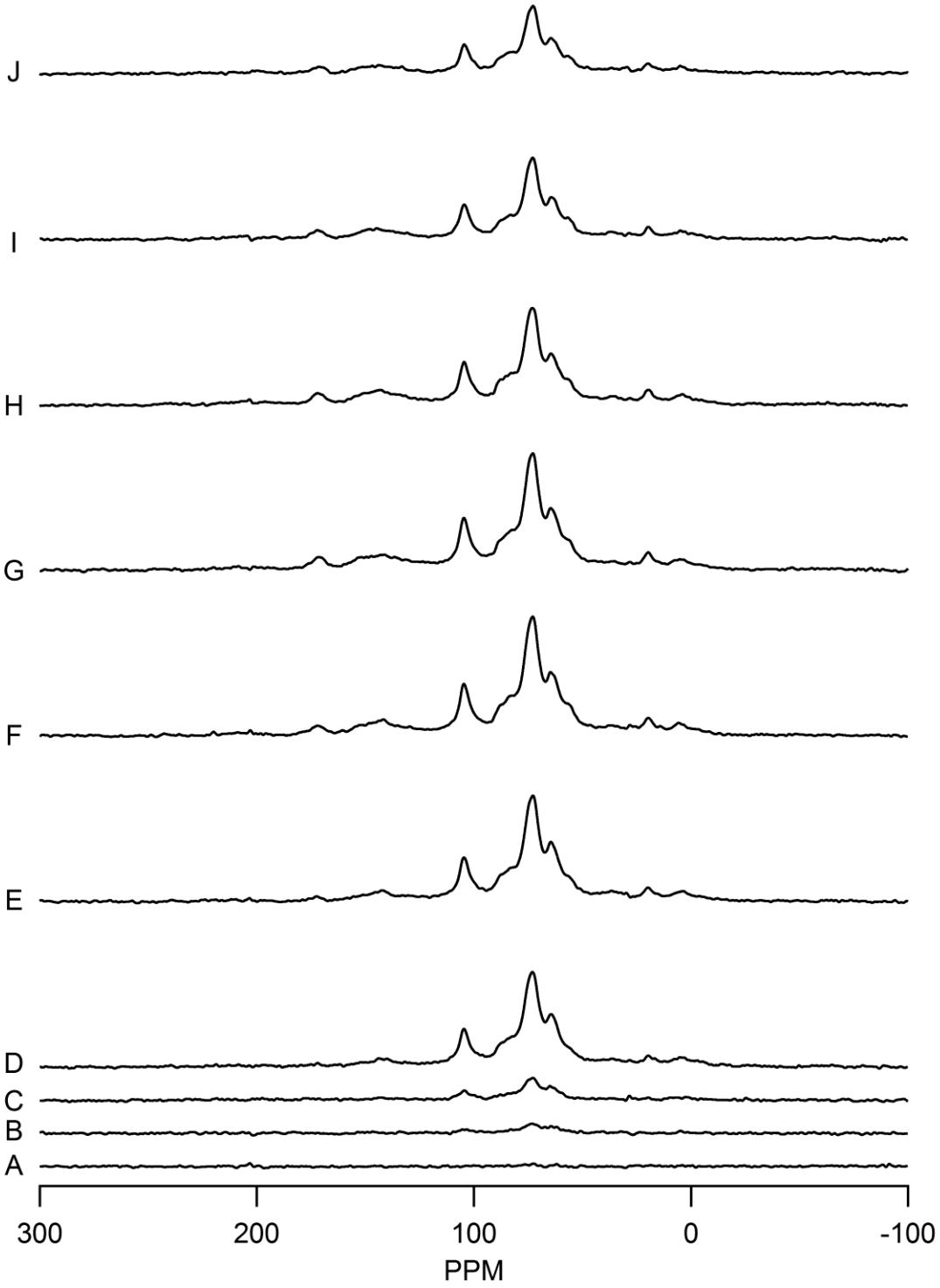

Figure C3a. CP-MAS spectra acquired from variable-contact-time experiment on 20 mg enriched wood 10 % in 0.5 M H_2SO_4 at 150 ^oC *during* pretreatment. Contact times: A. 1 μs. B. 5 μs. C. 10 μs. D. 50 μs. E. 100 μs. F. 500 μs. G. 1 ms. H. 5 ms. I. 10 ms. J. 15 ms.

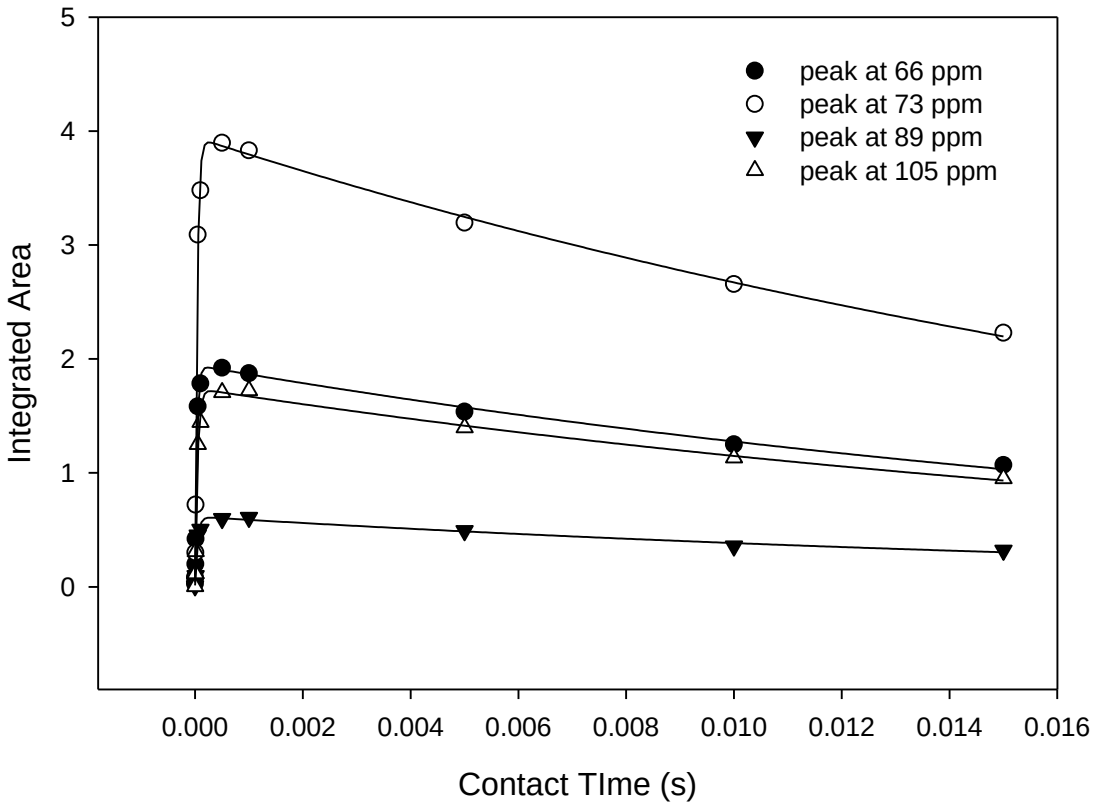

Figure C3b. Curve fitting of variable-contact-time results for integrated intensities of cellulose peaks in CP-MAS ^{13}C NMR spectra (Fig. C3a) on 20 mg enriched wood 10 % in 0.5 M H_2SO_4 at 150 ^{o}C *during* pretreatment to eq. 2.1.

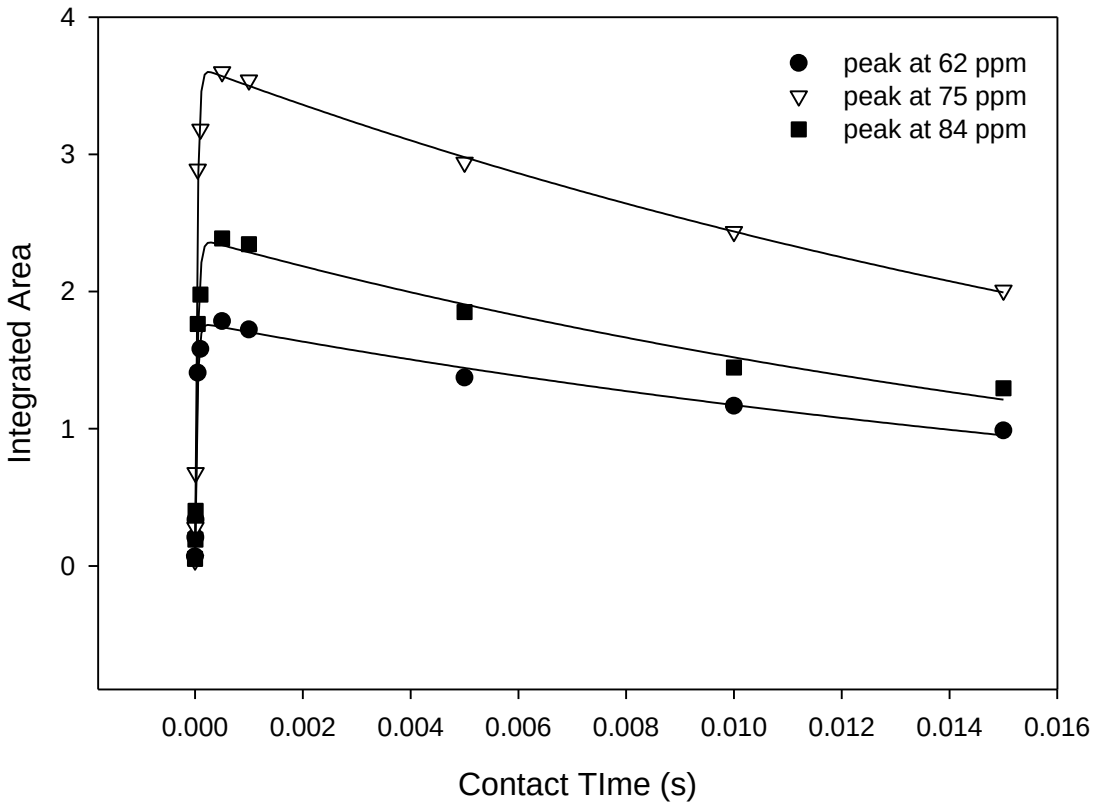

Figure C3c. Curve fitting of variable-contact-time results for integrated intensities of hemicellulose peaks in CP-MAS ^{13}C NMR spectra (Fig. C3a) on 20 mg enriched wood 10 % in 0.5 M H_2SO_4 at 150 ^{o}C *during* pretreatment to eq. 2.1.

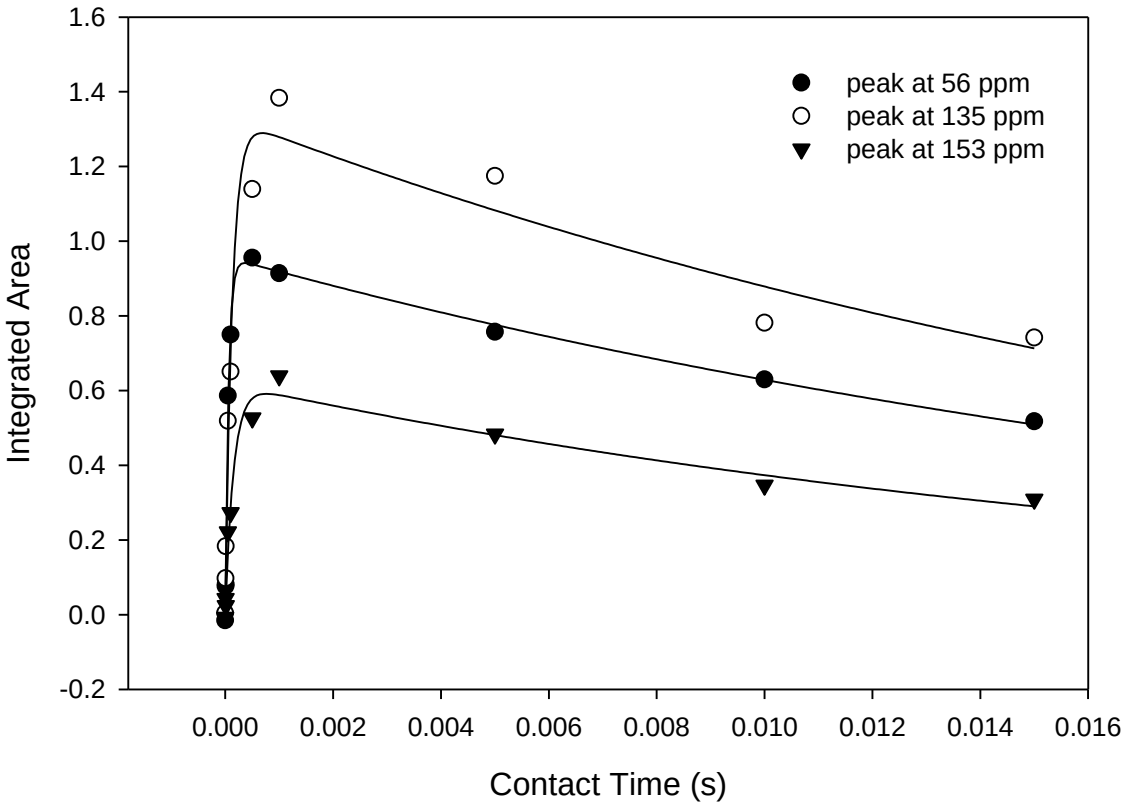

Figure C3d. Curve fitting of variable-contact-time results for integrated intensities of lignin peaks in CP-MAS ^{13}C NMR spectra (Fig. C3a) on 20 mg enriched wood 10 % in 0.5 M H_2SO_4 at 150 ^{o}C *during* pretreatment to eq. 2.1.

Table C3. Variable-contact-time **c**urve fitting results on 10 % poplar in 0.5 M H_2SO_4 at 30 ^oC *before* pretreatment.

Peak[a]		M_∞[b]	M^*_∞[c]	$T_{1\rho H}$ (ms)	T_{CH} (μs)
	22	[d]	[d]	[d]	[d]
L	56	1.0 ± 0.1	1.5 ± 0.1	24 ± 1	36 ± 5
	62	1.8 ± 0.1	2.7 ± 0.1	24 ± 2	37 ± 4
C	66	1.9 ± 0.1	2.8 ± 0.1	24 ± 2	34 ± 3
C	73	3.9 ± 0.1	5.8 ± 0.1	26 ± 3	39 ± 4
	75	3.6 ± 0.1	5.3 ± 0.1	25 ± 3	38 ± 4
	84	2.4 ± 0.1	3.5 ± 0.1	22 ± 3	44 ± 5
C	89	0.6 ± 0.1	0.9 ± 0.1	21 ± 3	46 ± 6
C	105	1.7 ± 0.1	2.5 ± 0.1	24 ± 2	46 ± 4
L	135	1.3 ± 0.1	1.8 ± 0.1	24 ± 5	130 ± 30
L	153	0.6 ± 0.1	0.8 ± 0.1	20 ± 3	160 ± 30
	173	[d]	[d]	[d]	[d]

[a] Peak positions in ppm. L signifies a lignin peak, C signifies a 'crystalline' cellulose peak and others are from hemicellulose and minor contributions from amorphous cellulose.

[b] M_∞ represents the transverse ^{13}C magnetization that would have been generated if the CP transfer had been infinitely fast and if rotating-frame ^1H spin-lattice relaxation had been infinitely slow.

[c] M^*_∞ is the corresponding M_∞ value that has been corrected by the factor, $\{1 - \exp(-t/T_{1H})\}^{-1}$, for incomplete ^1H spin-lattice relaxation between CP scans.

[d] The signals at 22 and 173 ppm were not observed under these conditions.

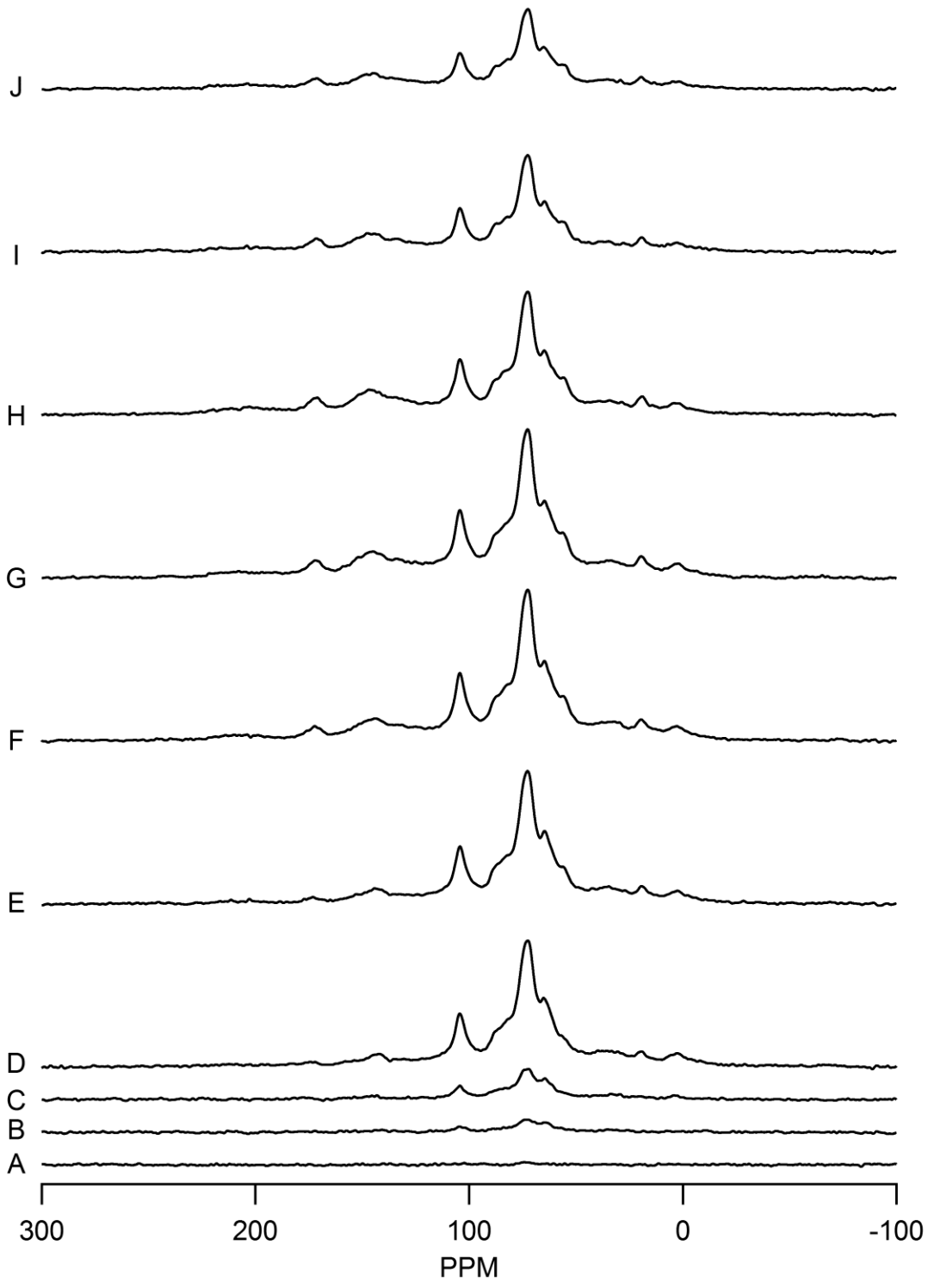

Figure C4a. CP-MAS spectra acquired from variable-contact-time experiment on 20 mg enriched wood 10 % in 0.5 M H_2SO_4 at 30 ^oC *after* pretreatment. Contact times: A. 1 μs. B. 5 μs. C. 10 μs. D. 50 μs. E. 100 μs. F. 500 μs. G. 1 ms. H. 5 ms. I. 10 ms. J. 15 ms.

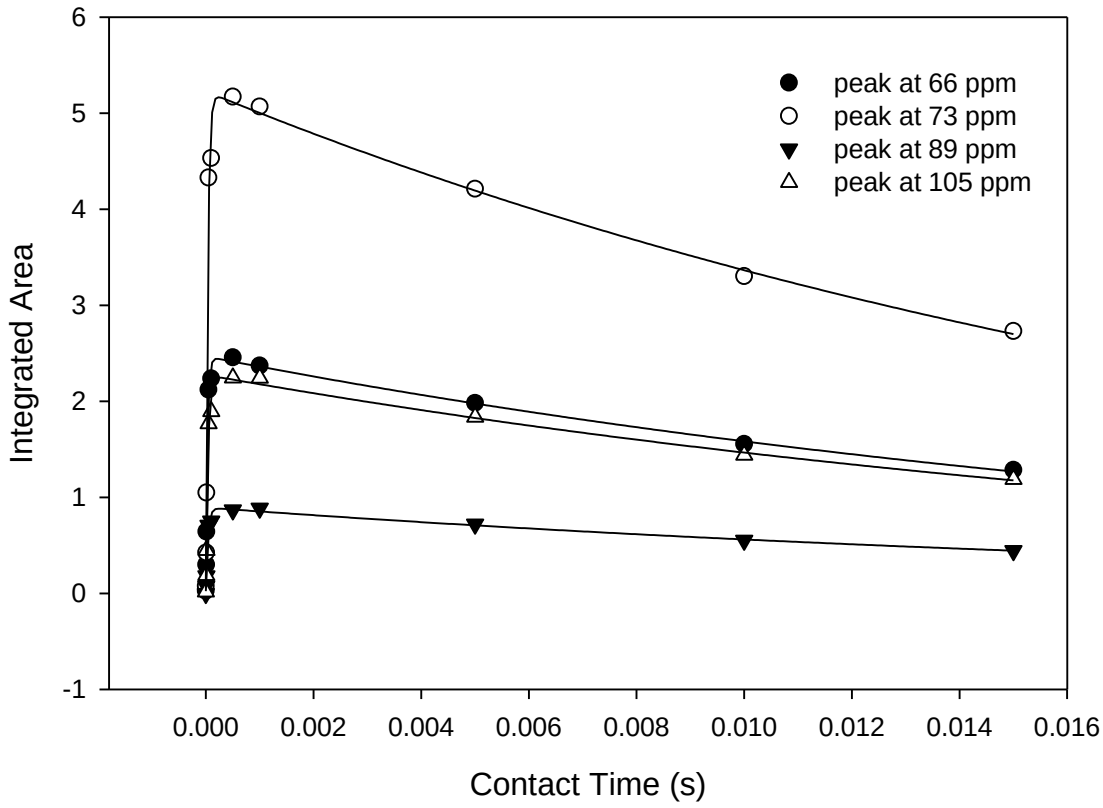

Figure C4b. Curve fitting of variable-contact-time results for integrated intensities of cellulose peaks in CP-MAS ^{13}C NMR spectra (Fig. C4a) on 20 mg enriched wood 10 % in 0.5 M H_2SO_4 at 30 ^{o}C *after* pretreatment to eq. 2.1.

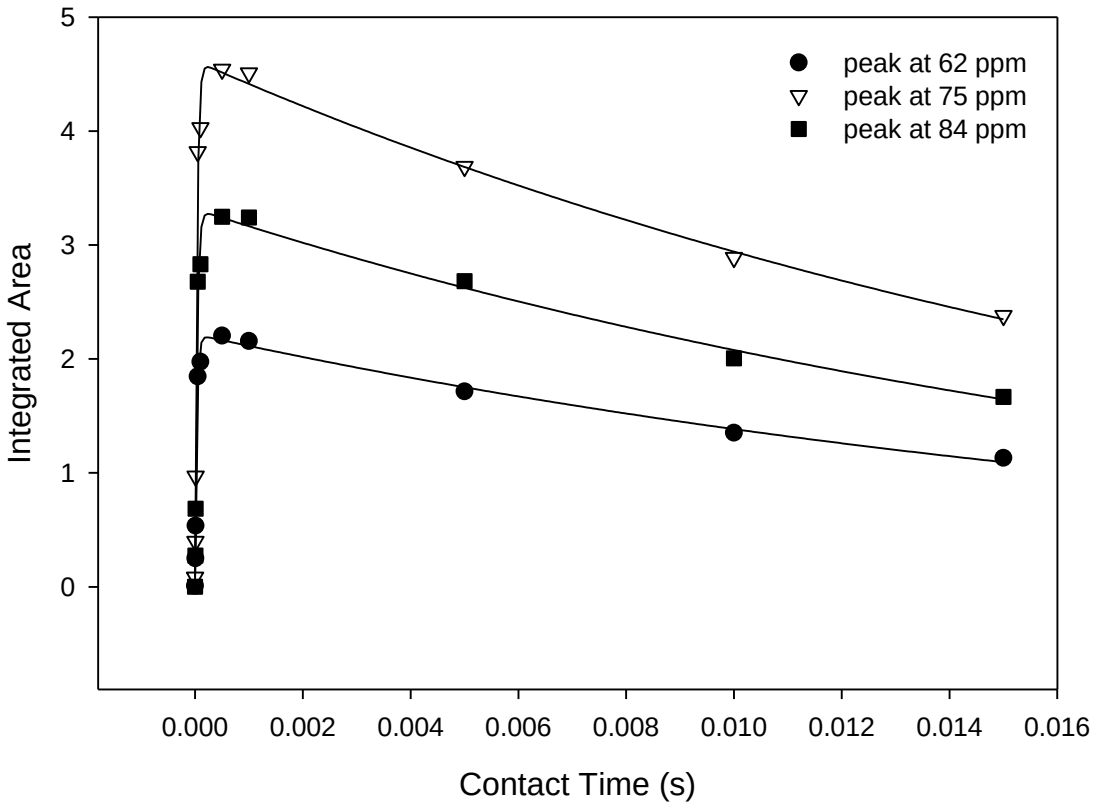

Figure C4c. Curve fitting of variable-contact-time results for integrated intensities of hemicellulose peaks in CP-MAS ^{13}C NMR spectra (Fig. C4a) on 20 mg enriched wood 10 % in 0.5 M H_2SO_4 at 30 ^{o}C *after* pretreatment to eq. 2.1.

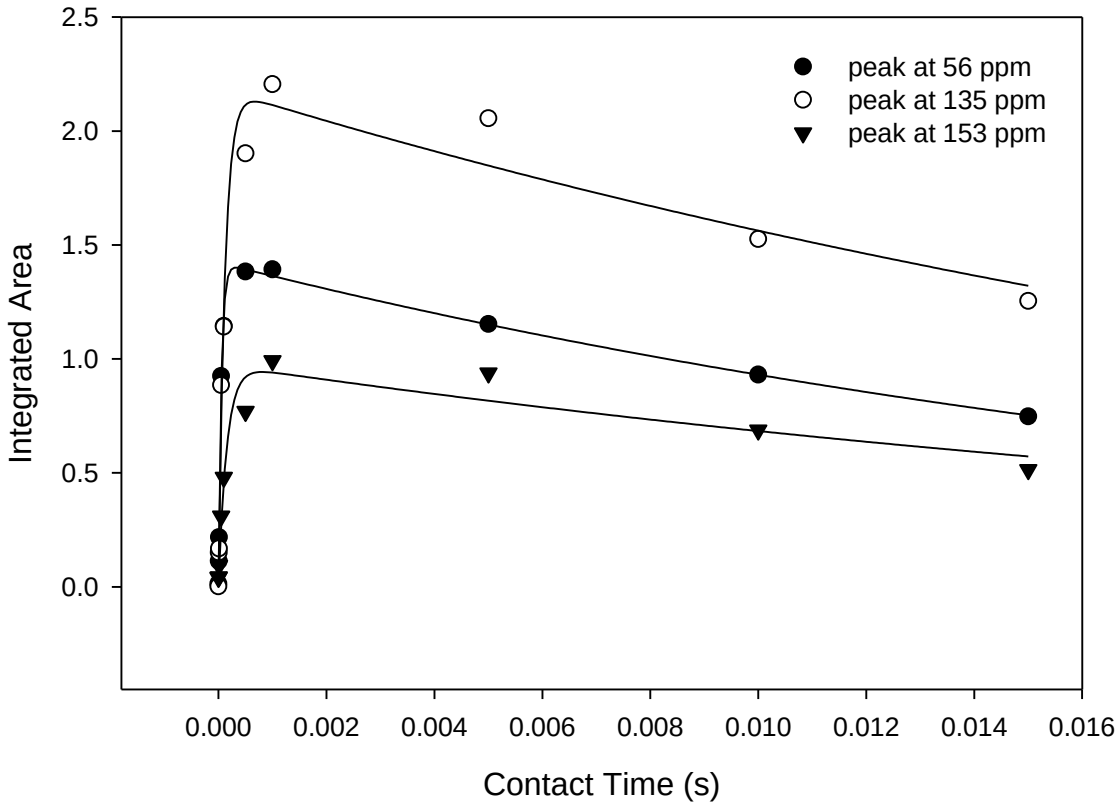

Figure C4d. Curve fitting of variable-contact-time results for integrated intensities of lignin peaks in CP-MAS ^{13}C NMR spectra (Fig. C4a) on 20 mg enriched wood 10 % in 0.5 M H_2SO_4 at 30 ^{o}C *after* pretreatment to eq. 2.1.

Table C4. Variable-contact-time **c**urve fitting results on 10 % poplar in 0.5 M H_2SO_4 at 30 ^oC *after* pretreatment.

Peak[a]		M_∞[b]	M^*_∞[c]	$T_{1\rho H}$ (ms)	T_{CH} (μs)
	22	[d]	[d]	[d]	[d]
L	56	1.4 ± 0.1	1.7 ± 0.1	24 ± 3	53 ± 3
	62	2.2 ± 0.1	2.8 ± 0.1	21 ± 2	33 ± 3
C	66	2.5 ± 0.1	3.2 ± 0.1	23 ± 2	30 ± 3
C	73	5.2 ± 0.2	6.7 ± 0.2	23 ± 3	36 ± 5
	75	4.6 ± 0.1	5.9 ± 0.1	22 ± 3	35 ± 4
	84	3.3 ± 0.1	4.1 ± 0.1	21 ± 3	37 ± 5
C	89	1.0 ± 0.1	1.3 ± 0.1	21 ± 3	39 ± 5
C	105	2.3 ± 0.1	3.0 ± 0.1	23 ± 3	40 ± 5
L	135	2.2 ± 0.1	2.6 ± 0.1	30 ± 6	120 ± 20
L	153	1.0 ± 0.1	1.2 ± 0.1	28 ± 8	150 ± 40
	173	[d]	[d]	[d]	[d]

[a] Peak positions in ppm. L signifies a lignin peak, C signifies a 'crystalline' cellulose peak and others are from hemicellulose and minor contributions from amorphous cellulose.

[b] M_∞ represents the transverse ^{13}C magnetization that would have been generated if the CP transfer had been infinitely fast and if rotating-frame ^1H spin-lattice relaxation had been infinitely slow.

[c] M^*_∞ is the corresponding M_∞ value that has been corrected by the factor, $\{1 - \exp(-t/T_{1H})\}^{-1}$, for incomplete ^1H spin-lattice relaxation between CP scans.

[d] The signals at 22 and 173 ppm were not observed under these conditions.

Appendix D

Saturation recovery results

List of Figures

D4. Indirect measurement of T_{1H} by saturation recovery at 30 ^{o}C *after* pretreatment of poplar wood 10 % in 0.5 M H_2SO_4 at 150 ^{o}C.

D4a. Experimental ^{13}C CP-MAS NMR spectra.

D4b. Results of curve fitting of T_{1H}, M_{∞} to cellulose peaks in ^{13}C CP-MAS NMR spectra.

D4c. Results of curve fitting of T_{1H}, M_{∞} to hemicellulose peaks in ^{13}C CP-MAS NMR spectra.

D4d. Results of curve fitting of T_{1H}, M_{∞} to lignin peaks in ^{13}C CP-MAS NMR spectra.

List of Tables

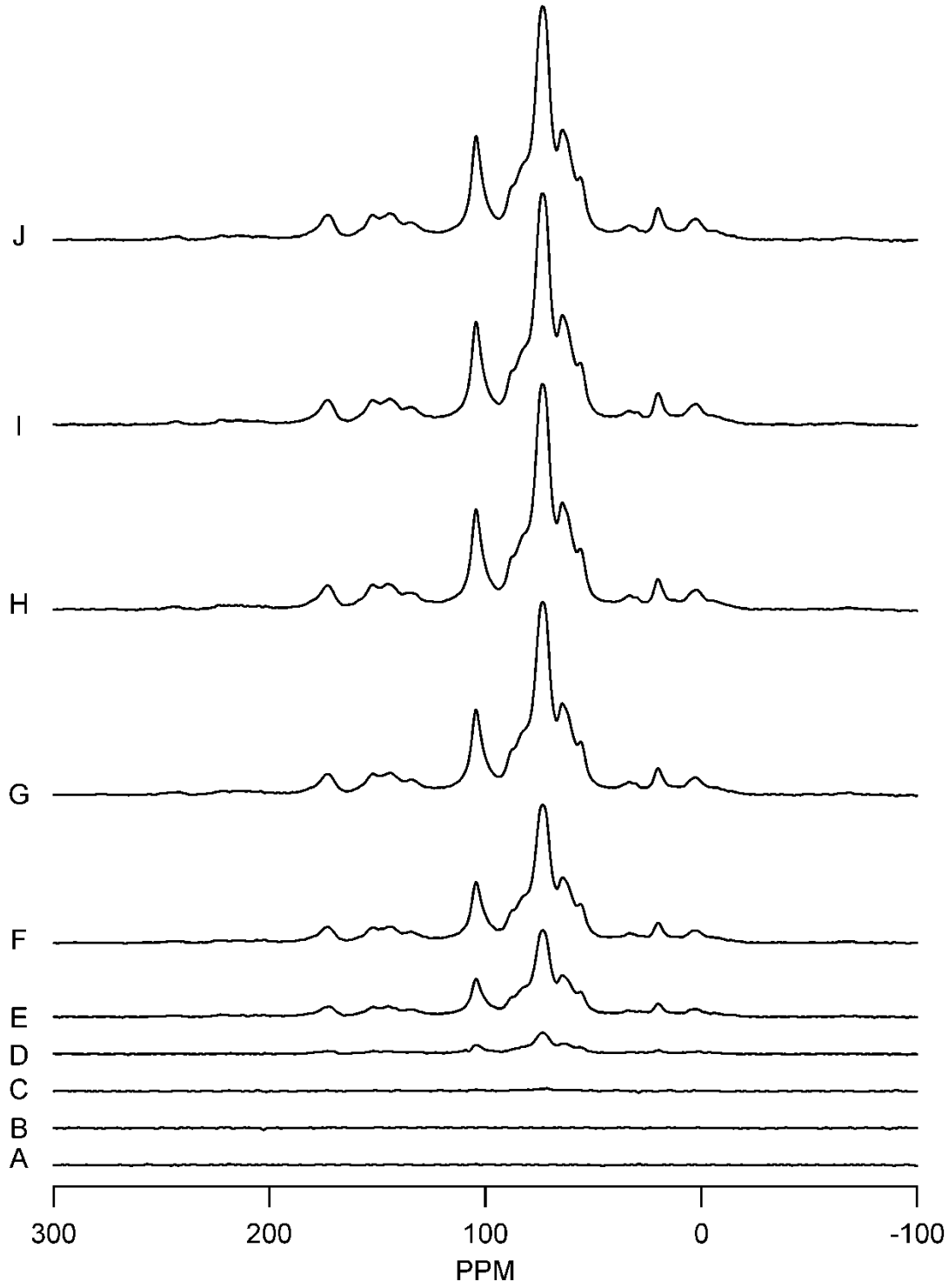

Figure D1a. Experimental ^{13}C CP-MAS NMR spectra from indirect measurement of T_{1H} by saturation recovery at 30 ^{o}C on dry wood. Recovery times: A. 0.1 ms. B. 1 ms. C. 10 ms. D. 100 ms. E. 500 ms. F. 1 s. G. 2 s. H. 4 s. I. 6 s. J. 8 s.

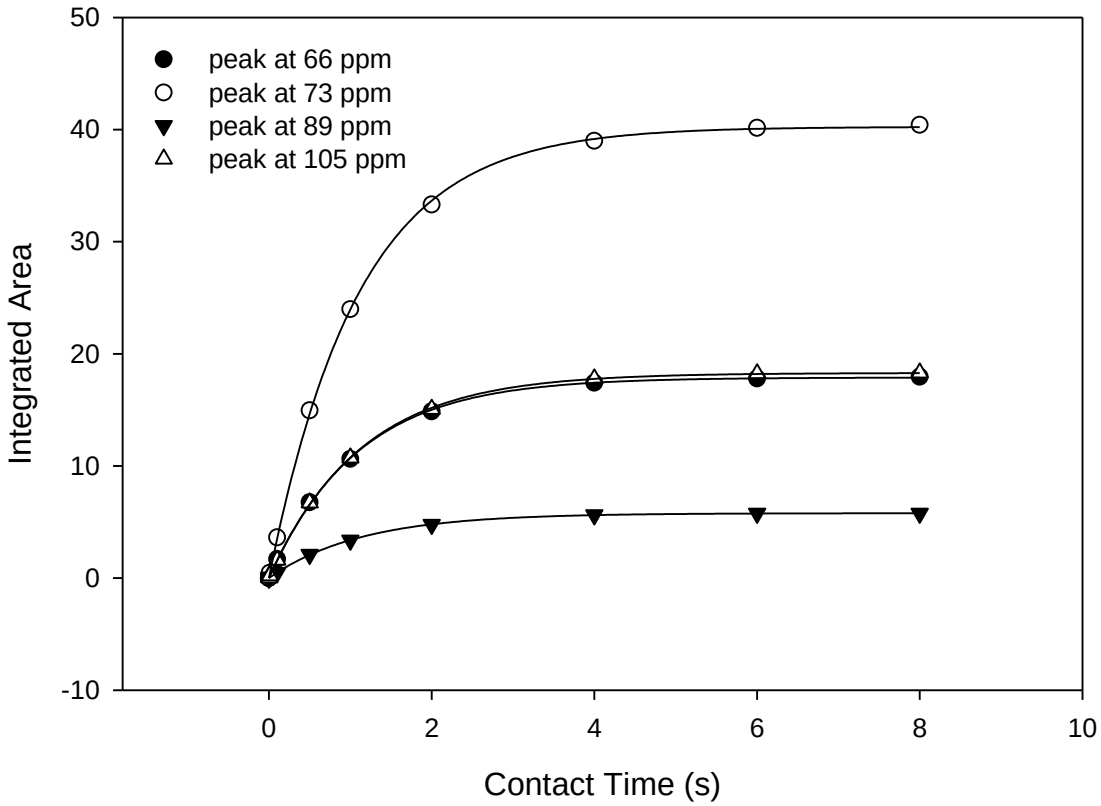

Figure D1b. Curve fitting of saturation recovery results for integrated intensities of cellulose peaks in CP-MAS ^{13}C NMR spectra (Fig. D1a) of dry poplar at 30 ^{o}C to eq. 2.2.

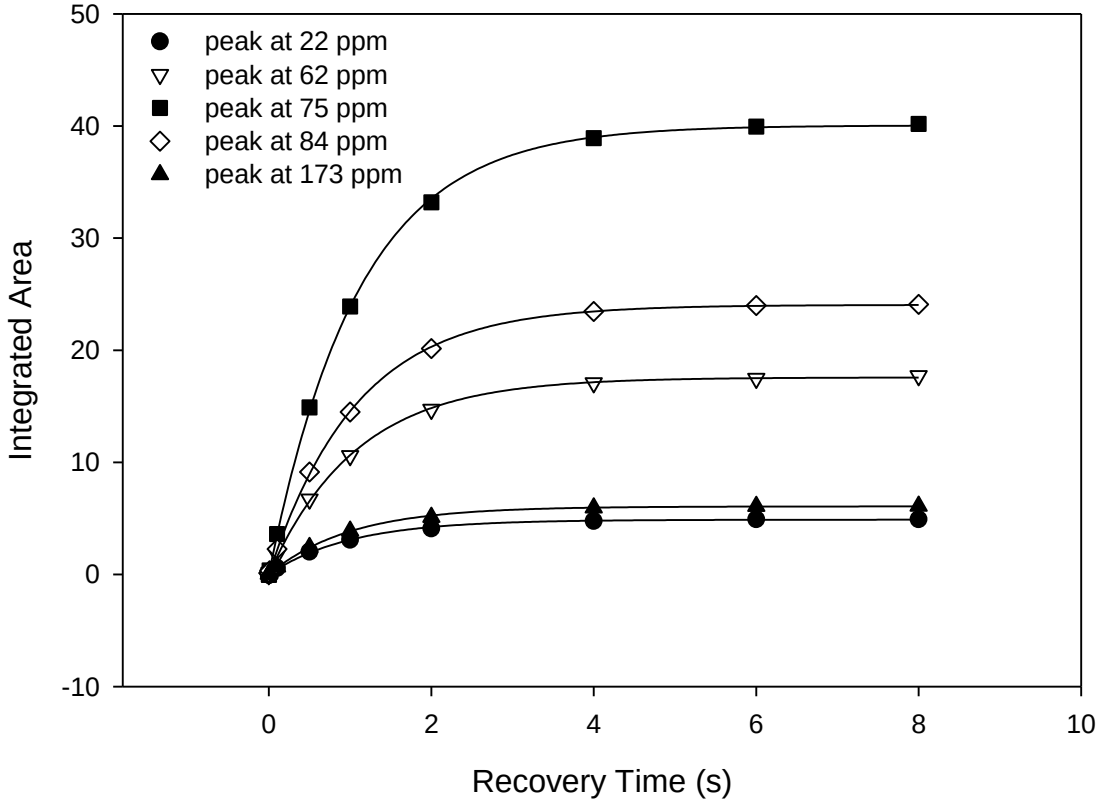

Figure D1c. Curve fitting of saturation recovery results for integrated intensities of hemicellulose peaks in CP-MAS ^{13}C NMR spectra (Fig. D1a) of dry poplar at 30 ^{o}C to eq. 2.2.

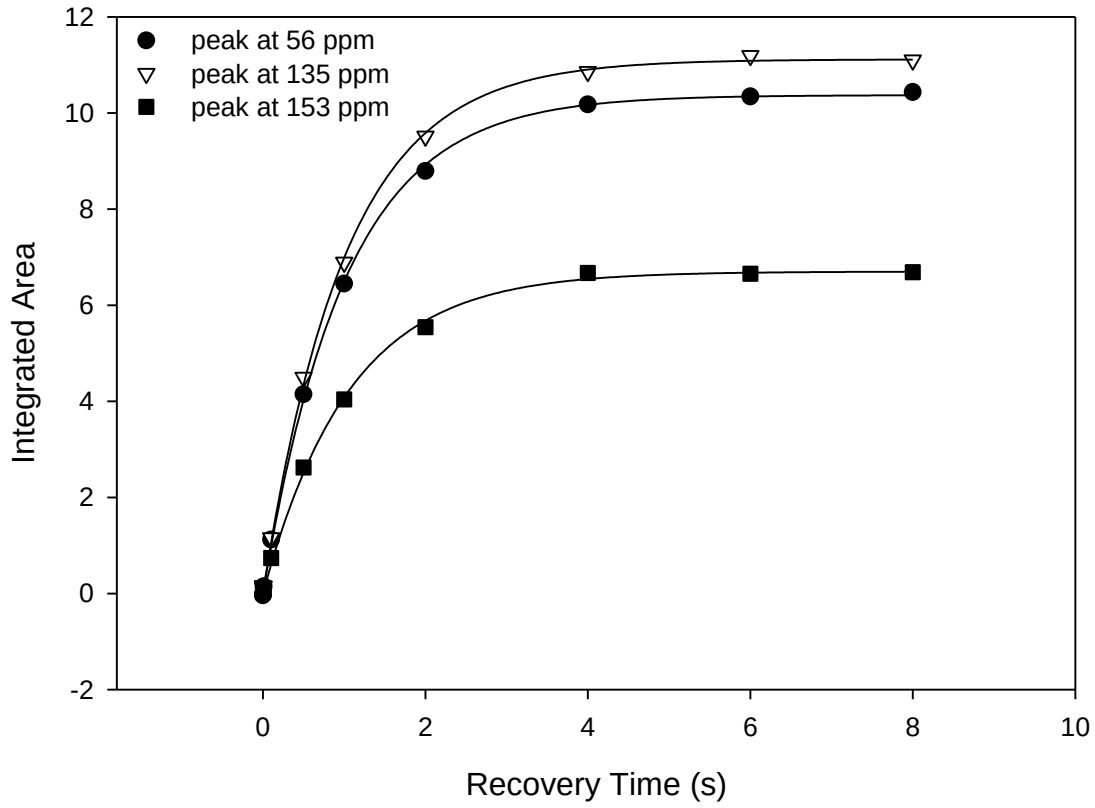

Figure D1d. Curve fitting of saturation recovery results for integrated intensities of lignin peaks in CP-MAS ^{13}C NMR spectra (Fig. D1a) of dry poplar at 30 ^{o}C to eq. 2.2.

Table D1. Results of curve fitting of integrated intensities in experimental indirect measurement of T_{1H} by saturation recovery on dry poplar at 30 ^{o}C.

Peak	M	T_{1H} (s)
21	4.9 ± 0.1	1.0 ± 0.1
56	10.4 ± 0.1	1.0 ± 0.1
62	17.6 ± 0.1	1.1 ± 0.1
65	17.9 ± 0.1	1.1 ± 0.1
72	40 ± 1	1.1 ± 0.1
75	40 ± 1	1.1 ± 0.1
83	24 ± 1	1.1 ± 0.1
89	5.8 ± 0.1	1.1 ± 0.1
105	18.3 ± 0.1	1.1 ± 0.1
135	11.1 ± 0.1	1.0 ± 0.1
153	6.7 ± 0.1	1.1 ± 0.1
173	2.5 ± 0.1	1.0 ± 0.1

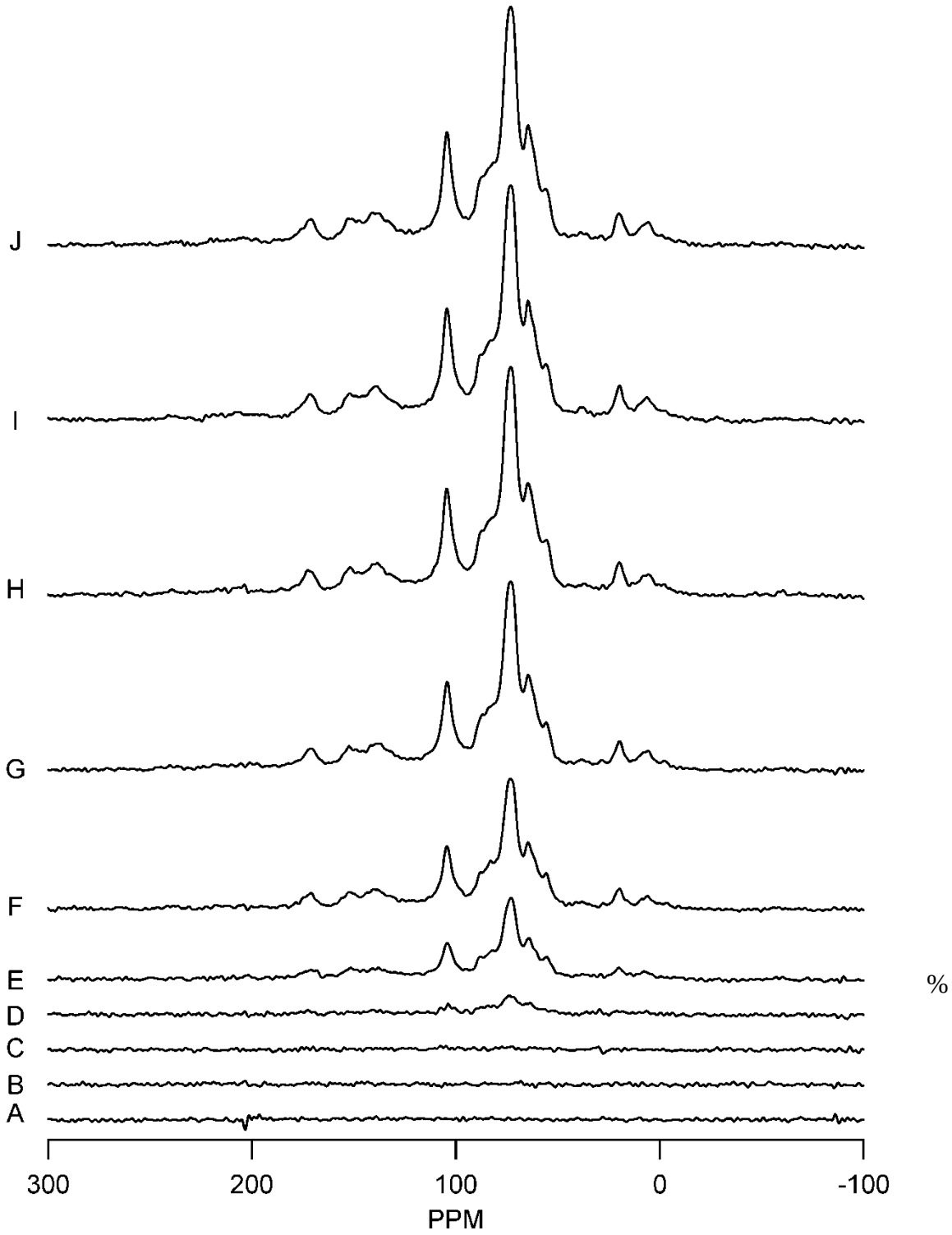

Figure D2a. Experimental ^{13}C CP-MAS NMR spectra from indirect measurement of T_{1H} by saturation recovery on 20 mg wood 10 % in 0.5 M H_2SO_4 at 30 ^{o}C *before* pretreatment at 150 ^{o}C. Recovery times: A. 0.1 ms. B. 1 ms. C. 10 ms. D. 100 ms. E. 500 ms. F. 1 s. G. 2 s. H. 4 s. I. 6 s. J. 8 s.

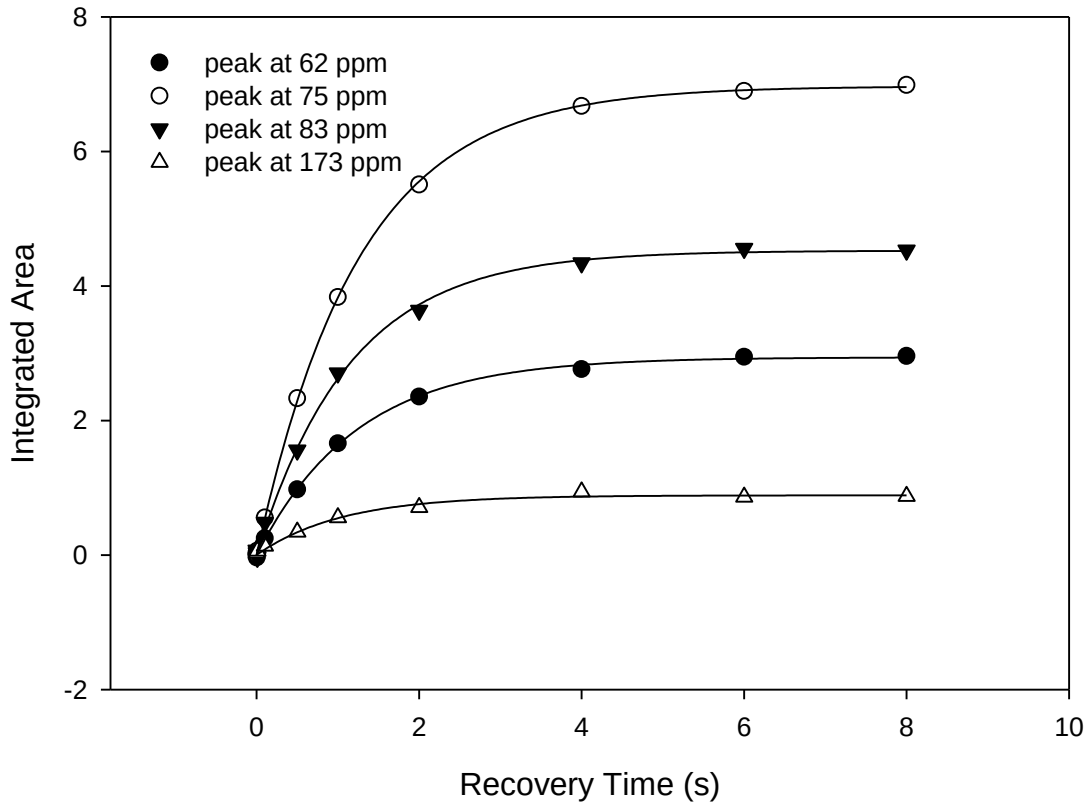

Figure D2c. Curve fitting of saturation recovery results for integrated intensities of hemicellulose peaks in CP-MAS ^{13}C NMR spectra (Fig. D2a) on 20 mg enriched wood 10 % in 0.5 M H_2SO_4 at 30 ^{o}C *before* pretreatment to eq. 2.2.

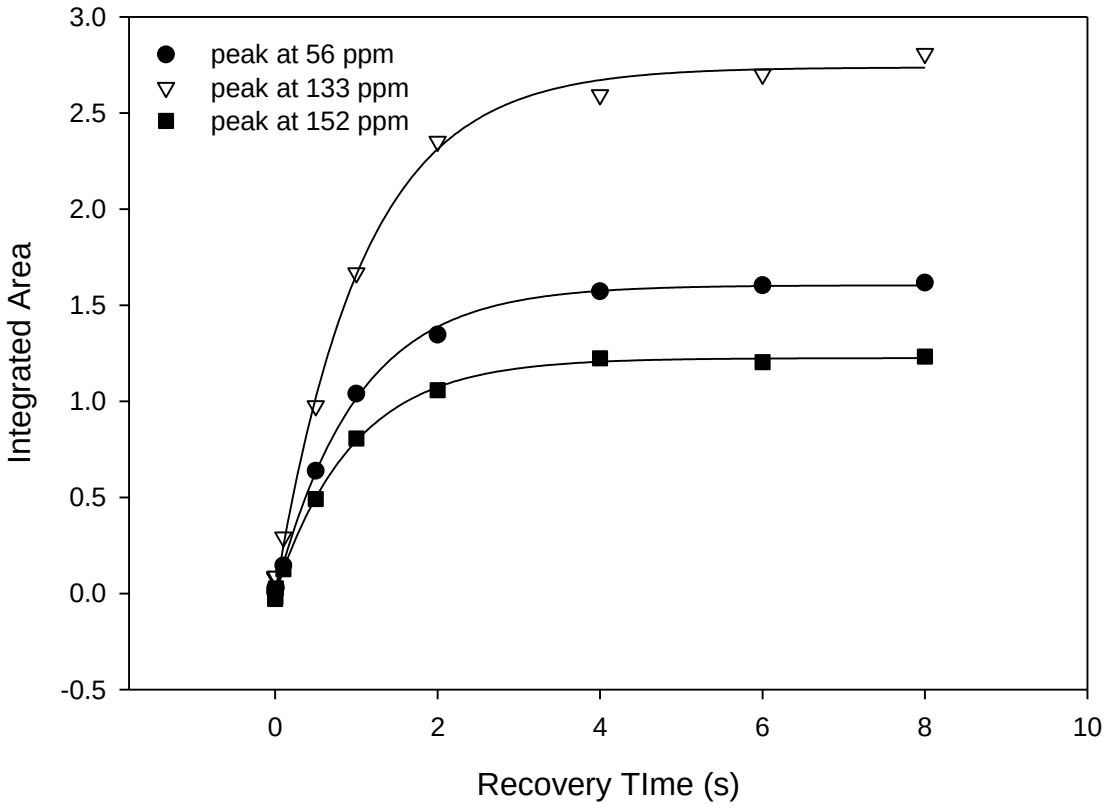

Figure D2d. Curve fitting of saturation recovery results for integrated intensities of lignin peaks in CP-MAS ^{13}C NMR spectra (Fig. D2a) on 20 mg enriched wood 10 % in 0.5 M H_2SO_4 at 30 ^{o}C *before* pretreatment to eq. 2.2.

Table D2. Results of curve fitting of integrated intensities in experimental indirect measurement of T_{1H} by saturation recovery on 10 % poplar in 0.5 M H_2SO_4 at 30 ^{o}C *before* pretreatment at 150 ^{o}C.

Peak	M	T_{1H} (s)
21	0.9 ± 0.1	1.1 ± 0.1
56	1.6 ± 0.1	1.0 ± 0.1
62	2.9 ± 0.1	1.2 ± 0.1
65	3.4 ± 0.1	1.2 ± 0.1
72	7.3 ± 0.1	1.3 ± 0.1
75	6.7 ± 0.1	1.3 ± 0.1
83	4.5 ± 0.1	1.2 ± 0.1
89	1.3 ± 0.1	1.2 ± 0.1
105	3.5 ± 0.1	1.3 ± 0.1
135	2.7 ± 0.1	1.1 ± 0.1
153	1.2 ± 0.1	1.0 ± 0.1
173	0.9 ± 0.1	1.0 ± 0.1

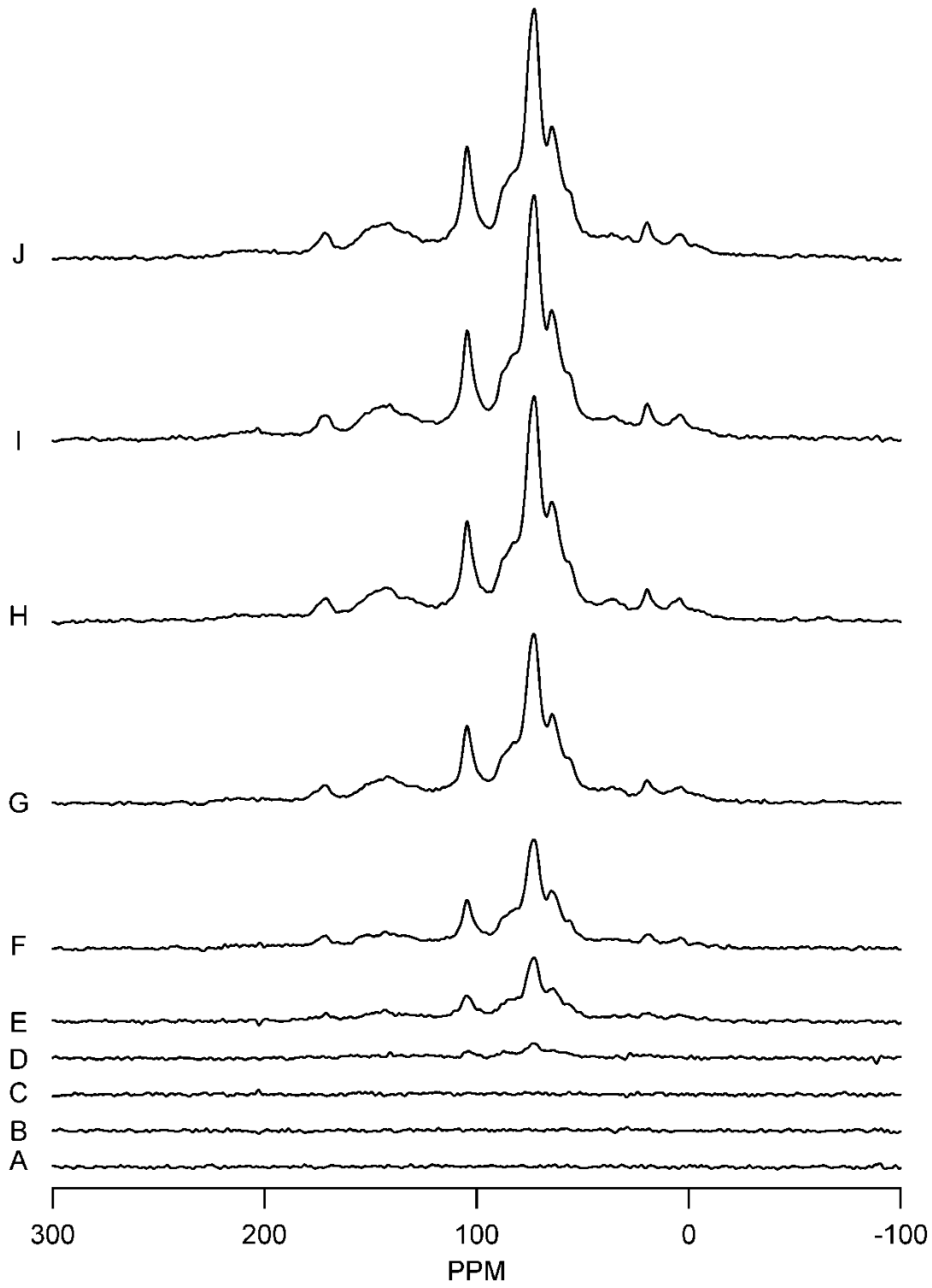

Figure D3a. Experimental ^{13}C CP-MAS NMR spectra from indirect measurement of T_{1H} by saturation recovery on 20 mg enriched wood 10 % in 0.5 M H_2SO_4 at 150 ^{o}C *during* pretreatment. Recovery times: A. 0.1 ms. B. 1 ms. C. 10 ms. D. 100 ms. E. 500 ms. F. 1 s. G. 2 s. H. 4 s. I. 6 s. J. 8 s.

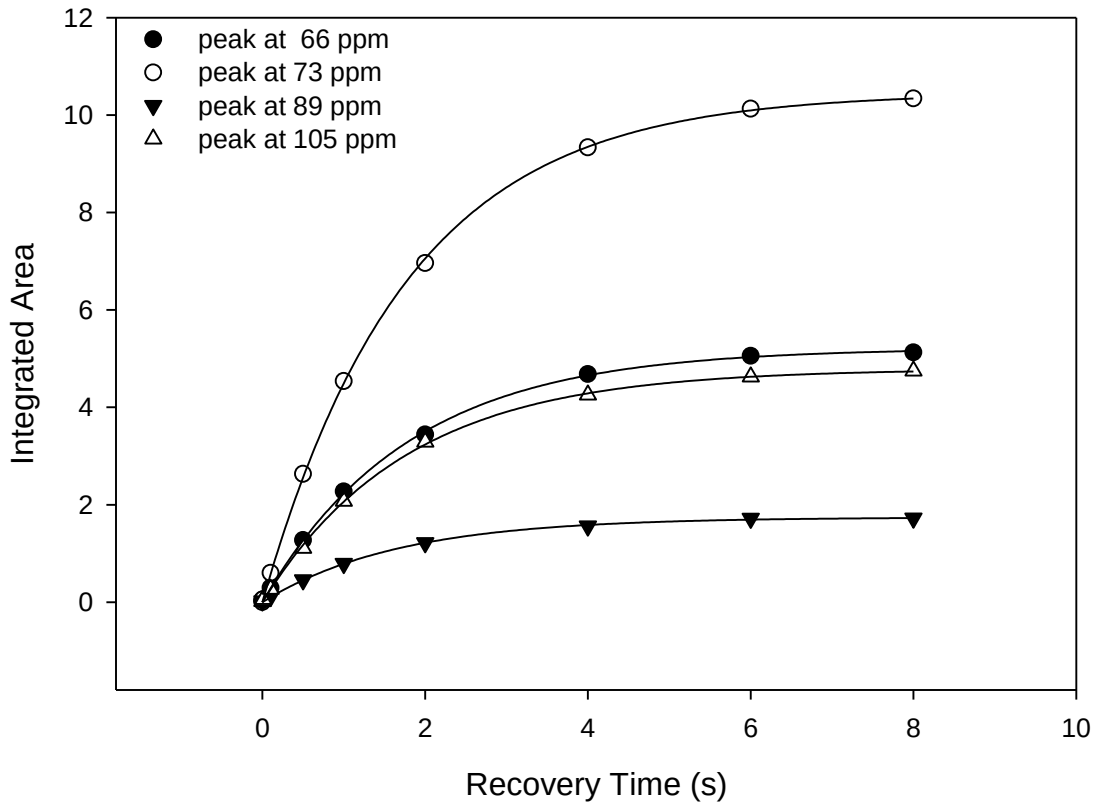

Figure D3b. Curve fitting of saturation recovery results for integrated intensities of cellulose peaks in CP-MAS ^{13}C NMR spectra (Fig. D3a) on 20 mg enriched wood 10 % in 0.5 M H_2SO_4 at 150 ^{o}C *during* pretreatment to eq. 2.2.

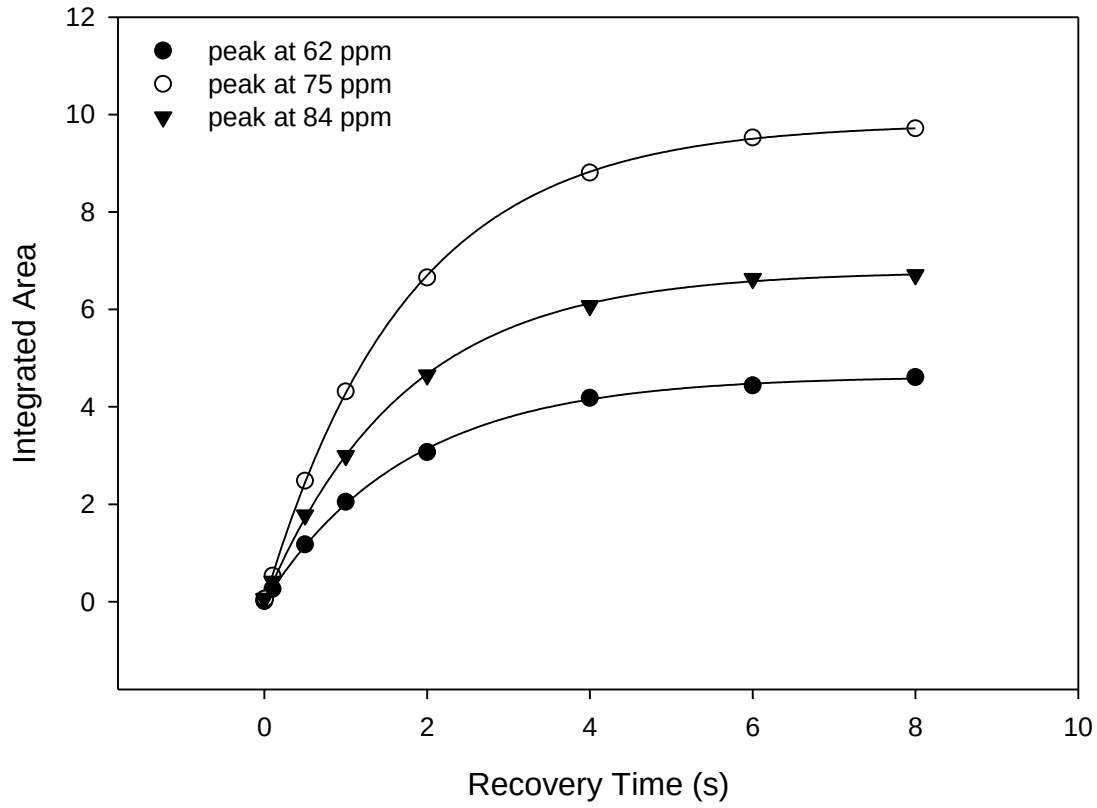

Figure D3c. Curve fitting of saturation recovery results for integrated intensities of hemicellulose peaks in CP-MAS ^{13}C NMR spectra (Fig. D3a) on 20 mg enriched wood 10 % in 0.5 M H_2SO_4 at 150 ^{o}C *during* pretreatment to eq. 2.2.

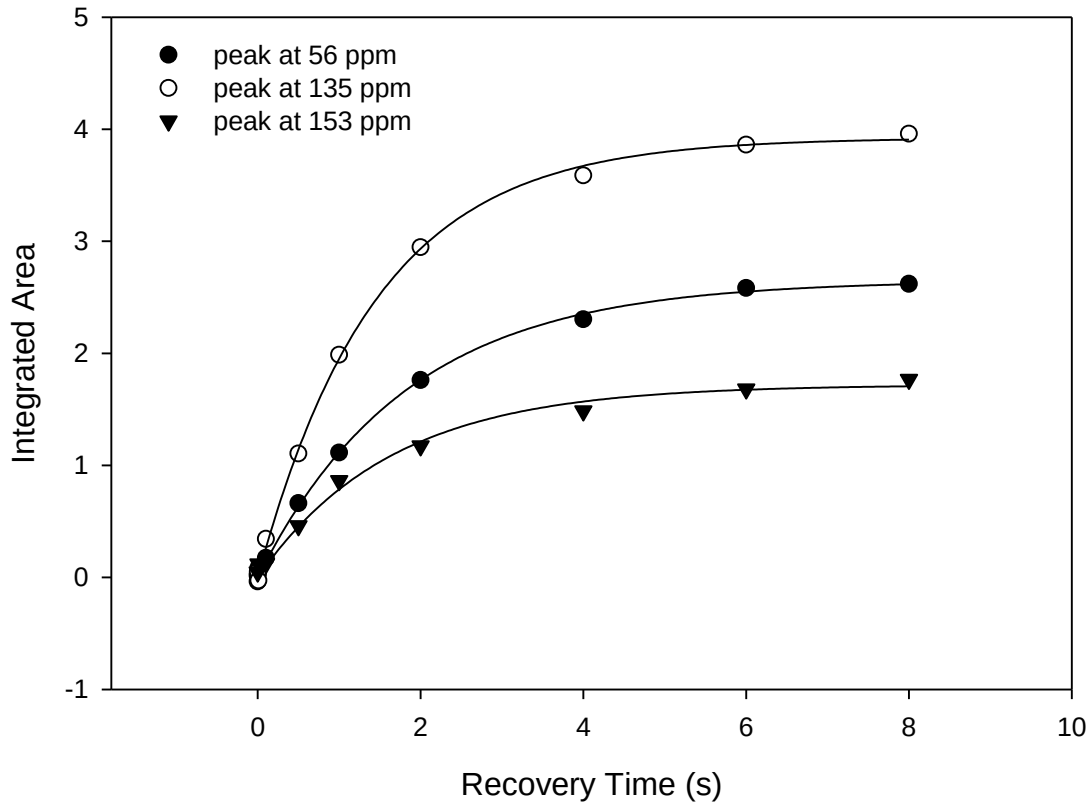

Figure D3d. Curve fitting of saturation recovery results for integrated intensities of lignin peaks in CP-MAS ^{13}C NMR spectra (Fig. D3a) on 20 mg enriched wood 10 % in 0.5 M H_2SO_4 at 150 ^{o}C *during* pretreatment to eq. 2.2.

Table D3. Results of curve fitting of integrated intensities in experimental indirect measurement of T_{1H} by saturation recovery on 10 % poplar in 0.5 M H_2SO_4 at 150 ^{o}C *during* pretreatment.

Peak	M	T_{1H} (s)
22	[d]	[d]
56	2.7 ± 0.1	1.8 ± 0.1
62	4.6 ± 0.1	1.8 ± 0.1
66	5.2 ± 0.1	1.8 ± 0.1
73	10.5 ± 0.1	1.8 ± 0.1
75	9.8 ± 0.1	1.7 ± 0.1
84	6.7 ± 0.1	1.7 ± 0.1
89	1.7 ± 0.1	1.7 ± 0.1
105	4.8 ± 0.1	1.8 ± 0.1
135	3.9 ± 0.1	1.5 ± 0.1
153	1.7 ± 0.1	1.6 ± 0.2
173	[d]	[d]

[d] not observed under these conditions

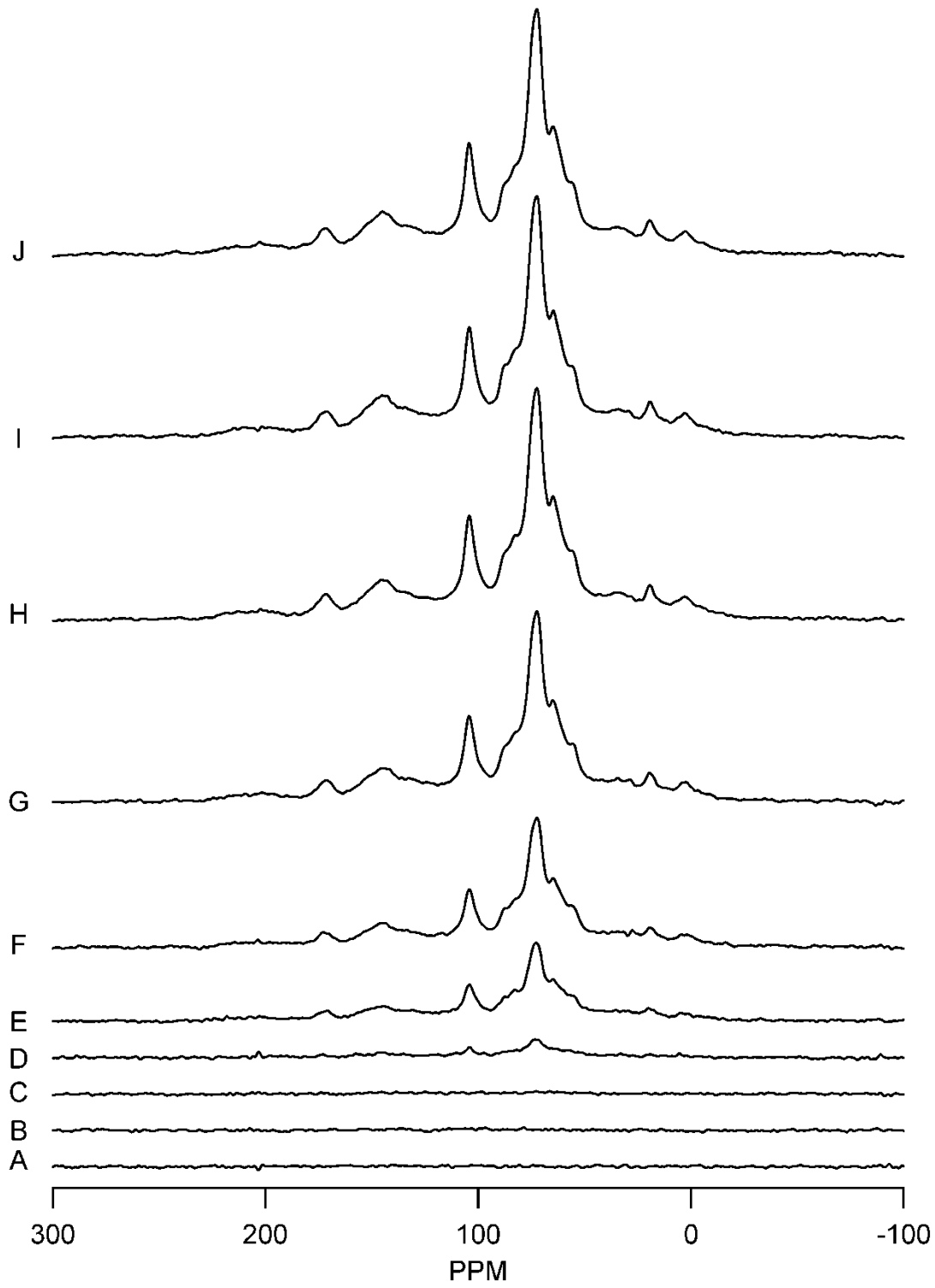

Figure D4a. Experimental ^{13}C CP-MAS NMR spectra from indirect measurement of T_{1H} by saturation recovery on 20 mg enriched wood 10 % in 0.5 M H_2SO_4 at 30 ^{o}C *after* pretreatment. Recovery times: A. 0.1 ms. B. 1 ms. C. 10 ms. D. 100 ms. E. 500 ms. F. 1 s. G. 2 s. H. 4 s. I. 6 s. J. 8 s.

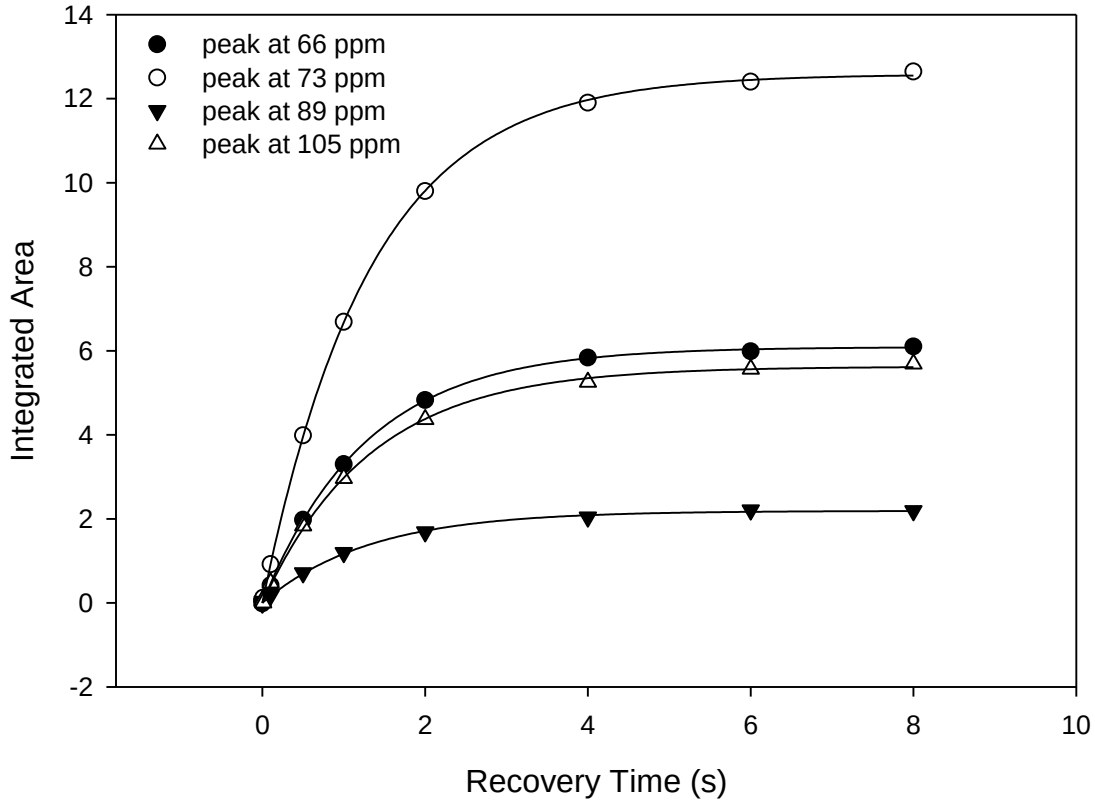

Figure D4b. Curve fitting of saturation recovery results for integrated intensities of cellulose peaks in CP-MAS ^{13}C NMR spectra (Fig. D4a) on 20 mg enriched wood 10 % in 0.5 M H_2SO_4 at 30 ^{o}C *after* pretreatment to eq. 2.2.

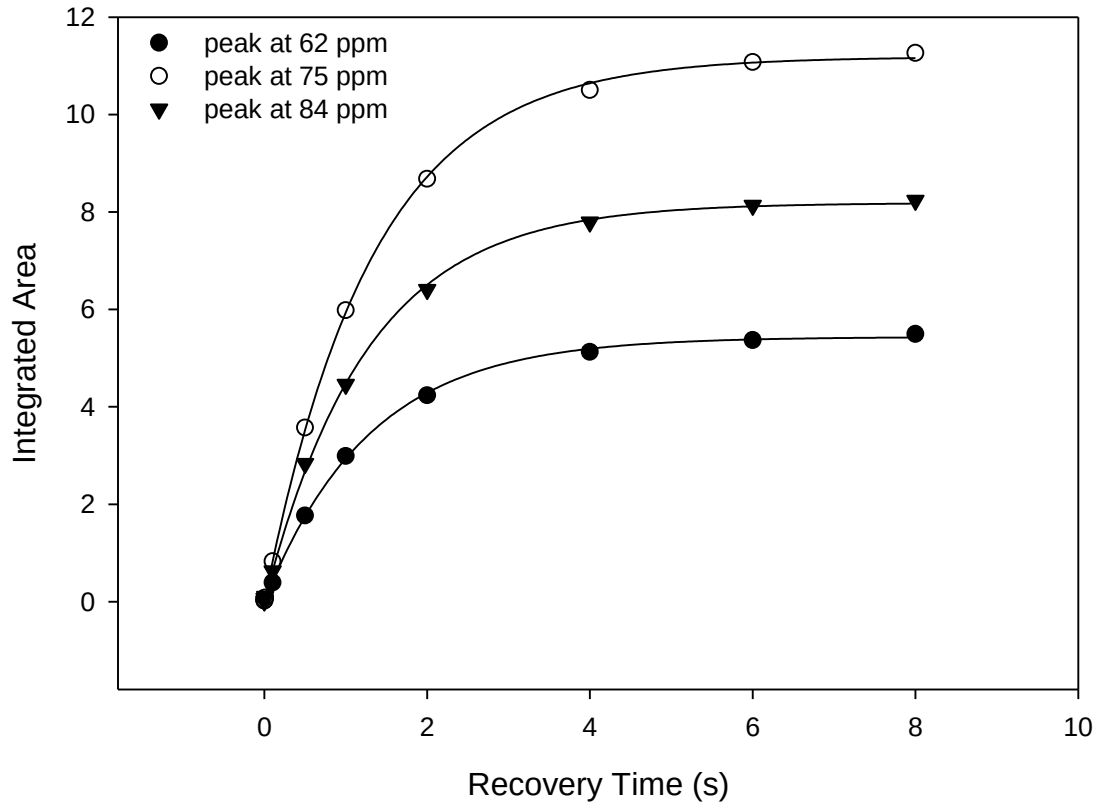

Figure D4c. Curve fitting of saturation recovery results for integrated intensities of hemicellulose peaks in CP-MAS ^{13}C NMR spectra (Fig. D4a) on 20 mg enriched wood 10 % in 0.5 M H_2SO_4 at 30 ^{o}C *after* pretreatment to eq. 2.2.

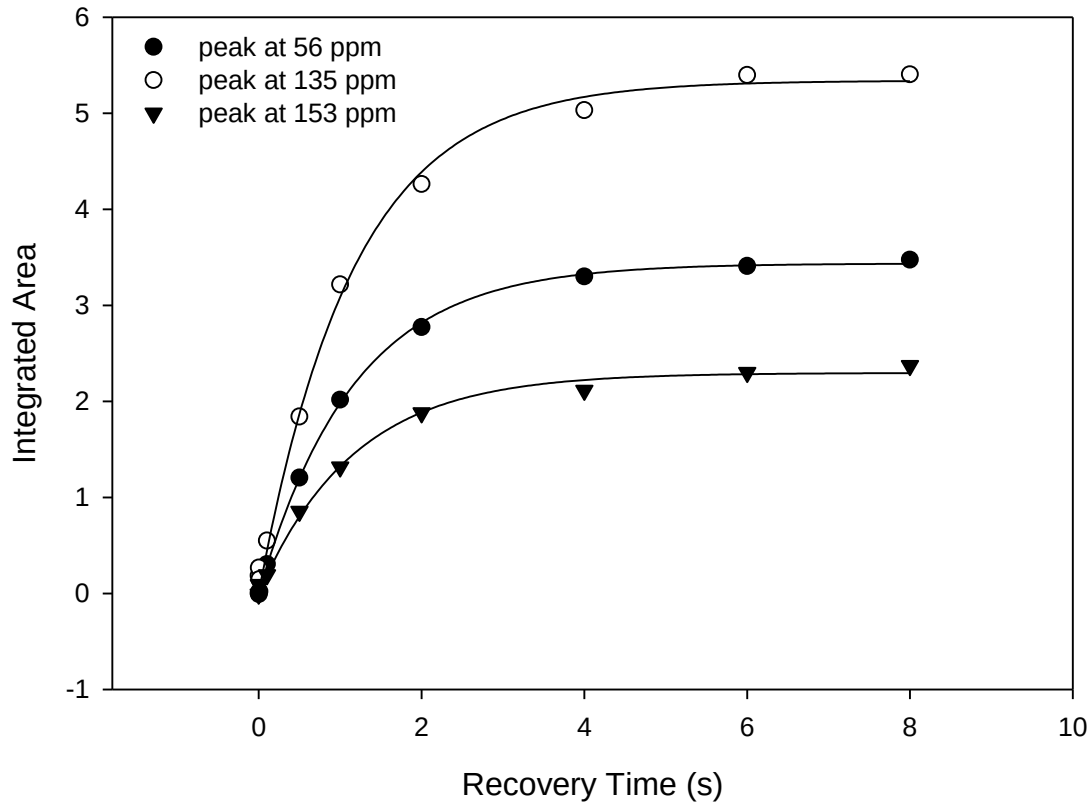

Figure D4d. Curve fitting of saturation recovery results for integrated intensities of lignin peaks in CP-MAS ^{13}C NMR spectra (Fig. D4a) on 20 mg enriched wood 10 % in 0.5 M H_2SO_4 at 30 ^{o}C *after* pretreatment to eq. 2.2

Table D4. Results of curve fitting of integrated intensities in experimental indirect measurement of T_{1H} by saturation recovery on 10 % poplar in 0.5 M H_2SO_4 at 30 ^{o}C *after* pretreatment at 150 ^{o}C.

Peak	M	T_{1H} (s)
22	[d]	[d]
56	3.4 ± 0.1	1.2 ± 0.1
62	5.4 ± 0.1	1.3 ± 0.1
66	6.1 ± 0.1	1.3 ± 0.1
73	12.6 ± 0.1	1.3 ± 0.1
75	11.2 ± 0.1	1.3 ± 0.1
84	8.2 ± 0.1	1.3 ± 0.1
89	2.2 ± 0.1	1.3 ± 0.1
105	5.6 ± 0.1	1.3 ± 0.1
135	5.3 ± 0.1	1.1 ± 0.1
153	2.3 ± 0.1	1.2 ± 0.1
173	[d]	[d]

[d] not observed under these conditions

Appendix E

^{13}C spin lattice measurement by the Torchia method.

List of Figures

E4. Determination of T_{1C} on 10 % poplar in 0.5 M H_2SO_4 by Torchia's method at 30 ^{o}C *after* pretreatment at 150 ^{o}C..

E4a. Experimental ^{13}C CP-MAS NMR spectra.

E4b. Results of curve fitting of T_{1C}, M to cellulose peaks in experimental ^{13}C CP-MAS NMR spectra.

E4c. Results of curve fitting of T_{1C}, M to hemicellulose peaks in experimental ^{13}C CP-MAS NMR spectra.

E4d. Results of curve fitting of T_{1C}, M to lignin peaks in experimental ^{13}C CP-MAS NMR spectra.

List of Tables

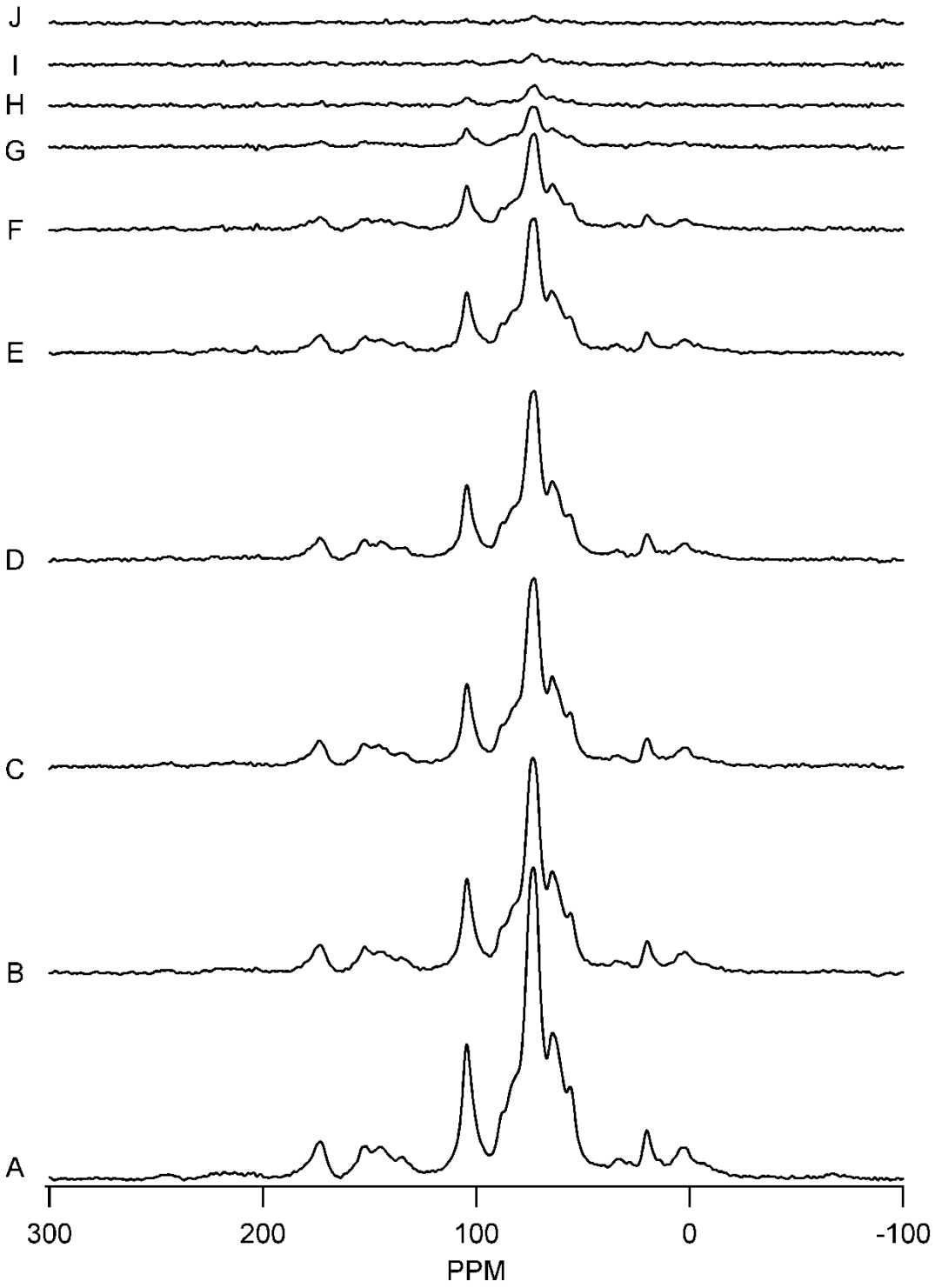

Figure E1a. CP-MAS spectra acquired from Torchia T_{1C} experiments on 20 mg dry enriched wood at 30 ^{o}C. Recovery times: A. 1 ms. B. 1.5 s. C. 2 s. D. 2.5 s. E. 3.5 s. F. 5 s. G. 9 s. H. 13 s. I. 17 s. J. 20 s.

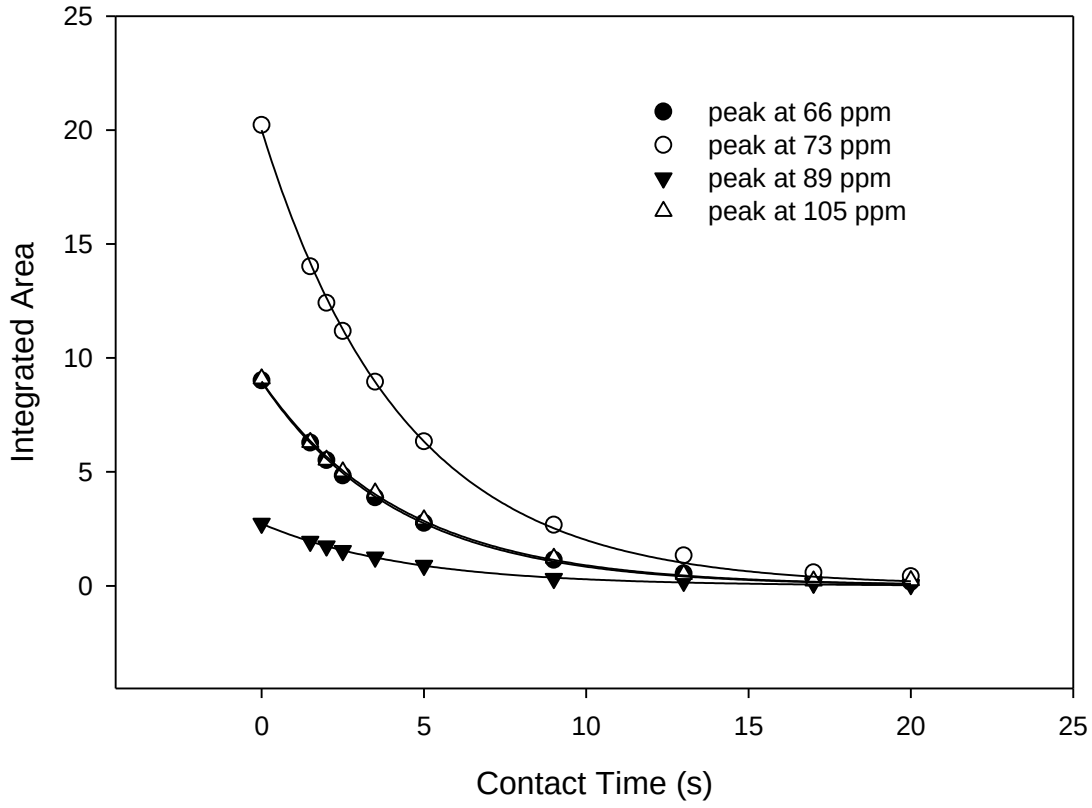

Figure E1b. Curve fitting of integrated intensities of cellulose peaks in ^{13}C CP-MAS NMR spectra (Fig. E1a) of dry poplar at 30 ^{o}C to eq. 2.3.

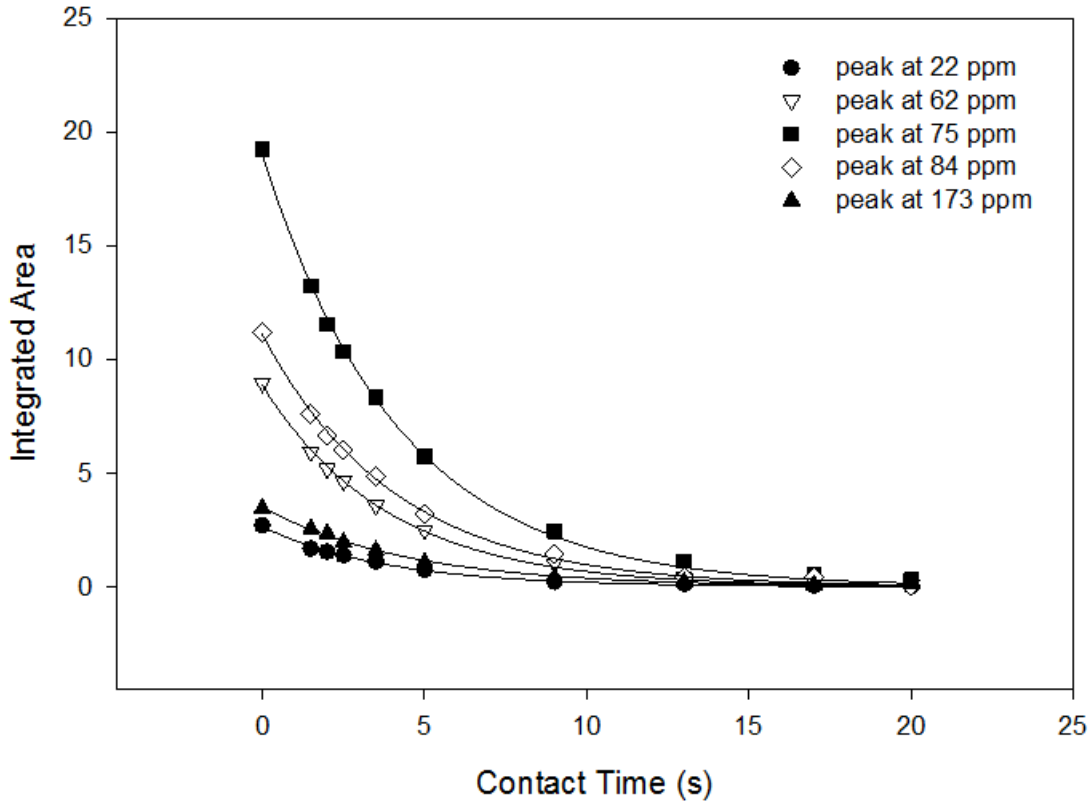

Figure E1c. Curve fitting of integrated intensities of hemicellulose peaks in ^{13}C CP-MAS NMR spectra (Fig. E1a) of dry poplar at 30 ^{o}C to eq. 2.3.

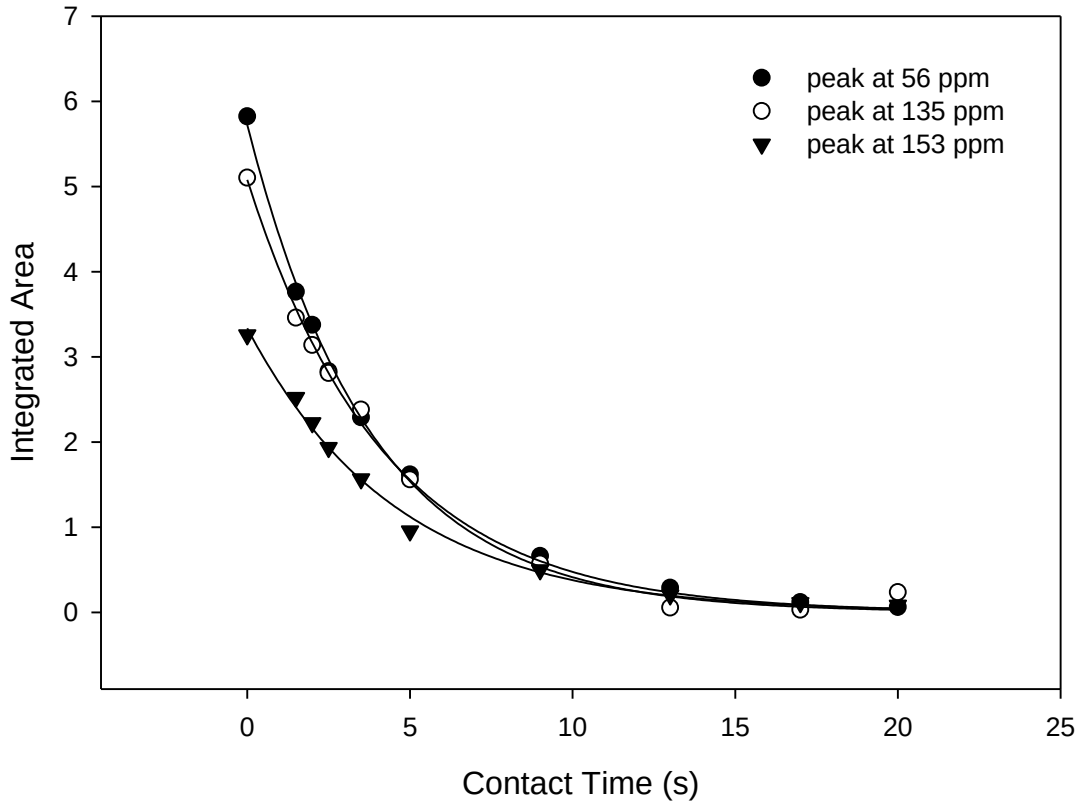

Figure E1d. Curve fitting of integrated intensities of lignin peaks in ^{13}C CP-MAS NMR spectra (Fig. E1a) of dry poplar at 30 ^{o}C to eq. 2.3.

Table E1. Curve fitting results of integrated intensities from peaks measured by Torchia's method at 30 ^{o}C on dry poplar.

Peak	M	T_{1C} (s)
21	2.6 ± 0.1	3.9 ± 0.1
56	5.7 ± 0.1	3.8 ± 0.1
62	8.9 ± 0.1	3.9 ± 0.1
65	8.9 ± 0.1	4.2 ± 0.1
72	20 ± 1	4.3 ± 0.1
75	19 ± 1	4.2 ± 0.1
83	11 ± 1	4.1 ± 0.2
89	2.7 ± 0.1	4.4 ± 0.1
105	9.0 ± 0.1	4.4 ± 0.1
135	5.1 ± 0.1	4.2 ± 0.2
153	3.3 ± 0.1	4.6 ± 0.2
173	3.5 ± 0.1	4.5 ± 0.2

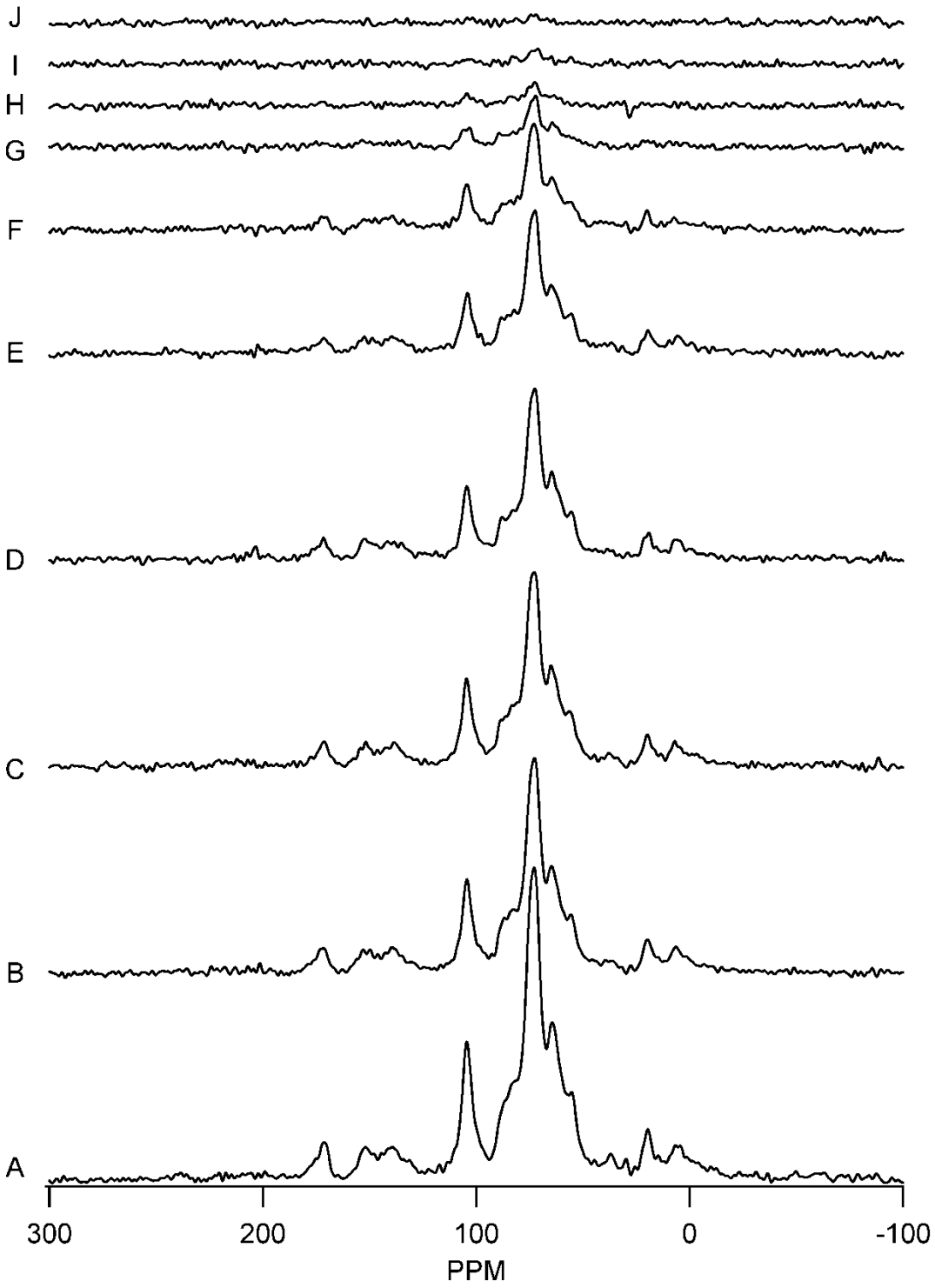

Figure E2a. CP-MAS spectra acquired from Torchia T_{1C} experiments on 20 mg enriched wood 10 % in 0.5 M H_2SO_4 at 30 ^{o}C *before* pretreatment. Recovery times: A. 1 ms. B. 1.5 s. C. 2 s. D. 2.5 s. E. 3.5 s. F. 5 s. G. 9 s. H. 13 s. I. 17 s. J. 20 s.

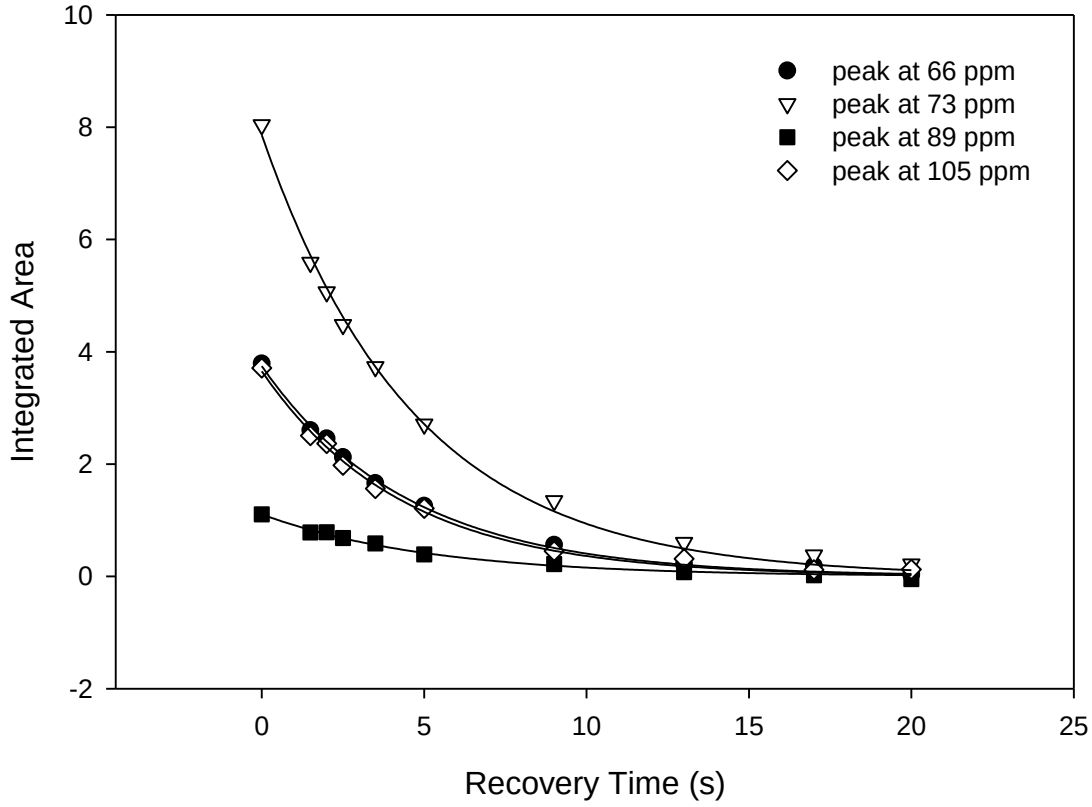

Figure E2b. Curve fitting of integrated intensities of cellulose peaks in ^{13}C CP-MAS NMR spectra (Fig. E2a) on 20 mg enriched wood 10 % in 0.5 M H_2SO_4 at 30 ^{o}C *before* pretreatment to eq. 2.3.

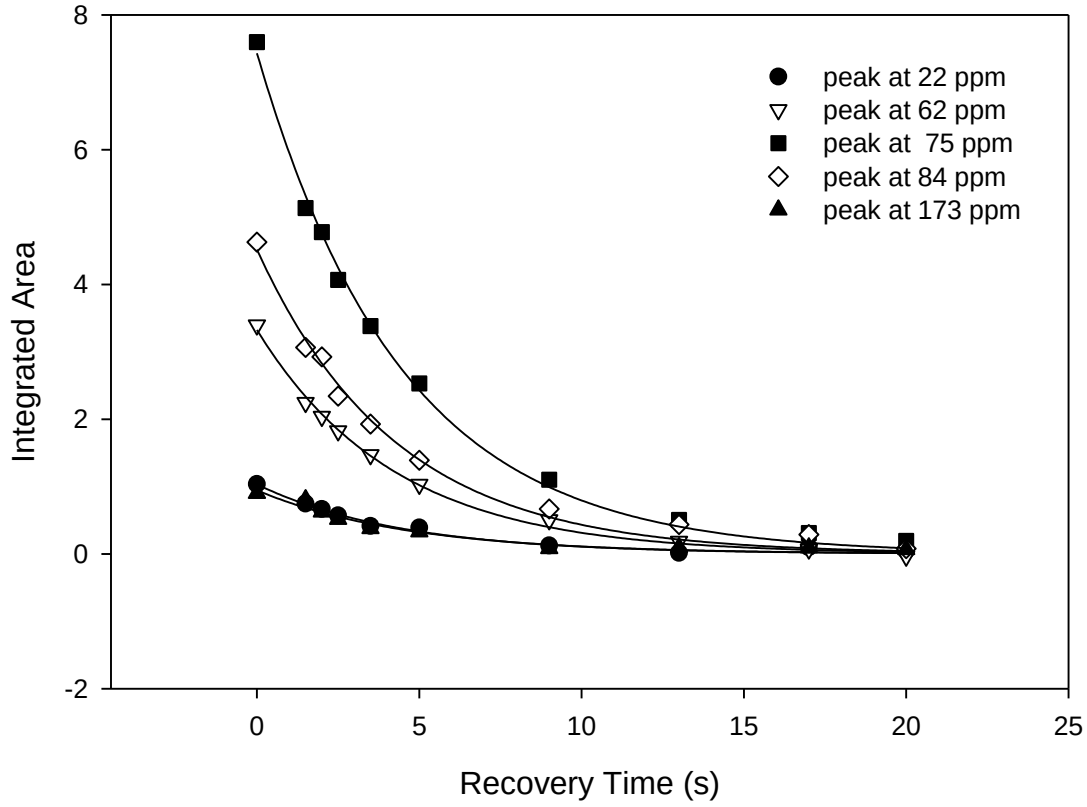

Figure E2c. Curve fitting of integrated intensities of hemicellulose peaks in ^{13}C CP-MAS NMR spectra (Fig. E2a) on 20 mg enriched wood 10 % in 0.5 M H_2SO_4 at 30 ^{o}C *before* pretreatment to eq. 2.3.

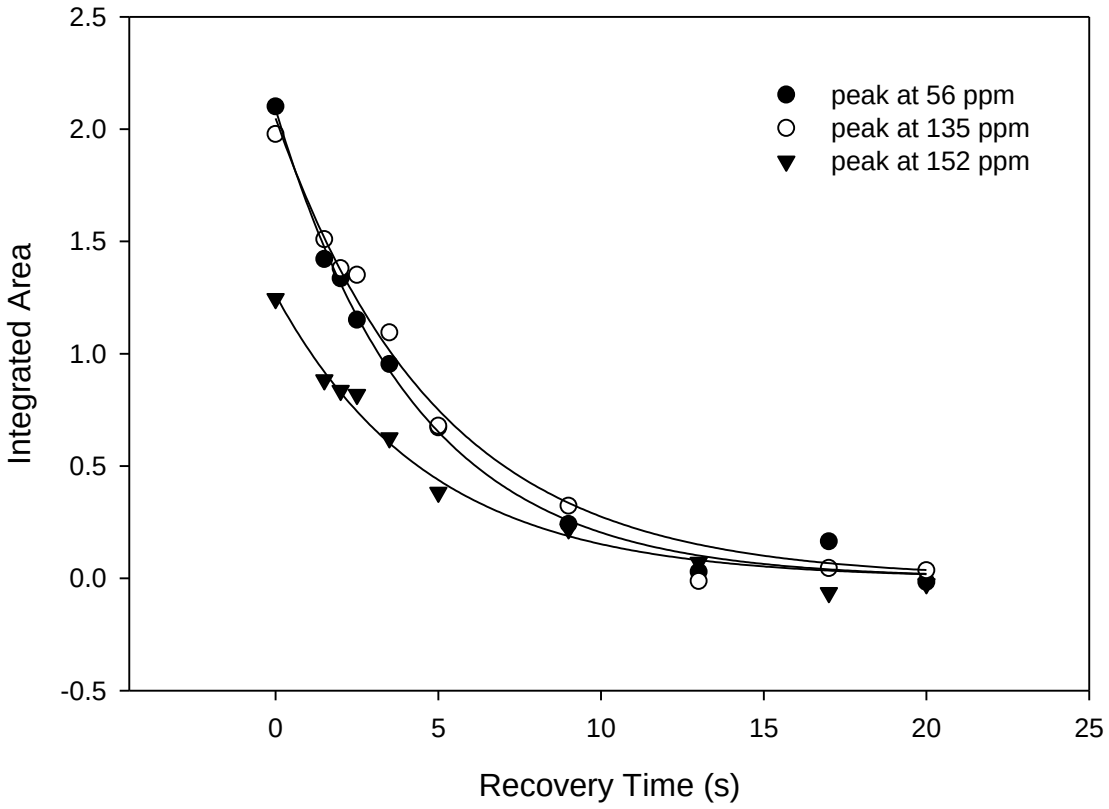

Figure E2d. Curve fitting of integrated intensities of lignin peaks in ^{13}C CP-MAS NMR spectra (Fig. E2a) on 20 mg enriched wood 10 % in 0.5 M H_2SO_4 at 30 ^{o}C *before* pretreatment to eq. 2.3.

Table E2. Curve fitting results of integrated intensities from peaks measured by Torchia's method on 10 % poplar in 0.5 M H_2SO_4 at 30 ^oC *before* pretreatment at 150 ^oC.

Peak	M	T_{1C} (s)
21	1.0 ± 0.1	4.4 ± 0.3
56	2.1 ± 0.1	4.3 ± 0.2
62	3.3 ± 0.1	4.2 ± 0.1
65	3.7 ± 0.1	4.5 ± 0.1
72	7.9 ± 0.1	4.7 ± 0.1
75	7.4 ± 0.1	4.5 ± 0.1
83	4.5 ± 0.1	4.3 ± 0.2
89	1.1 ± 0.1	5.1 ± 0.3
105	3.7 ± 0.1	4.3 ± 0.2
135	2.1 ± 0.1	5.0 ± 0.4
153	1.3 ± 0.1	4.7 ± 0.4
173	0.9 ± 0.1	4.7 ± 0.6

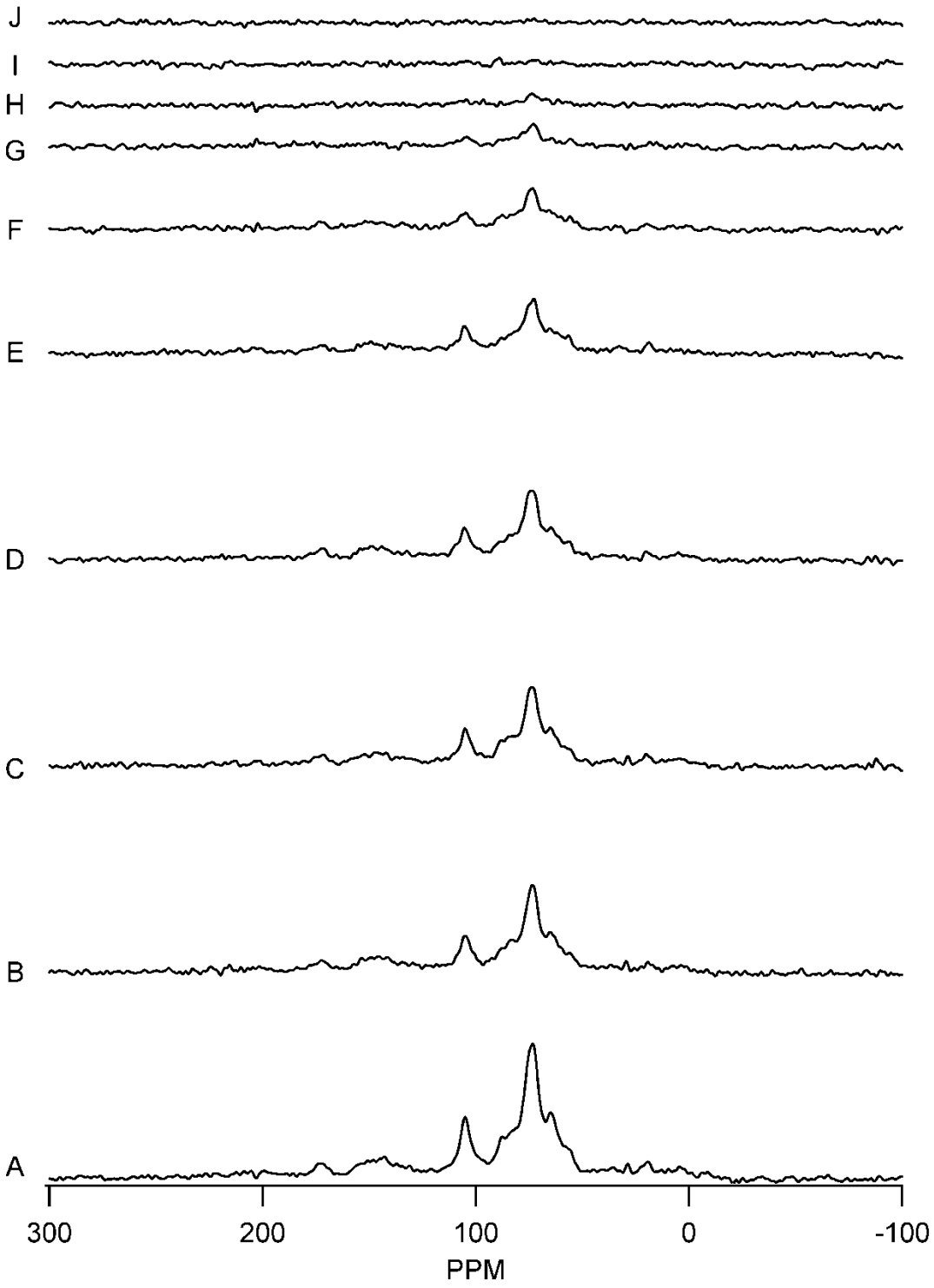

Figure E3a. CP-MAS spectra acquired from Torchia T_{1C} experiments on 20 mg enriched wood 10 % in 0.5 M H_2SO_4 at 150 ^{o}C *during* pretreatment. Recovery times: A. 1 ms. B. 1.5 s. C. 2 s. D. 2.5 s. E. 3.5 s. F. 5 s. G. 9 s. H. 13 s. I. 17 s. J. 20 s.

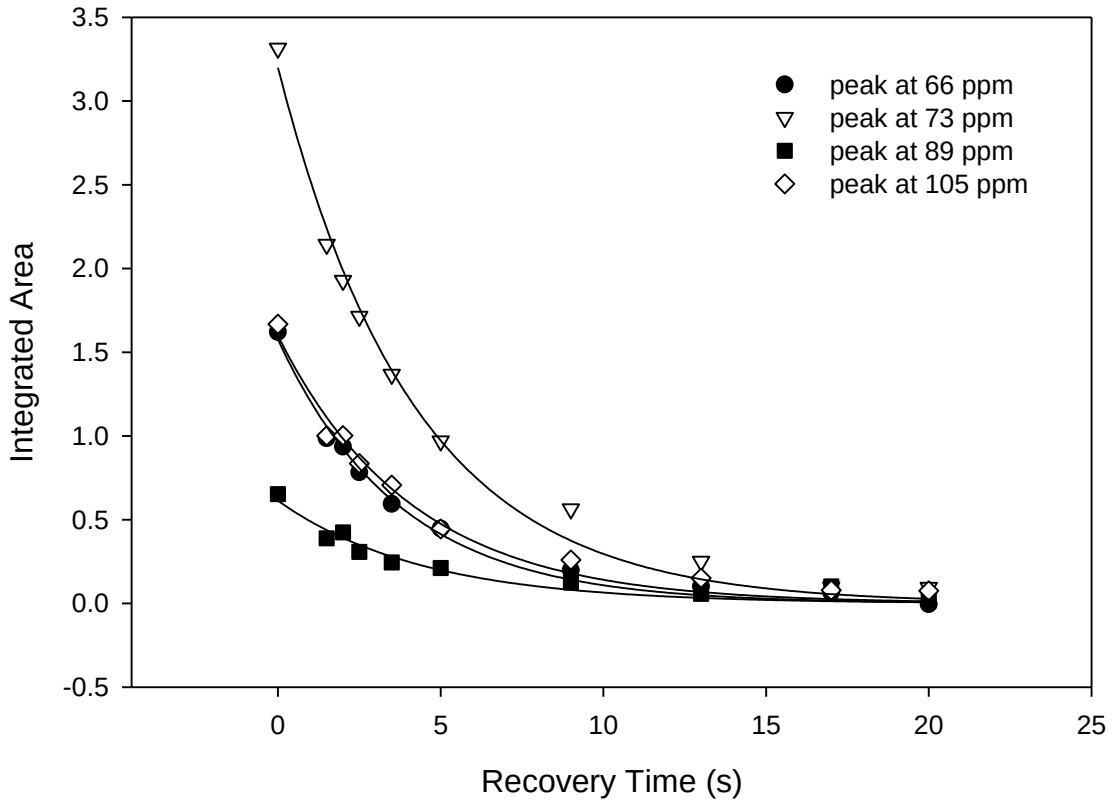

Figure E3b. Curve fitting of integrated intensities of cellulose peaks in ^{13}C CP-MAS NMR spectra (Fig. E3a) on 20 mg enriched wood 10 % in 0.5 M H_2SO_4 at 150 ^{o}C *during* pretreatment to eq. 2.3.

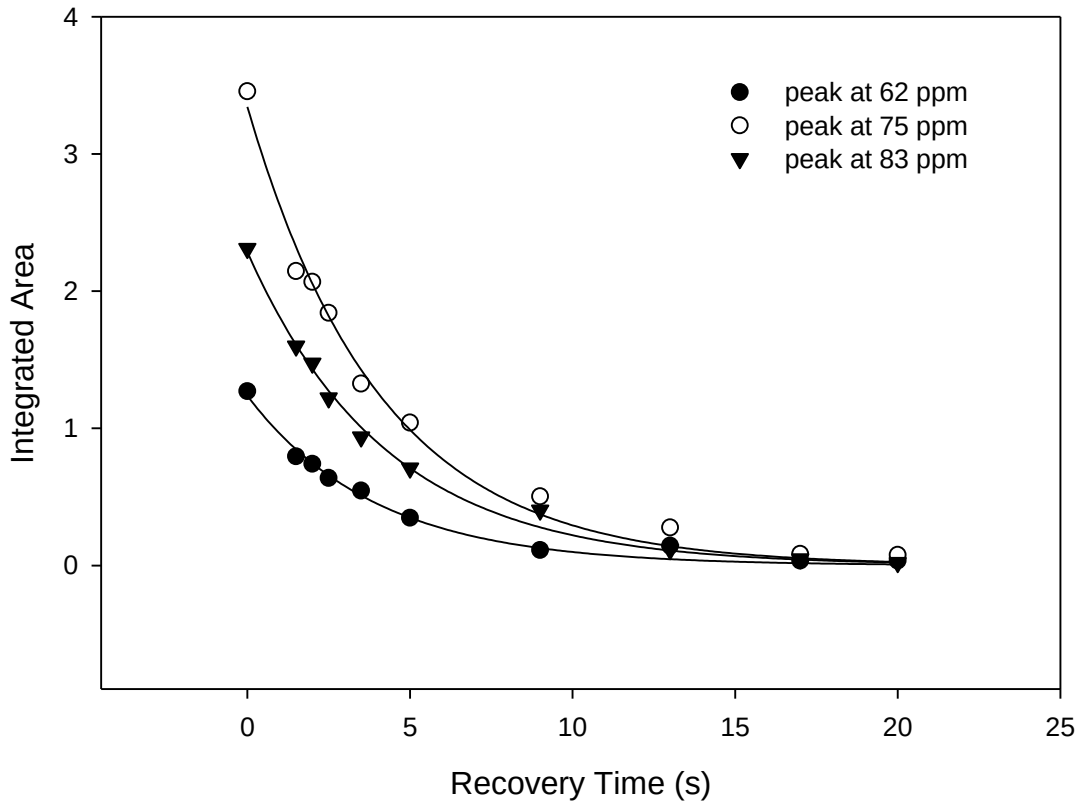

Figure E3c. Curve fitting of integrated intensities of hemicellulose peaks in ^{13}C CP-MAS NMR spectra (Fig. E3a) on 20 mg enriched wood 10 % in 0.5 M H_2SO_4 at 150 ^{o}C *during* pretreatment to eq. 2.3.

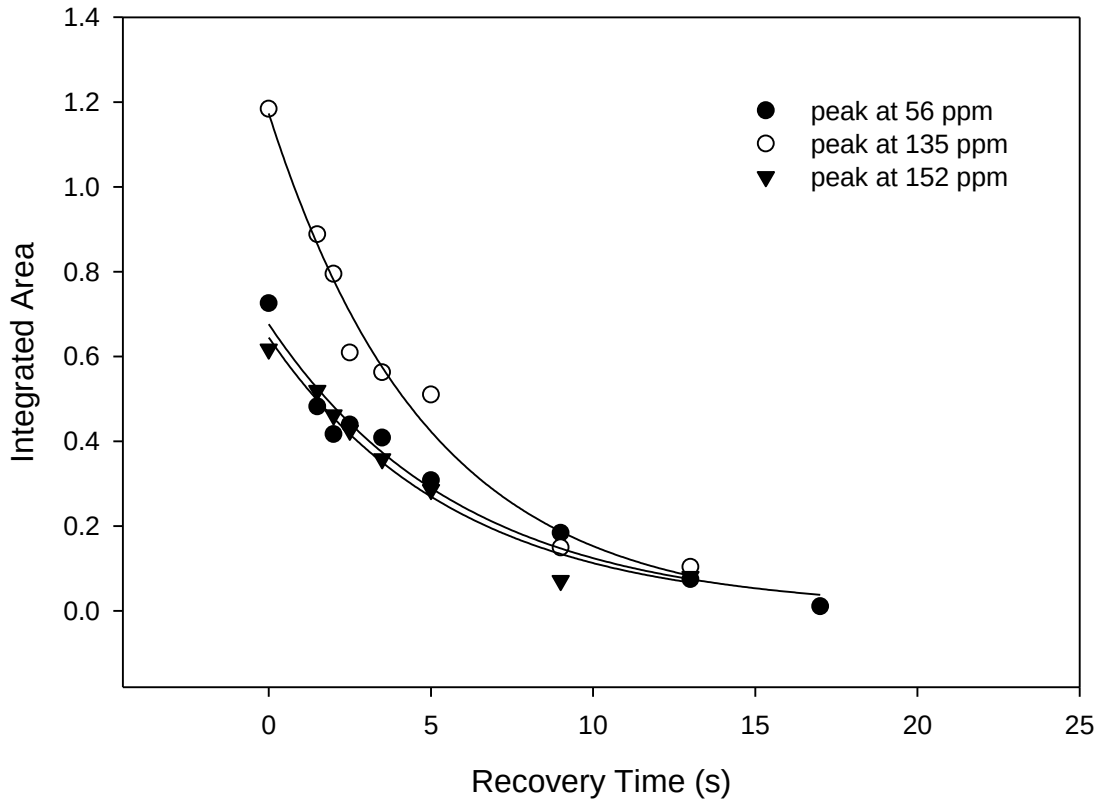

Figure E3d. Curve fitting of integrated intensities of lignin peaks in ^{13}C CP-MAS NMR spectra (Fig. E3a) on 20 mg enriched wood 10 % in 0.5 M H_2SO_4 at 150 ^{o}C *during* pretreatment to eq. 2.3.

Table E3. Curve fitting results of integrated intensities from peaks measured by Torchia's method *during* pretreatment on 10 % poplar in 0.5 M H_2SO_4 at 150 ^oC.

Peak	M	T_{1C} (s)
21	[d]	[d]
56	0.7 ± 0	5.9 ± 0.6
62	1.2 ± 0	3.9 ± 0.3
65	1.6 ± 0	3.7 ± 0.2
72	3.2 ± 0	4.1 ± 0.2
75	3.3 ± 0	4.1 ± 0.2
83	2.3 ± 0	4.3 ± 0.2
89	0.6 ± 0	4.4 ± 0.6
105	1.6 ± 0	4.1 ± 0.3
135	1.2 ± 0	4.7 ± 0.4
153	0.7 ± 0	4.1 ± 0.2
173	[d]	[d]

[d] not observed under these conditions

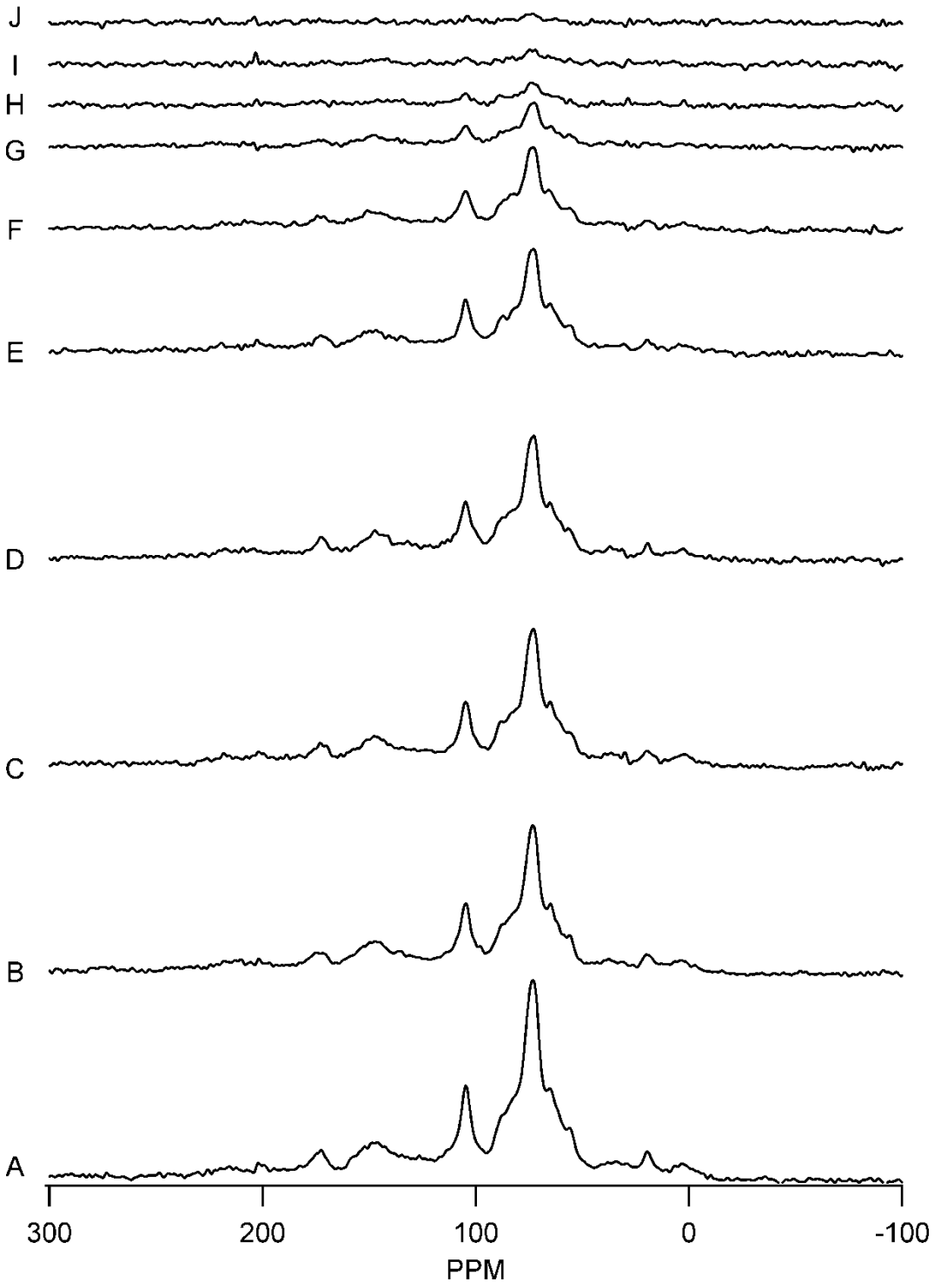

Figure E4a. CP-MAS spectra acquired from Torchia T_{1C} experiments on 20 mg enriched wood 10 % in 0.5 M H_2SO_4 at 30 ^{o}C *after* pretreatment. Recovery times: A. 1 ms. B. 1.5 s. C. 2 s. D. 2.5 s. E. 3.5 s. F. 5 s. G. 9 s. H. 13 s. I. 17 s. J. 20 s.

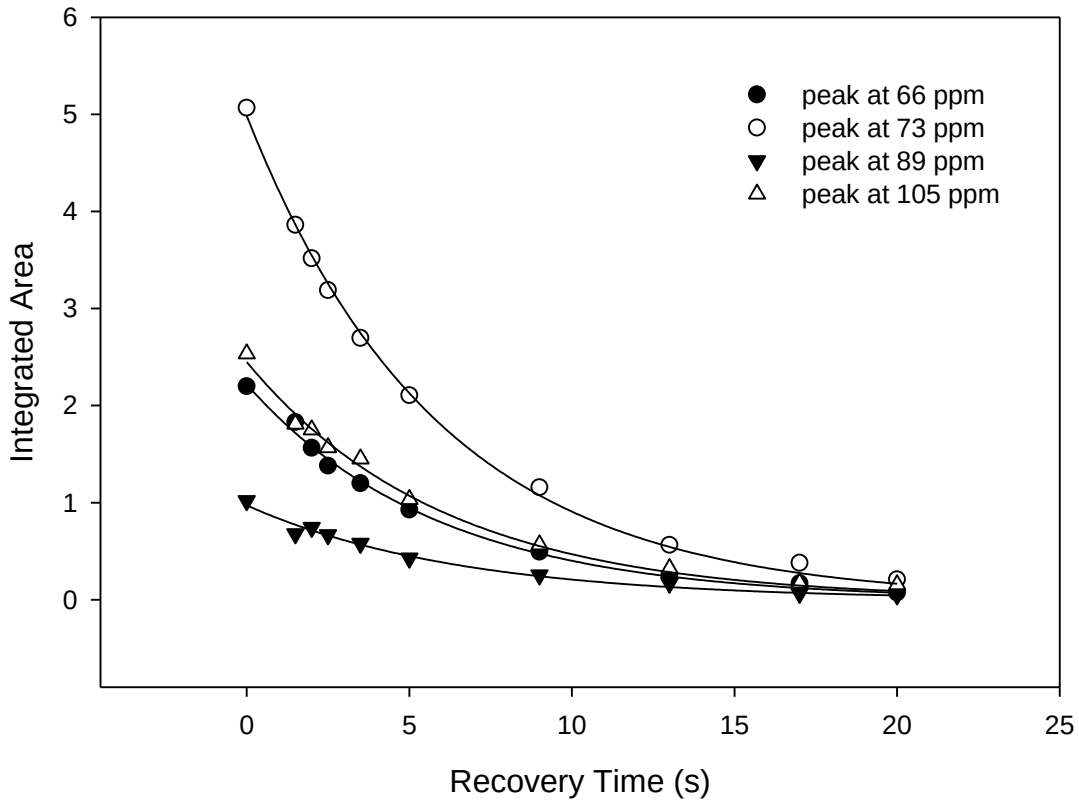

Figure E4b. Curve fitting of integrated intensities of cellulose peaks in ^{13}C CP-MAS NMR spectra (Fig. E4a) on 20 mg enriched wood 10 % in 0.5 M H_2SO_4 at 30 ^{o}C *after* pretreatment to eq. 2.3.

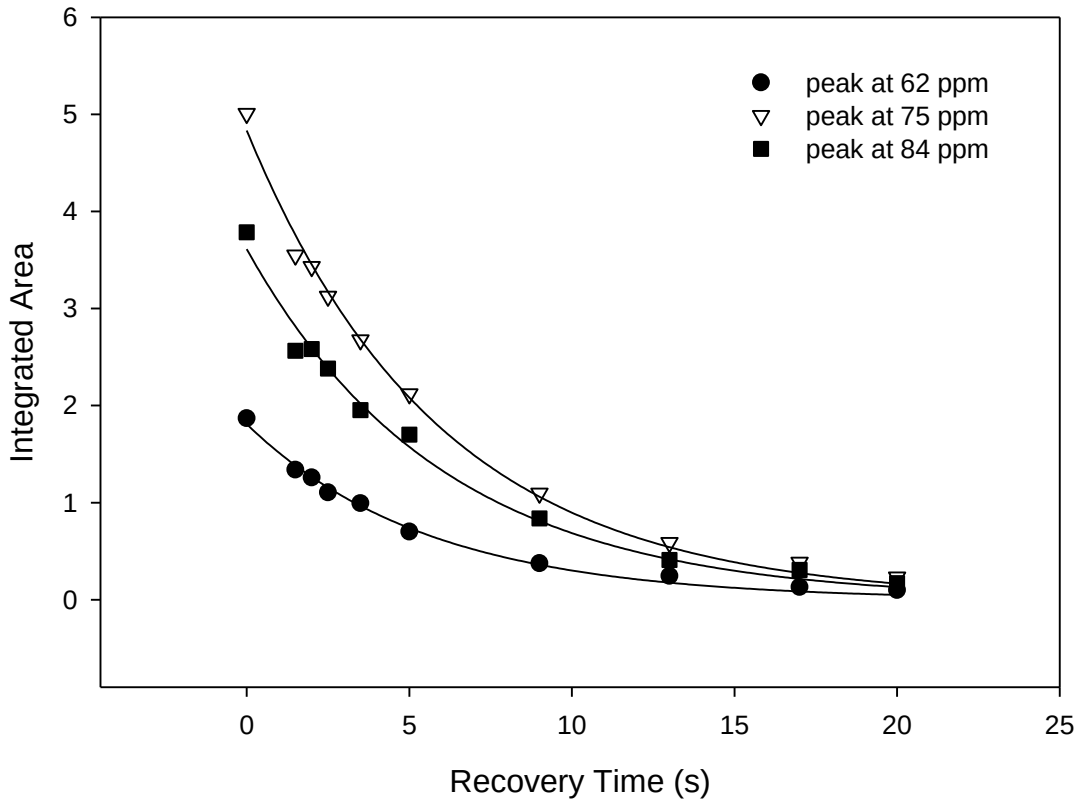

Figure E4c. Curve fitting of integrated intensities of hemicellulose peaks in ^{13}C CP-MAS NMR spectra (Fig. E4a) on 20 mg enriched wood 10 % in 0.5 M H_2SO_4 at 30 ^{o}C *after* pretreatment to eq. 2.3.

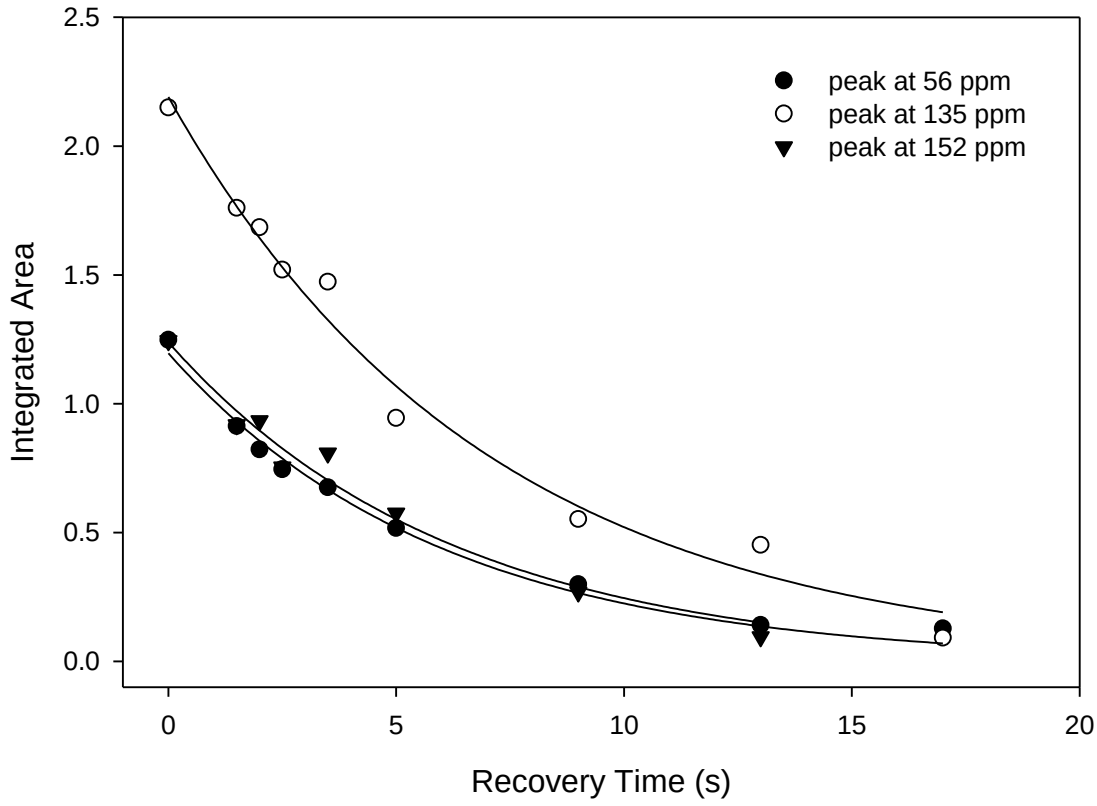

Figure E4d. Curve fitting of integrated intensities of lignin peaks in ^{13}C CP-MAS NMR spectra (Fig. E4a) on 20 mg enriched wood 10 % in 0.5 M H_2SO_4 at 30 ^{o}C *after* pretreatment to eq. 2.3.

Table E4. Curve fitting results of integrated intensities from peaks measured by Torchia's method on 10 % poplar in 0.5 M H_2SO_4 at 30 ^oC *after* pretreatment at 150 ^oC.

Peak	M	T_{1C} (s)
21	[d]	[d]
56	1.2 ± 0	5.9 ± 0.4
62	1.8 ± 0	5.6 ± 0.3
65	2.2 ± 0	5.8 ± 0.2
72	5.0 ± 0	5.9 ± 0.1
75	4.8 ± 0	5.9 ± 0.2
83	3.6 ± 0	6.0 ± 0.4
89	1.0 ± 0	6.5 ± 0.5
105	2.4 ± 0	6.0 ± 0.3
135	2.2 ± 0	6.6 ± 0.5
153	1.2 ± 0	5.8 ± 0.4
173	[d]	[d]

[d] not observed under these conditions

Appendix F

Complete set of Alternating ^{13}C CP-MAS and ^{13}C DP-MAS spectra on 10 % poplar in H_2O obtained in situ at 150 ^{o}C.

The first in situ solid state nuclear magnetic resonance ^{13}C observations of the biomass pretreatment process, using 20 mg ^{13}C enriched poplar wood in a 10 % slurry with H_2O at 150 ^{o}C, were performed by alternating data acquisition between the CP mode and the DP mode as described in the experimental section of this thesis. For CP data acquisition, a one second pulse delay was used to acquire 60 scans, resulting in a total time of one minute for ^{13}C NMR data acquisition. The DP spectra were acquired with a 4.5 s delay to acquire 120 scans, resulting in 9 minutes total acquisition time. The Figure F1 shows the CP results on the left side of the page and the corresponding DP spectra on the right side of the page.

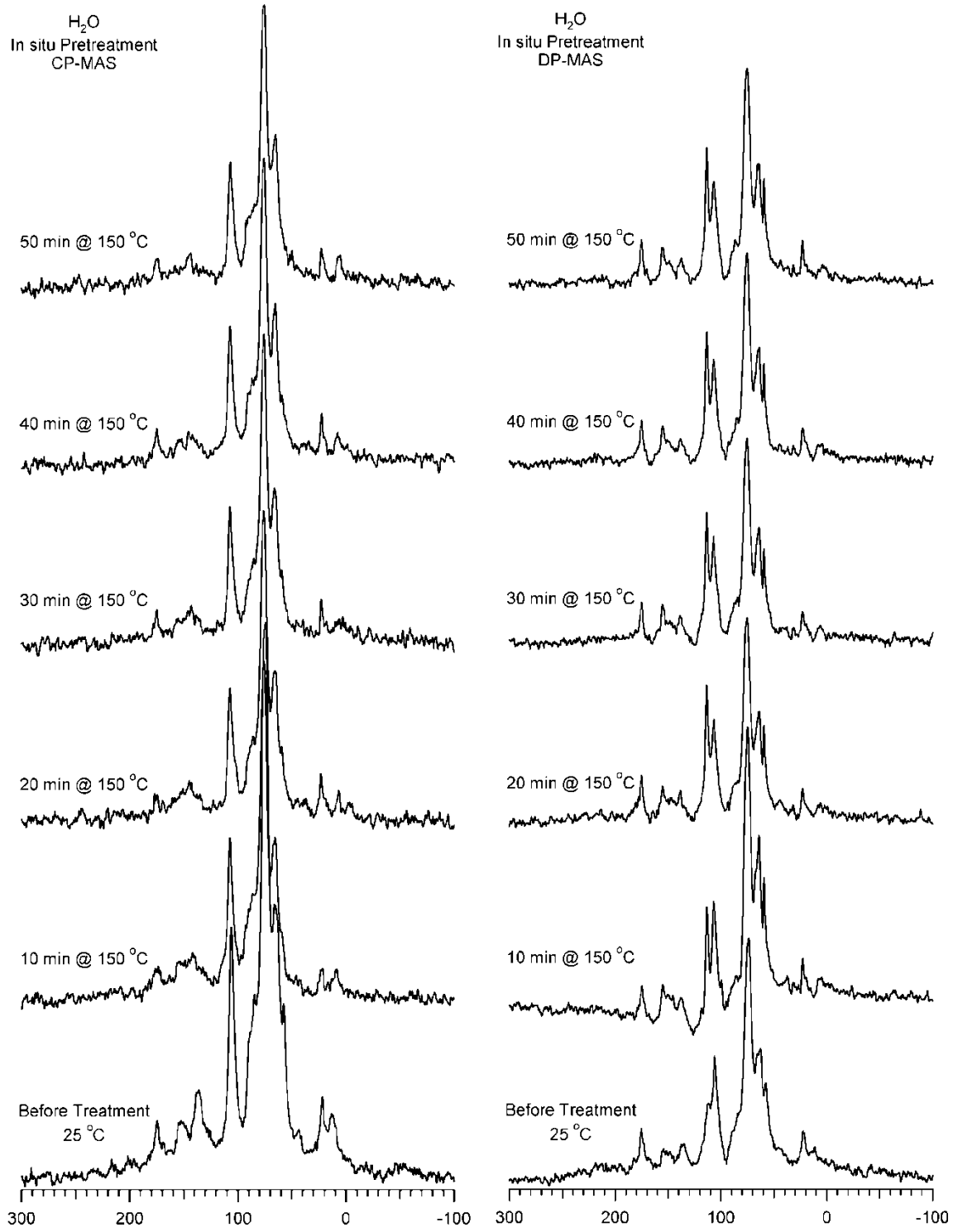

Figure F1. Left: ^{13}C CP-MAS results on 20 mg wood, 10 % in H_2O at 150 ^oC, time span of one min., separated by nine min. DP segments. Right: ^{13}C DP-MAS results on 20 mg wood, 10 % in H_2O, time span of nine min., separated by one min. CP segments. A more detailed version of Figure 9.

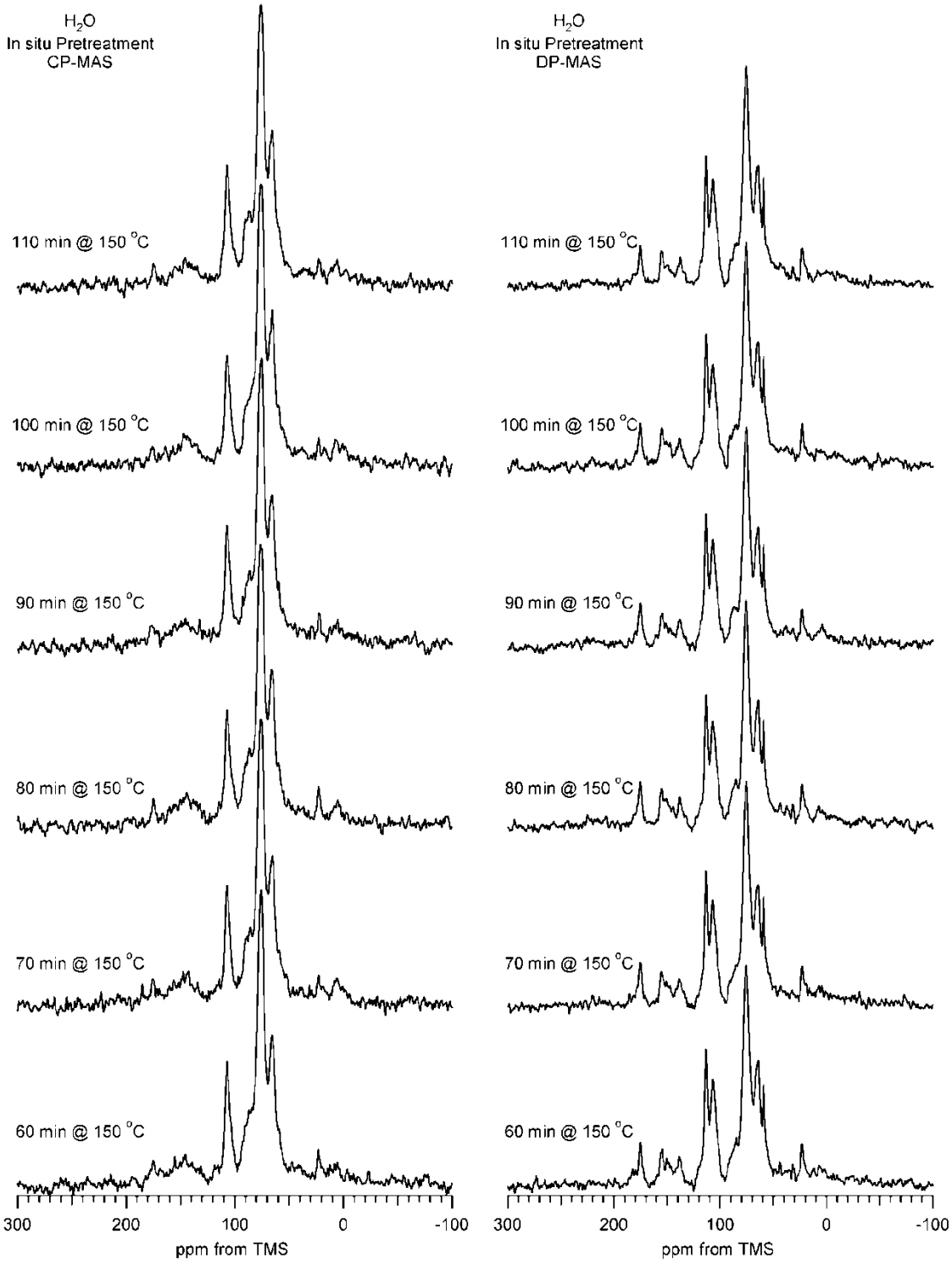

Figure F1. Continued.

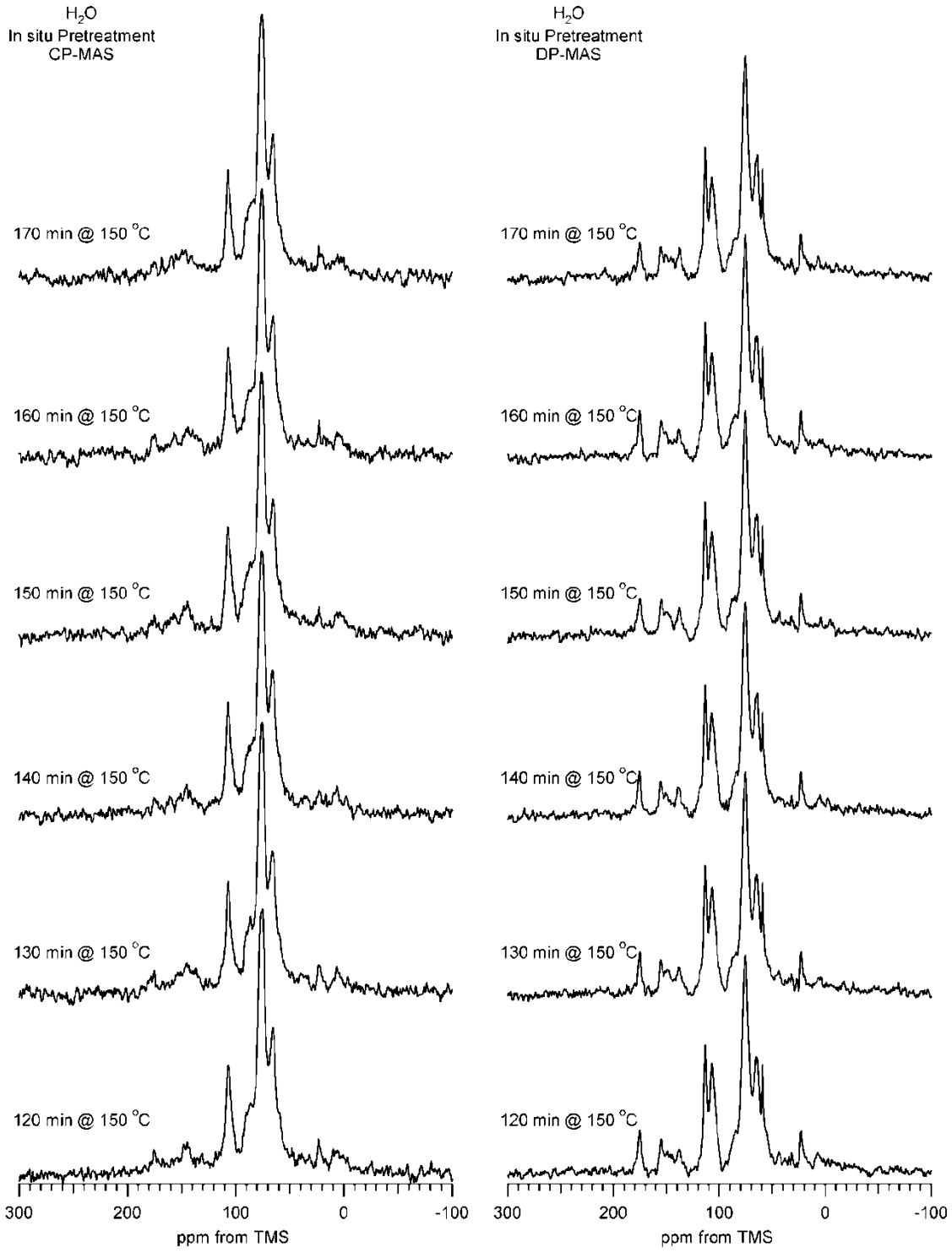

Figure F1. Continued.

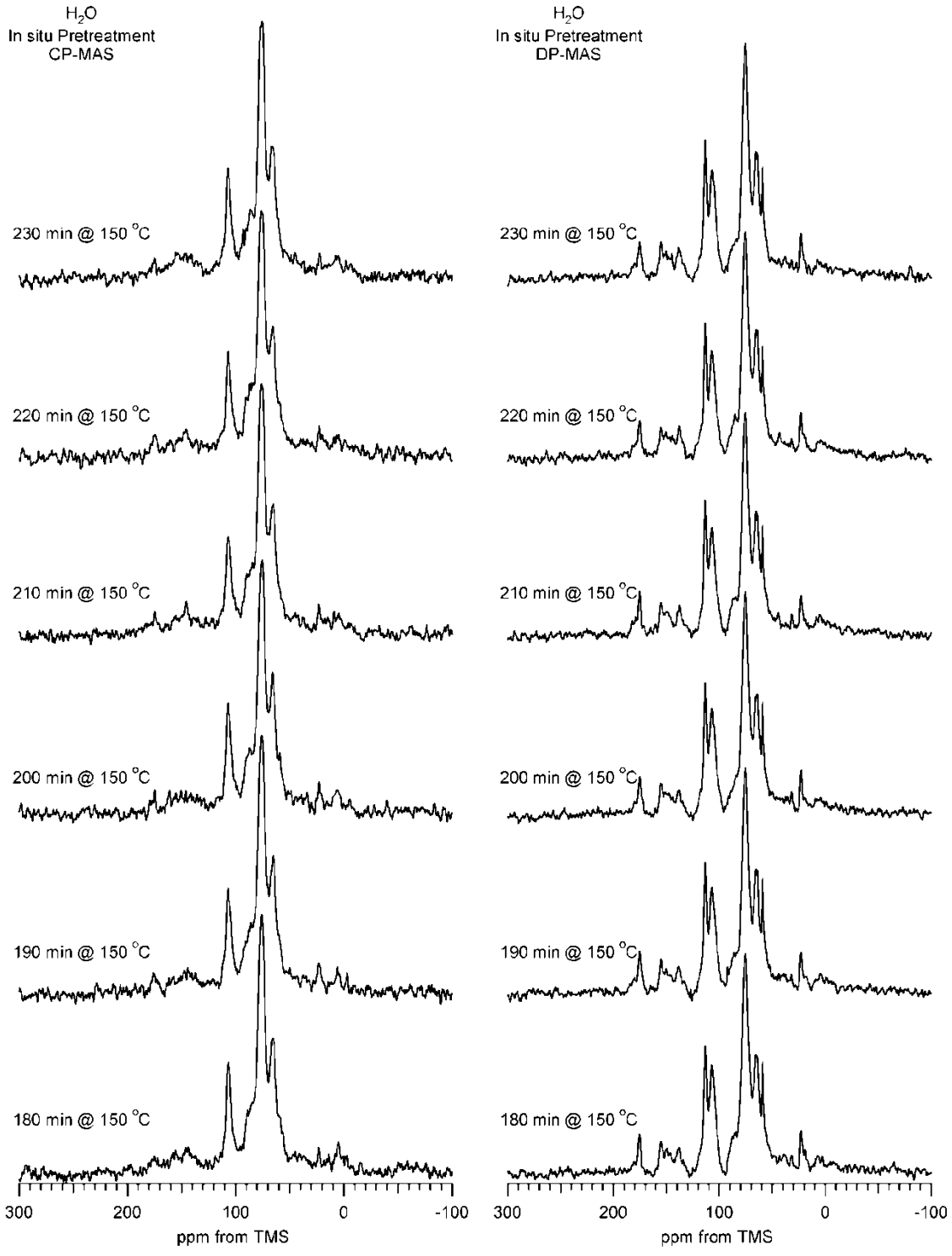

Figure F1. Continued.

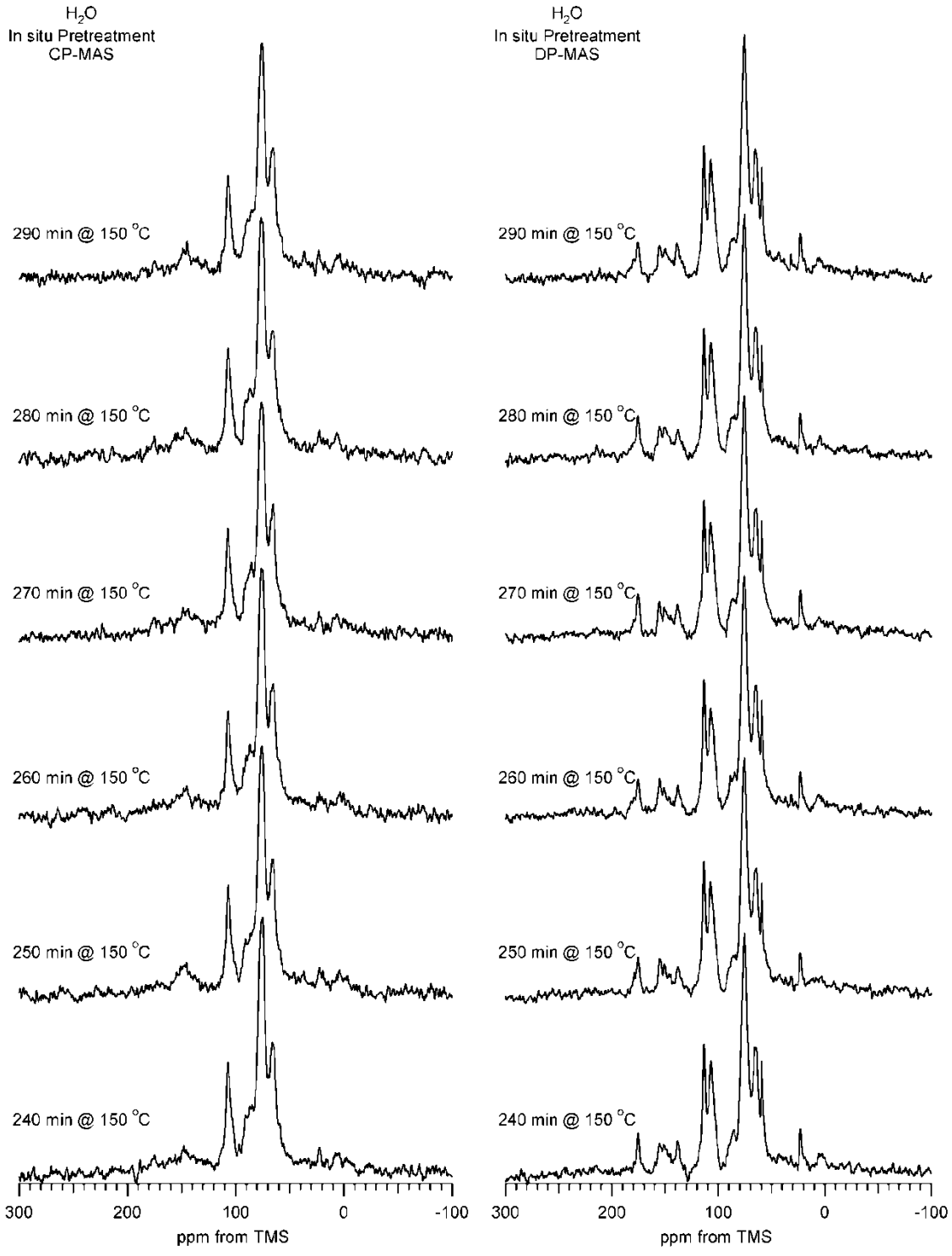

Figure F1. Continued.

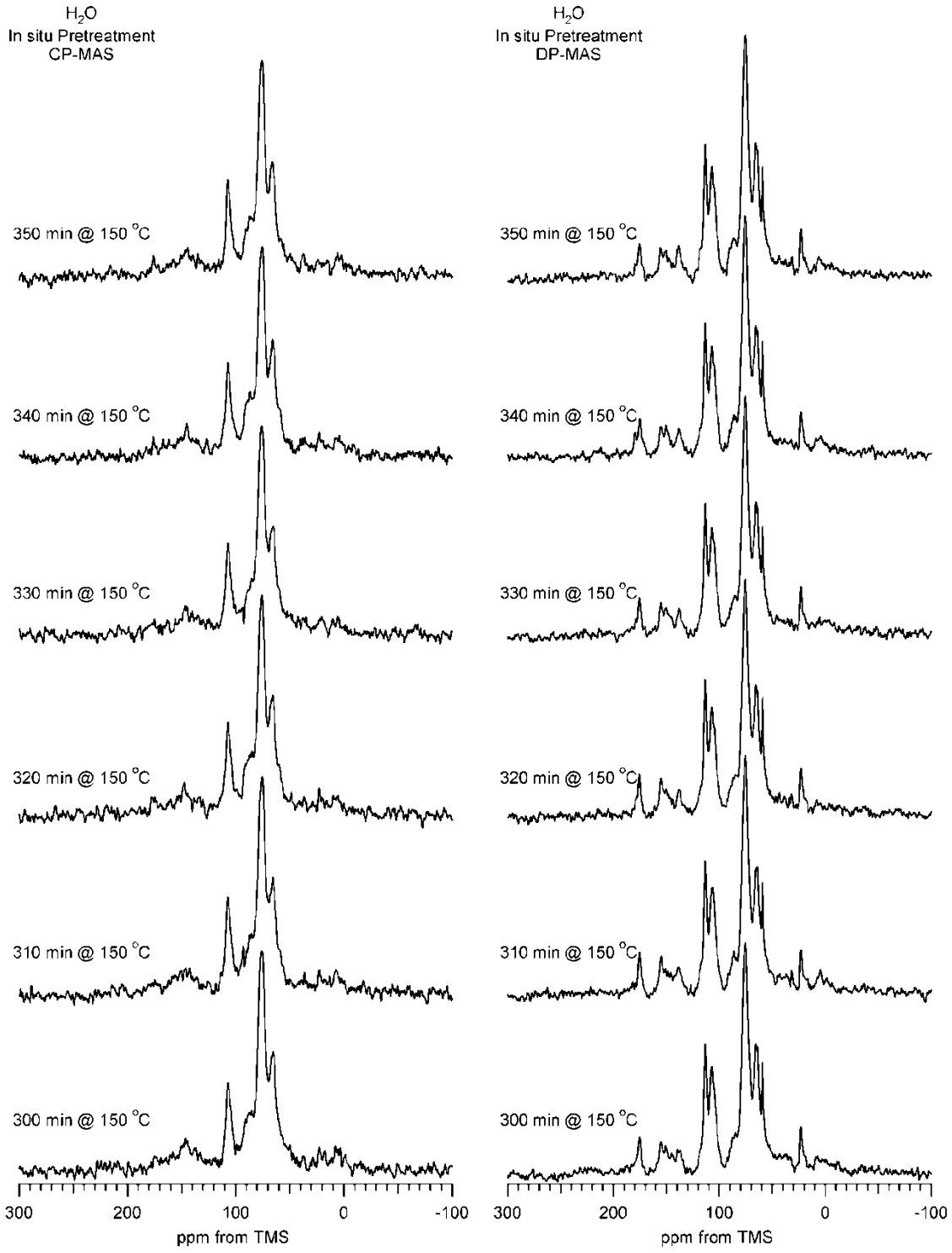

Figure F1. Continued.

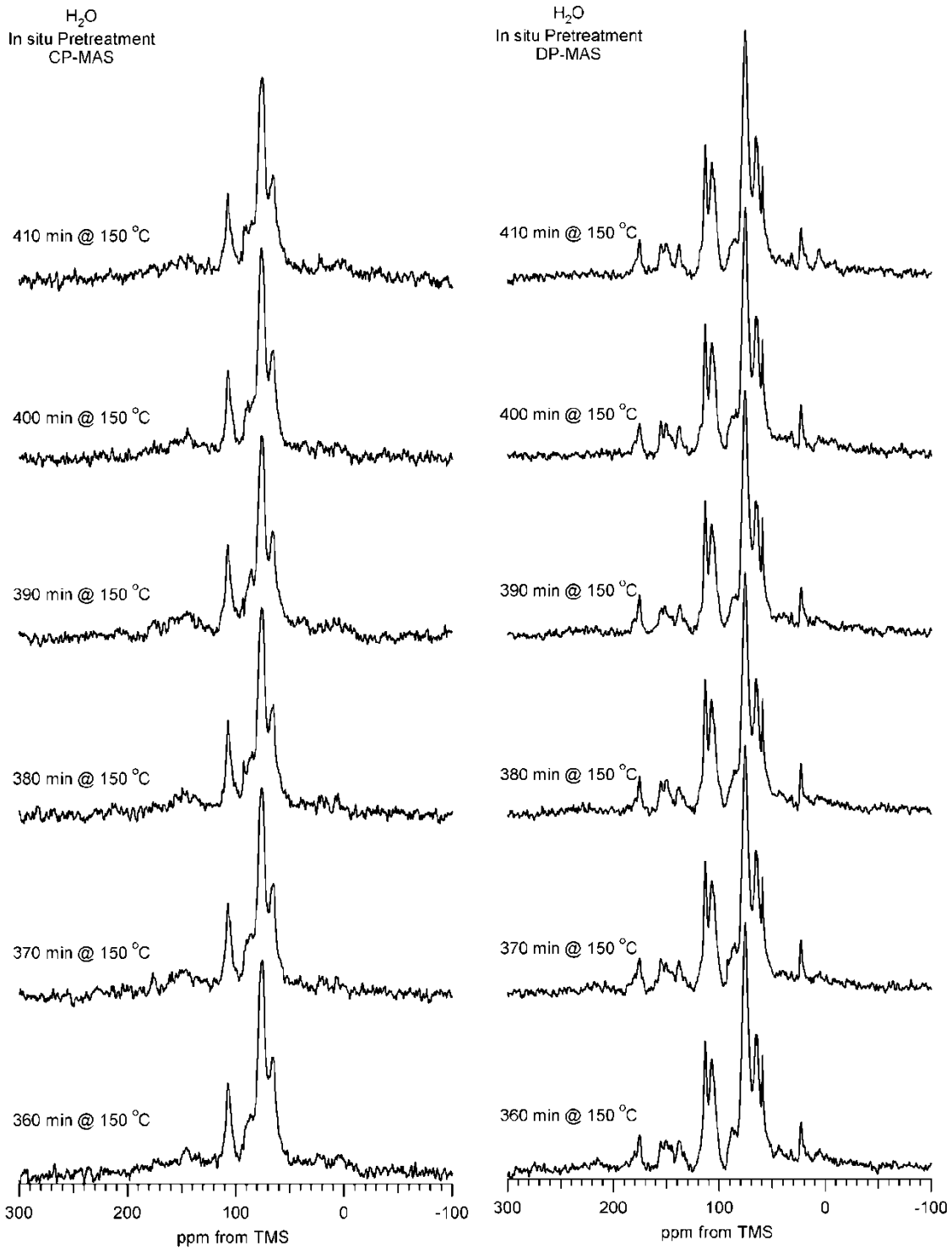

Figure F1. Continued.

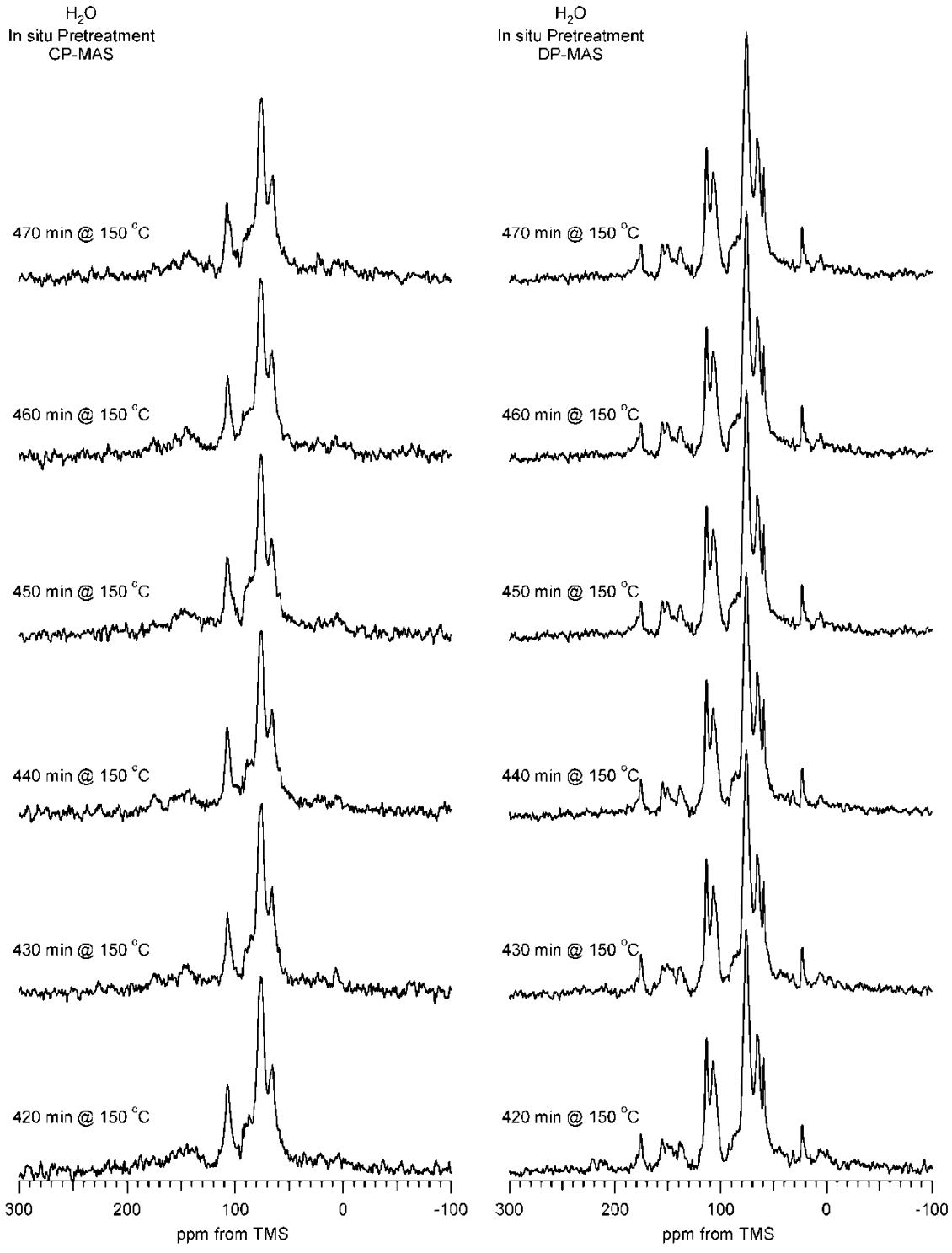

Figure F1. Continued.

Appendix G.

Complete set of Alternating ^{13}C CP-MAS and ^{13}C DP-MAS spectra on 10 % poplar in 0.5 M H_2SO_4 obtained in situ at 150 ^{o}C.

The first in situ solid state nuclear magnetic resonance ^{13}C observations of the biomass pretreatment process, using 20 mg ^{13}C enriched poplar wood in a 10 % slurry with H_2SO_4 at 150 ^{o}C, were performed by alternating data acquisition between the CP mode and the DP mode as described in the experimental section of this thesis. For CP data acquisition, a one second pulse delay was used to acquire 60 scans, resulting in a total time of one minute for ^{13}C NMR data acquisition. The DP spectra were acquired with a 4.5 s delay to acquire 120 scans, resulting in 9 minutes total acquisition time. The Figure G1 shows the CP results on the left side of the page and the corresponding DP spectra on the right side of the page.

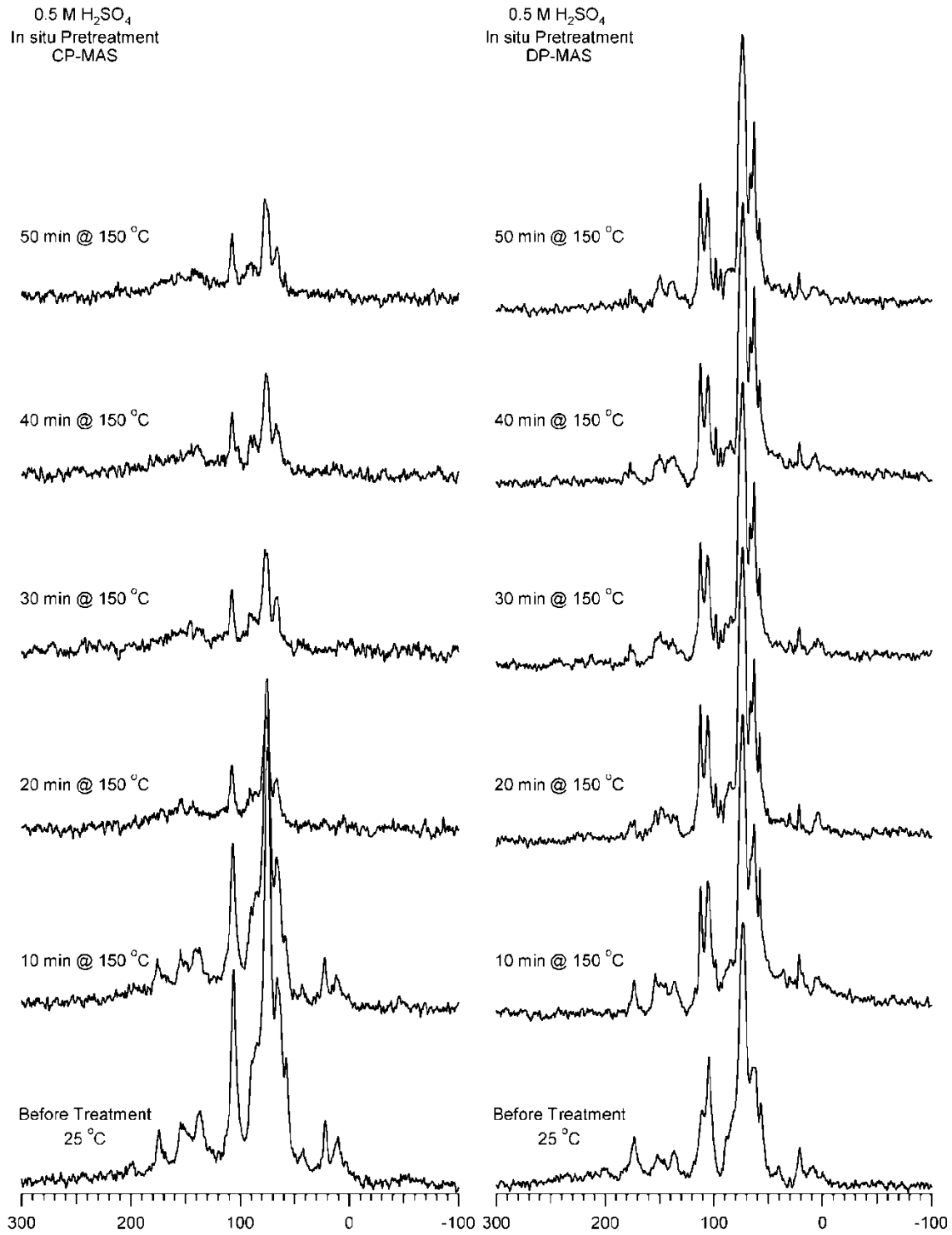

Figure G1. Left: ^{13}C CP-MAS results on 20 mg wood, 10 % in H_2SO_4 at 150 ^oC, time span of one min., separated by nine min. DP segments. Right: ^{13}C DP-MAS results on 20 mg wood, 10 % in H_2O, time span of nine min., separated by one min. CP segments. A more detailed version of Figure 10.

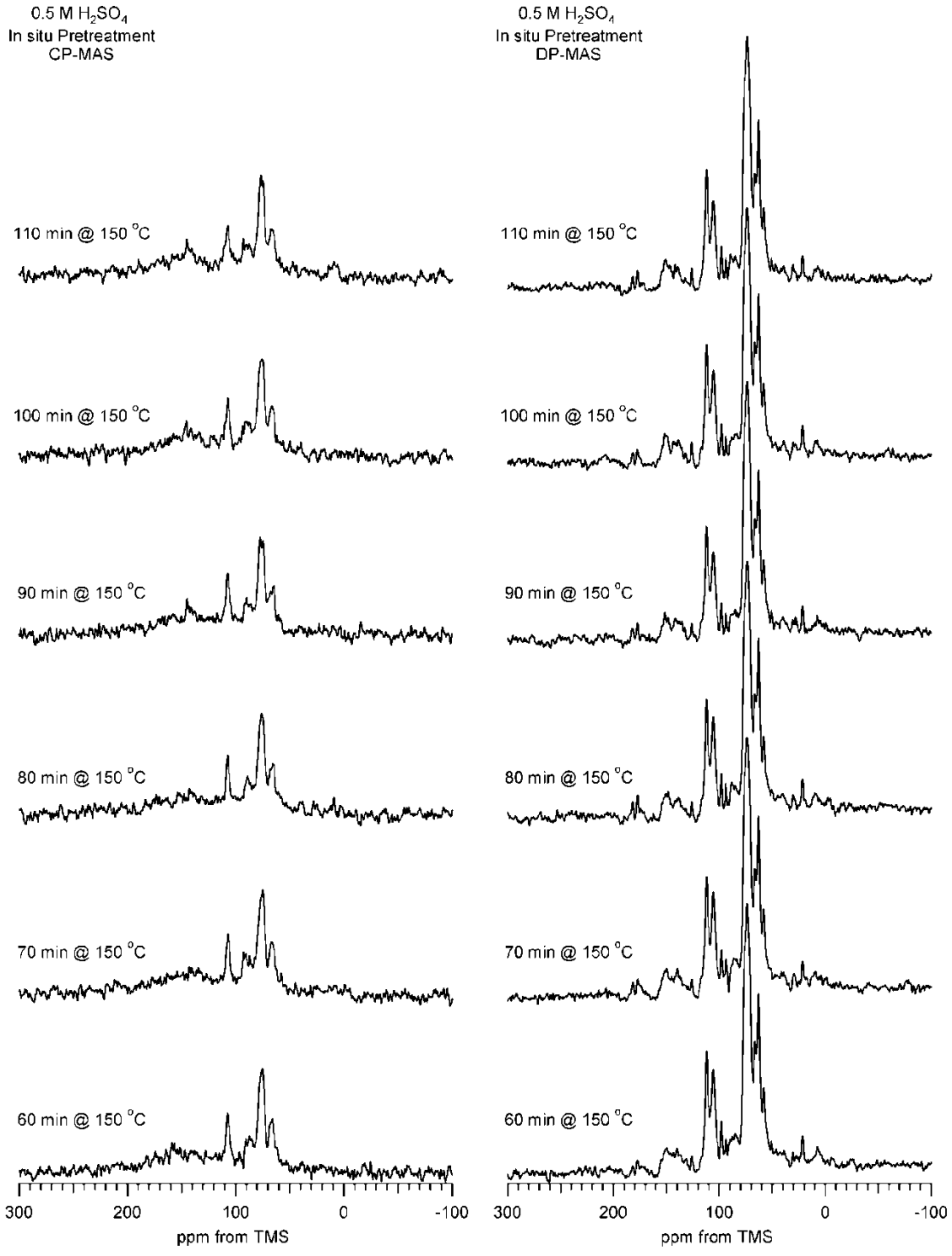

Figure G1. Continued.

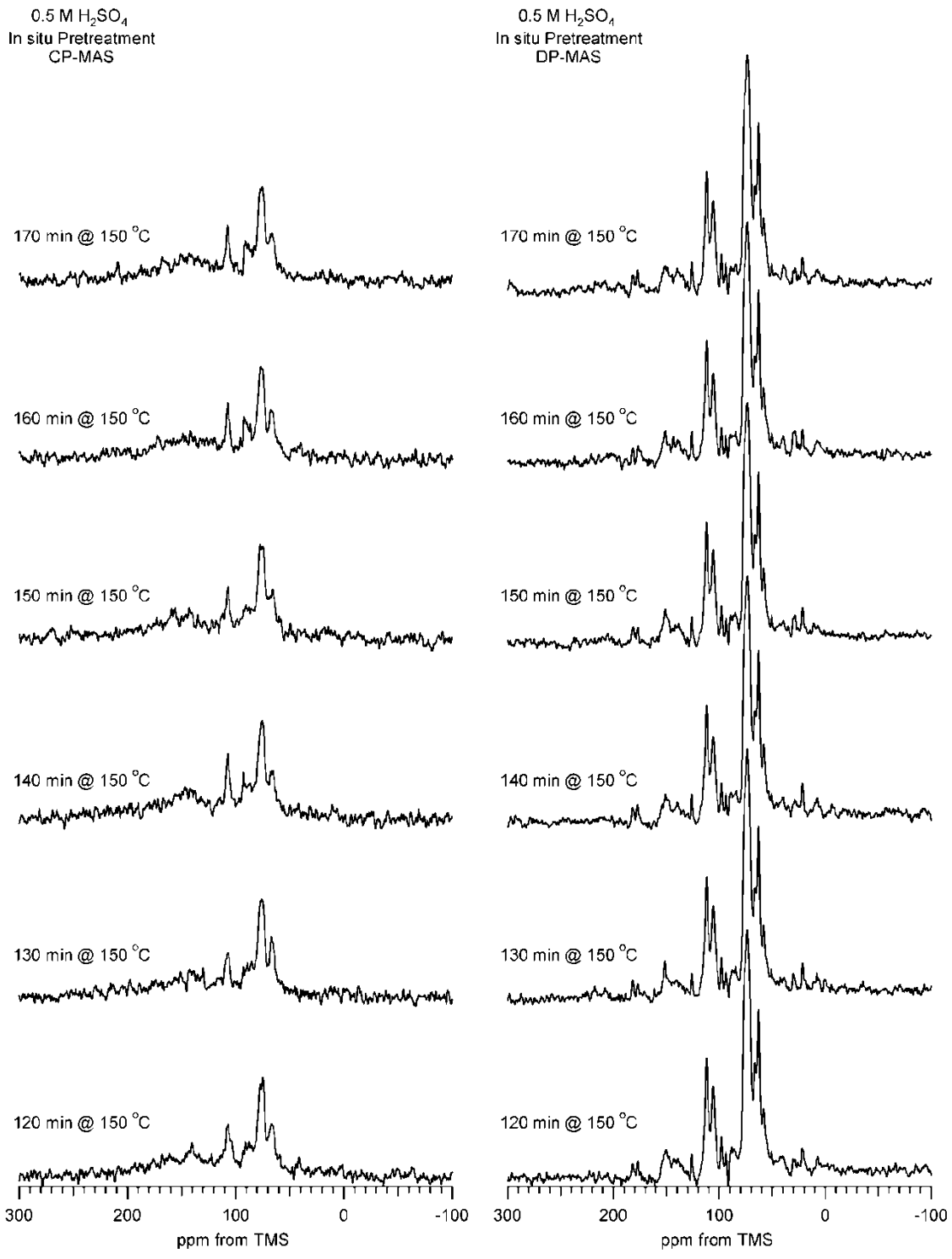

Figure G1. Continued.

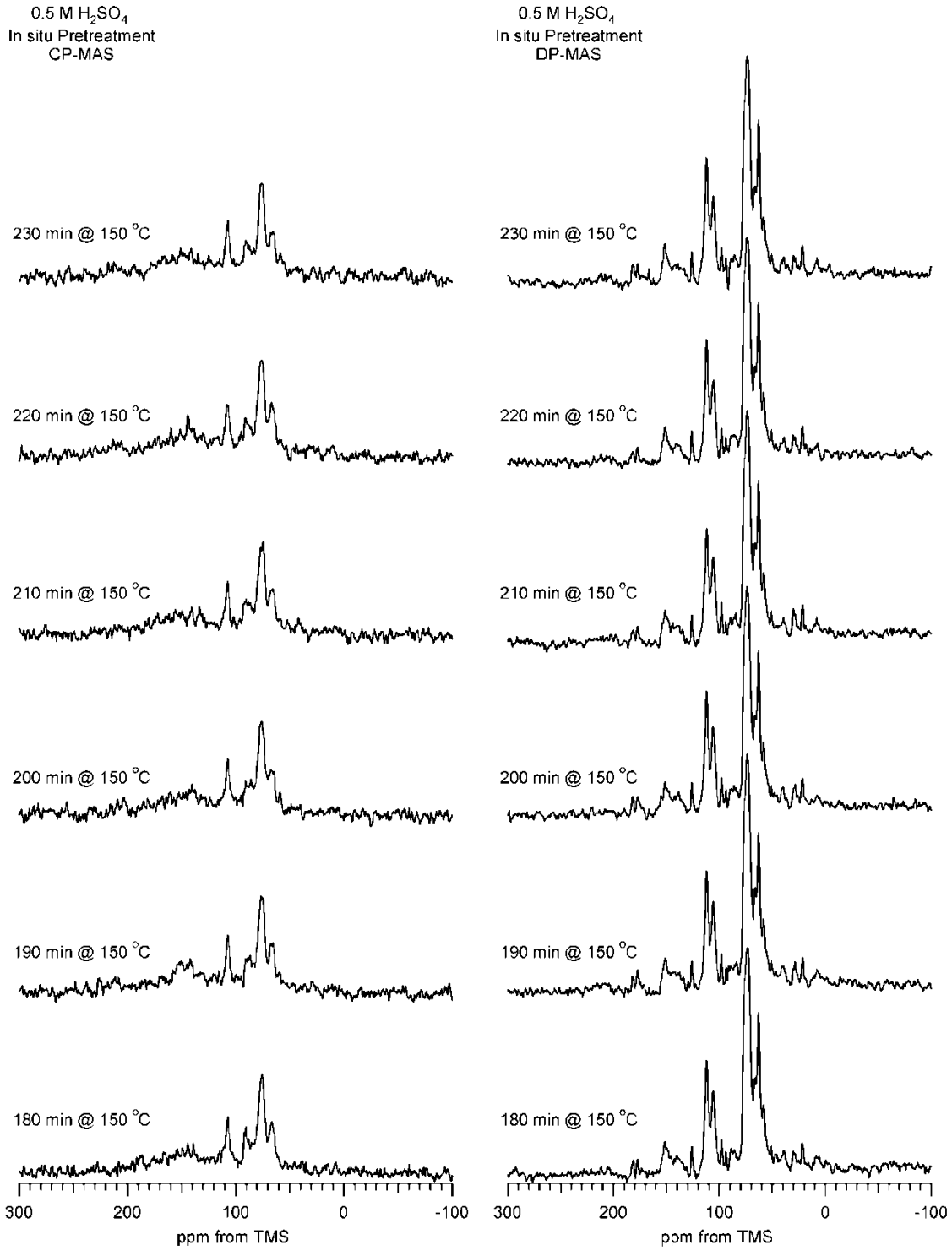

Figure G1. Continued.

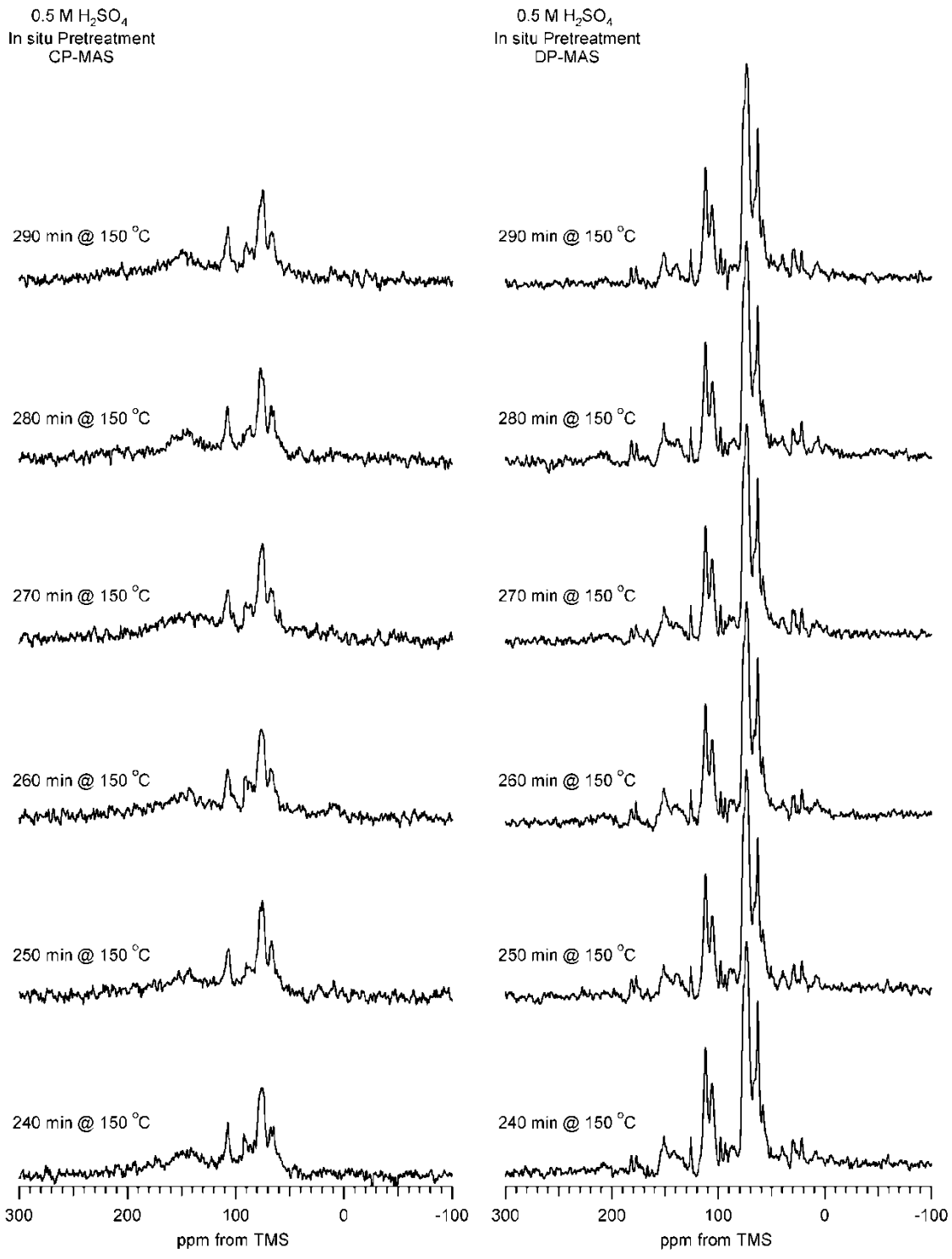

Figure G1. Continued.

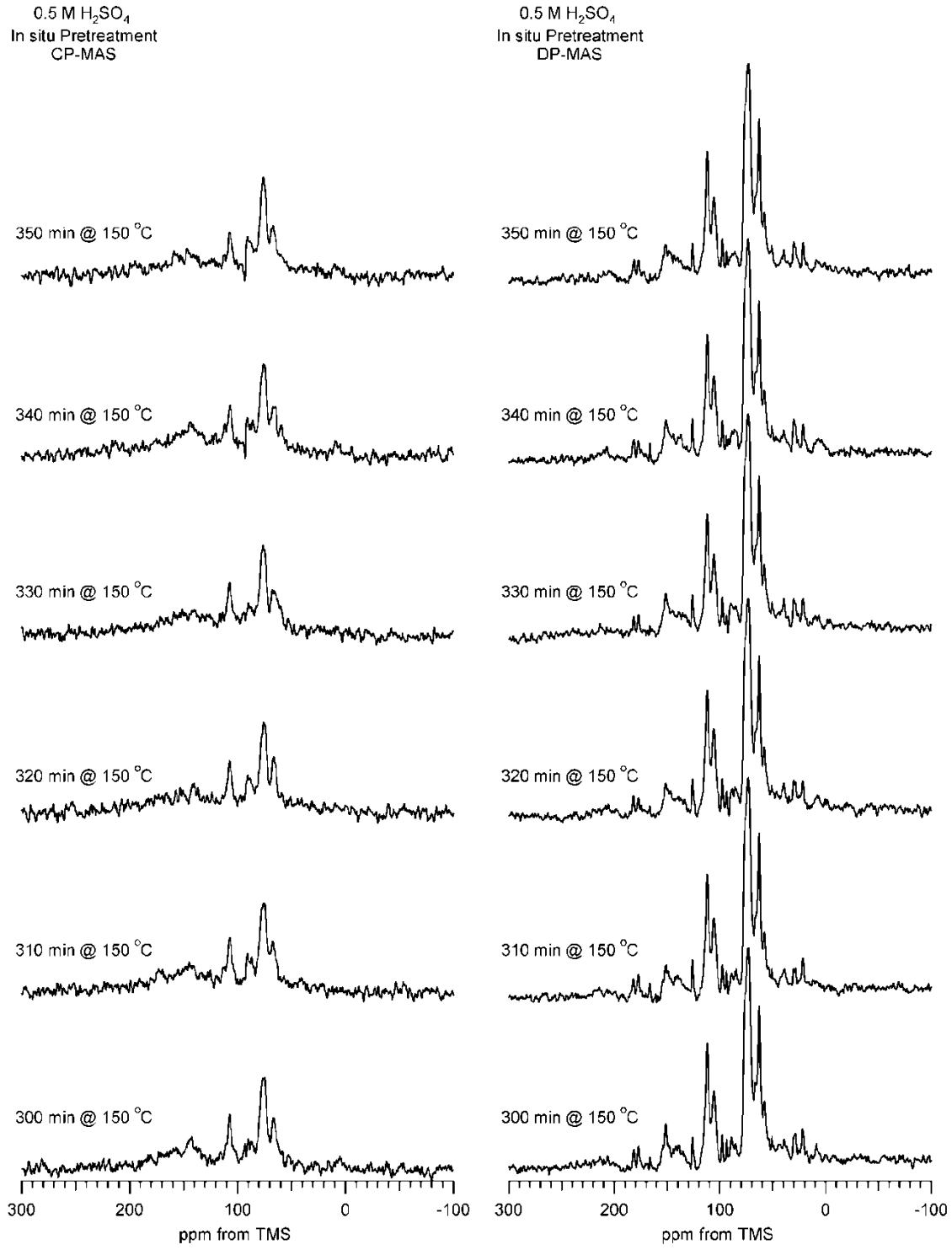

Figure G1. Continued.

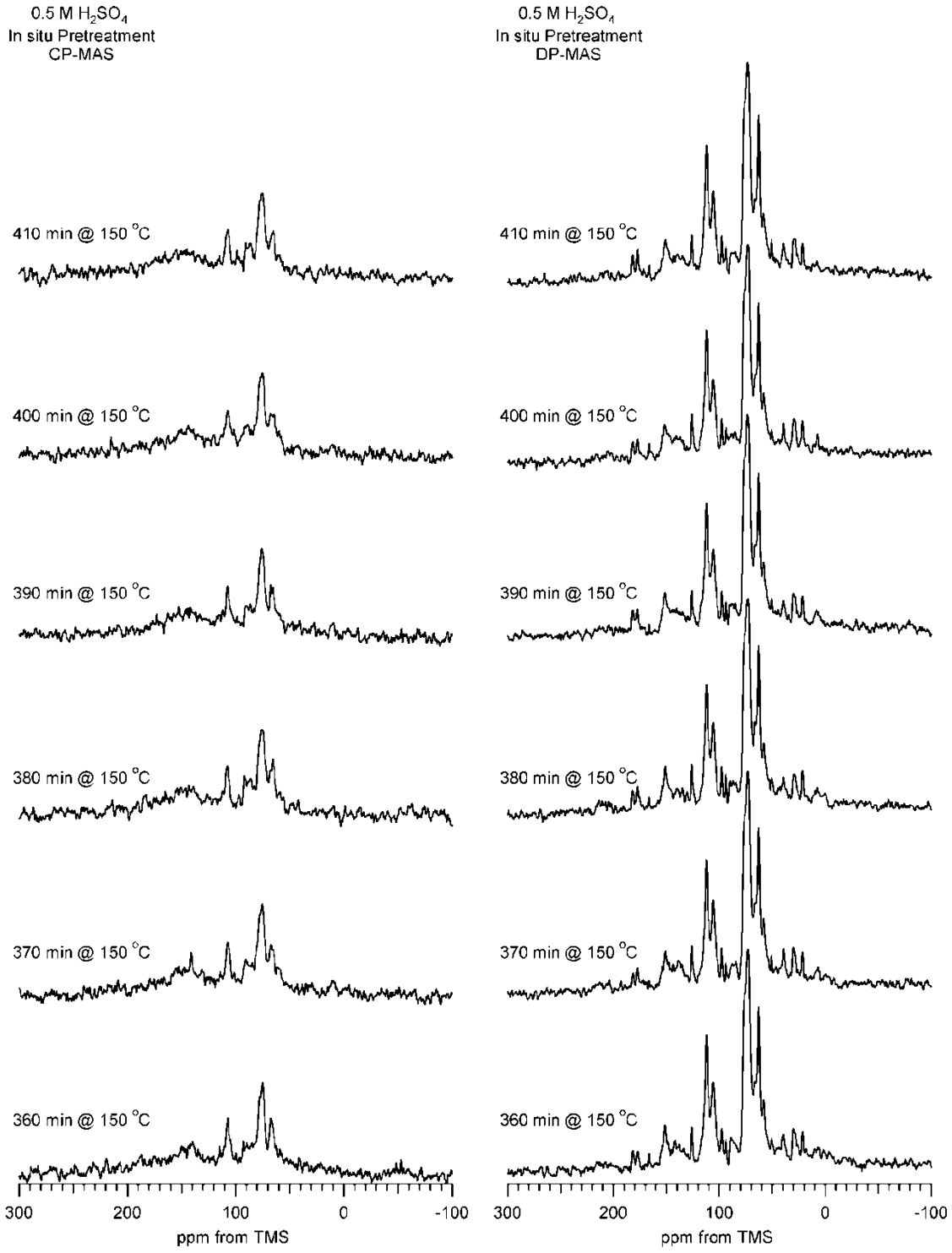

Figure G1. Continued.

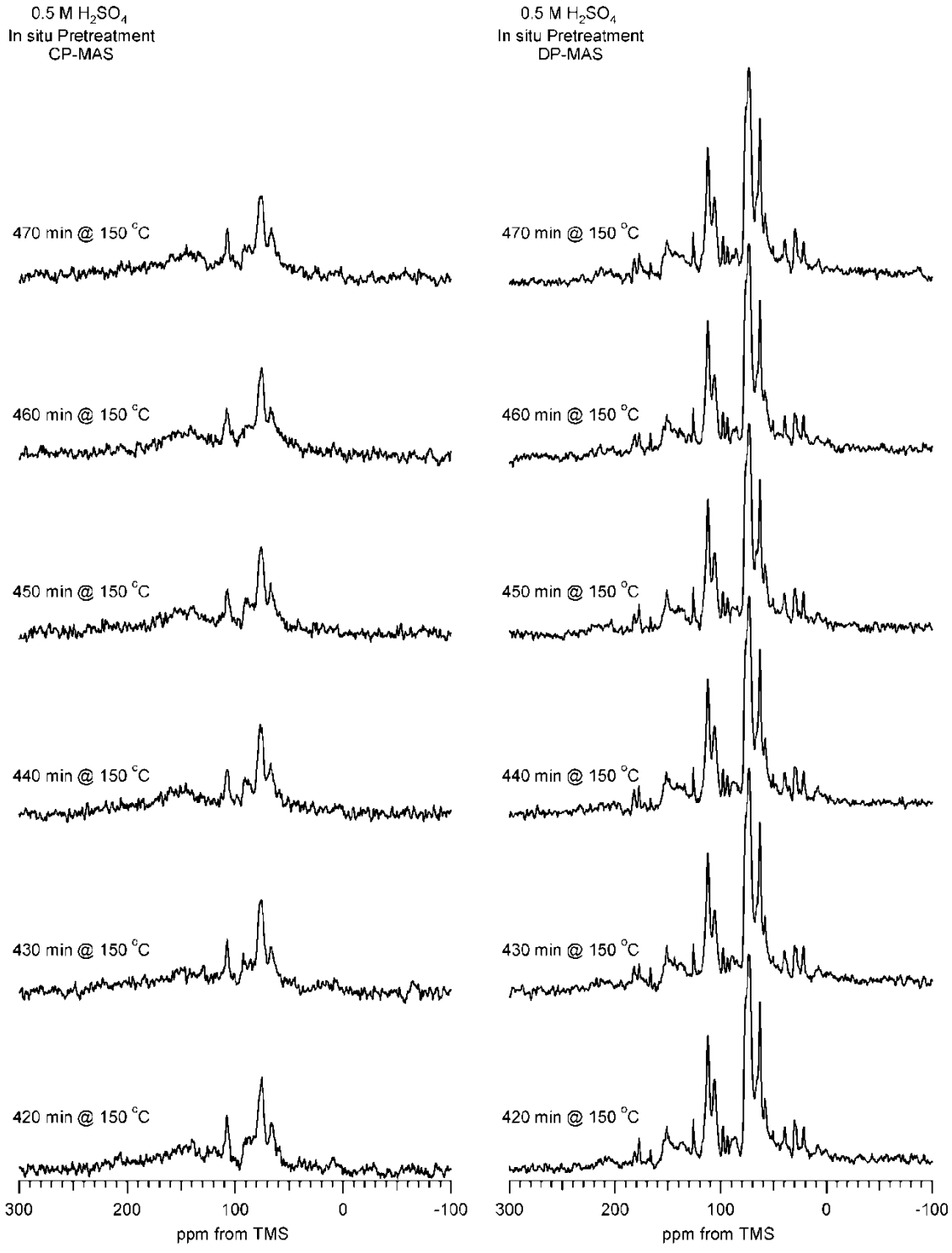

Figure G1. Continued.